

~~Adriaan Franken~~
DI 510

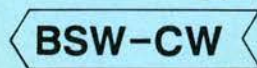
Kolkman, P.A.
Discharge relations for
hydraulic structures an...

~~WISN/118 B-02127 BDU~~

Discharge relations for hydraulic structures and head losses from different components

Desk study for Rijkswaterstaat and the International Association for Hydraulic Research, performed in cooperation with the Delft University of Technology

C67



BOUWSPEURWERK
CONSTRUCTIES EN WATER

December 1989

Z2331

Q 953

delft hydraulics

Preface

This report "Discharge Relations of Hydraulic Structures and Head Losses from Different Components" is conceived as part III of the future IAHR manual about discharge relations and losses in general. Part I, which is presented by Dr. D. Miller will deal with losses in internal flow systems, and part II (Dr. W.M. Hager) will deal with the design of discharge measuring structures. The content of this part of the manual is purely based on literature. It is providing designers both background information and easily applicable data. There are much data on discharge relations available and so the selection of topics and literature was one of the problems the author had to cope with and sometimes arbitrary decisions had to be taken. The problem was also the non-uniformity of symbols, and matters would have been easier when not at some time the water level and at another time the energy level had been introduced as a reference for the hydraulic condition. It was considered to be unpractical to redesign all figures, but for all the figures the meaning of the applied symbols is given.

It was inevitable that once again use was made of the design manuals of the Vickburg Waterways Experiment Station of the US Army and the US Bureau of Reclamation, the data of which are used worldwide because of their concise and user-friendly presentation. When presented here, however, all results were transformed into a dimensionless form. I could also make use of the open-channel-flow textbook by prof. E. Naudascher which fortunately had just been published.

This part III is certainly not sufficiently complete, to cover all the needs for design, but while also being a general introduction, a certain conciseness was aimed at. Only after a certain period of use and after receiving comments from users gaps may be filled.

I got help from a few colleagues of DELFT HYDRAULICS and RIJKSWATERSTAAT who corrected initial errors and indicated omissions. In particular I wish to thank prof. J. Battjes of Delft University of Technology for his close reading of the equations, symbols and text of the first draft, and prof. P. Novak of New Castle University for his corrections and proposed additions.

RIJKSWATERSTAAT financed, within the framework of the Hydraulic Structures Research (BSW-CW), the final editing of this report. This edition has been published in a limited number of copies, as a DELFT HYDRAULICS' report Q953.

December 1989

P.A. Kolkman

CONTENTS

List of Symbols

1. GENERAL ASPECTS OF DISCHARGE RELATIONS AND LOSSES	1
1.1 Introduction	1
1.2 Discharge relations of hydraulic structures introduced in far-field computations	6
1.3 The use of the Bernoulli-, the momentum- and the Carnot equations	8
1.4 Some general remarks before starting the calculation of losses	10
1.5 Modular flow equations	11
1.6 Fully submerged flow	15
1.7 The intermediate-flow relations at control sections	19
1.8 Remarks about entrance losses	23
1.9 Remarks about trash-rack and bridge pier losses	25
1.10 Required and obtainable accuracies	27
2. NUMERICAL PROCEDURE FOR COMPUTATION OF WATER LEVEL/DISCHARGE RELATIONS	29
2.1 Introduction	29
2.2 The search procedure	31
Appendix of Chapter 2: Iterative search procedure for h_2 using the ACORN-BBC computer.	
3. DISCHARGE RELATIONS FOR CONTROL SECTIONS	36
3.1 The sharp-crested weir	36
3.2 The weir with circular crest section	42
3.3 The nappe-shaped overflow weir	46
A modular flow.....	47
B submerged flow.....	48
C modular flow with piers	49
3.4 The nappe-shaped spillway with gate	54
3.5 Broadcrested weirs and dikes	56
3.6 The morning glory spillway	62

CONTENTS (continued)

3.7	Labyrinth weir	69
3.8	Gates with underflow	73
3.9	Gates with overflow	86
3.10	Gates with combined under- and overflow	90
3.11	The Howell Bunger valve	92
3.12	Conduit outlet	96
4.	LOSSES OF COMPONENTS UP- AND DOWNSTREAM OF THE CONTROL SECTION	97
4.1	Orifice and intake losses	97
4.2	Friction losses	105
4.3	Slots	109
4.4	Exit losses and hydraulic jump relations	112
	A abrupt expansions downstream of control section.....	114
	B hydraulic jump relations (two-dimensional).....	116
	C hydraulic jump on a slope.....	120
	D gradual expansions.....	122
	E hydraulic jump in a gradual expansion.....	125
4.5	Trash racks	127
4.6	Resistance of bridge piers	132

REFERENCES

LIST OF SYMBOLS

a	(gate) opening height	(m)
a and b	parts of the nappe at weir flow	(m)
A_c	culvert area	(m ²)
A_o	orifice area	(m ²)
C_{br}	loss coefficient by bridge piers	
C_c	contraction coefficient	
C_d	discharge coefficient	
C_{Do}	drag coefficient of bar or pier at internal flow or at free flow with low velocities, without blockage effect	
C_f	friction factor	
C_0	discharge coefficient at free flow (used also as a reference discharge coefficient)	
C_s	reduction factor by submergence	
C_{tr}	loss coefficient of trash rack	
d	gate thickness, diameter of semi-circular gate edge, waterdepth	(m)
d_j	jet thickness	(m)
d_0	upstream waterdepth	(m)
d_1	waterdepth in or just downstream of control section	
d_1	waterdepth upstream of hydraulic jump	(m)
d_2	downstream waterdepth	(m)
d_c	critical depth = $(q^2/g)^{1/3}$	(m)
d_c	waterdepth in culvert	(m)
d_s	waterdepth at submerged supercritical flow	(m)
D	pipe diameter, height of roofed culvert	(m)
D_h	hydraulic diameter (4 x hydraulic radius)	(m)
F	Froude number V/\sqrt{gh} (F_2 refers to section 2 etc)	
F_1	Froude number upstream of hydraulic jump	
g	acceleration of gravity	(ms ⁻²)
G_0	height of gate opening	(m)
h	upstream water level related to crest level at modular flow	(m)
h_0	upstream head related to weir crest or culvert bottom	(m)
h_1	downstream head in or just downstream of control section	(m)
h_2	downstream head further downstream	(m)
H	upstream energy head (above weir crest) at modular flow	(m)
H_0	upstream energy head above weir crest or culvert bottom	(m)
H_c	energy head in culvert	(m)
H_d	crest-design value of upstream energy head	(m)
H_e	(effective) energy head upstream of a weir	(m)

LIST OF SYMBOLS (continued)

K	coefficient in the bridge-resistance formula of Yarnell	
K_s	loss coefficient of slots	
K_a	abutment coefficient	
K_p	pier flow-contraction coefficient	
L	length of crest in flow direction	(m)
L	bruto length of labyrinth weir	(m)
L	lip length of gate	(m)
L	length of hydraulic jump	(m)
L_r	length of radial jump	(m)
m_1, m_2	discharge coefficients	
p	weir height	(m)
P	pressure	(Pa)
Pa	atmospheric pressure	(Pa)
q	discharge per unit width	(m^2s^{-1})
Q	discharge	(m^3s^{-1})
Q_g	gate discharge	(m^3s^{-1})
Q_1	real discharge over labyrinth weir	(m^3s^{-1})
Q_n	discharge at a sharp-crested straight weir	(m^3s^{-1})
Q_0	discharge at modular flow (used as reference discharge)	(m^3s^{-1})
r_o	ratio r_2/r_1	
r_1, r_2	radii up- and downstream of radial jump	(m)
R	bottom step	(m)
R_h	hydraulic radius	(m)
S	submergence factor (h_1/h_o) or (h_2/h_o)	
S_o	slope	
U	velocity of flow	($m s^{-1}$)
\bar{U}	average pipe flow velocity	($m s^{-1}$)
V	flow velocity	($m s^{-1}$)
V_c	culvert velocity	($m s^{-1}$)
V_o	orrifice velocity	($m s^{-1}$)
w	width of opening, weir, sluice, culvert or gate	(m)
w	repeating distance at labyrinth weir	(m)
w	bar thickness of trash rack	(m)
W	canal width	(m)
W	distance between trash rack bars	(m)
W_e	Weber number	
y	waterdepth on a slope, measured vertically	(m)
Y_0	ratio d_2/d_1	

LIST OF SYMBOLS (continued)

z	coordinate in vertical direction	(m)
α	correction factor in the Bernoulli equation for uneven flow distribution	
α	divergence angle at one side of diffuser	(degrees)
β	correction factor in the momentum equation for uneven flow distribution	
δ	boundary layer thickness	(m)
δ_d	displacement thickness of boundary layer	(m)
δ_0	shape coefficient of bridge piers in Rehbock formula	
ΔH	loss of energy head	(m)
τ	wall shear stress	(kg m ⁻¹ s ⁻²)
θ	divergence angle (= 2 α)	(rad)
ξ	coefficient for loss of energy head related to $V^2/2g$ or to $(V_1 - V_2)^2/2g$	
ξ_e	entrance loss coefficient etc.	
ρ	fluid density	(kg m ⁻³)
ψ	rate of submergence of submerged hydraulic jump (= d_s/d_1)	

1. GENERAL ASPECTS OF DISCHARGE RELATIONS AND LOSSES

1.1 Introduction

Hydraulic losses are among the classic research topics in laboratories for hydraulic research, and a continuous flow of publications has been the result.

In contrast to publications about internal flow, only a limited number of publications about losses and discharge relations of free surface flow structures are of more general value. Because at free surface flow many more parameters (compared to internal flow) are involved, the chance is small that exactly similar conditions occur as compared to data from literature.

Because internal flow is discussed in Part I of the IAHR manual, in the following only data and computation methods are presented which are related to free surface flow. The application of scale models is not further discussed.

The data of this manual will mainly be used for estimating in the pre-design stage the dimensions of a structure through which a certain discharge should pass at a given combination of up- and downstream water levels (or difference of water levels).

Another use of these data can be the introduction of structures such as sluices, weirs, and so on in far-field computational models of canal networks and estuaries. Then it is important to have insight into the nature of the discharge relations with all sorts of combinations of the upstream and downstream water levels.

The following type of equation is called a "discharge relation":

$$Q = f(h_0, h_2, \text{geometry}) \quad (1a)$$

in which Q = discharge, h_0 = upstream water level, and h_2 = downstream water level (in general at a distance where the flow is redistributed over the flow section).

Instead of water levels, also the energy heads can be applied.

$$Q = f(H_0, H_2, \text{geometry}) \quad (1b)$$

When in a structure one section controls either in total or mainly the discharge relation, then this is called a "control section". In Chapter 3 the discharge relations of control sections are presented.

When the structure has a certain length (in flow direction) the "hydraulic losses from different components" are also involved, such as entrance- and exit-losses, friction losses, losses at a hydraulic jump etc.

A number of these losses are expressed in terms of losses of energy head.

As an example the entrance loss:

$$\Delta H_e = \xi_e V_c^2 / 2g \quad (2a)$$

where:

ΔH_e = loss of energy head at the entrance,

ξ_e = entrance loss coefficient,

V_c = culvert velocity and

g = acceleration of gravity.

At a free-surface condition this equation becomes:

$$\Delta H_e = \xi_e (Q/w_c d_c)^2 / 2g \quad (2b)$$

(w_c = culvert width, d_c = water depth in the culvert).

This relation differs markedly from Equation 1, and in equation 2b the depth d_c is coupled to both the up- and the downstream head. The following procedure is suitable to determine the discharge relation of the structure. The discharge relation of a control section, mostly expressed in the form of Equation (1), is transformed into:

$$h'_0 = f(Q, h_1)$$

(h_1 is the head just downstream of the control section and h'_0 is the water level just upstream of this section).

Now to h'_0 is added the effect of the different losses from elements upstream and from h_1 is subtracted the effect of the downstream losses which results in h_2 . (All these additional losses are found from expressions similar to equation 2b but then transformed into steps in water level).

When these calculations are performed for a sufficient number of combinations of Q , h_0 and h_1 then a new discharge relation of the type of Equation 1 can be established.

In this manual data are presented about discharge relations of control sections and about losses of components. Discharge relations of complete hydraulic structure are not presented here as these can only be considered as a special case. In certain cases the discharge relations of the control section might be representative for the whole structure. This applies when the flow at the control section is strongly throttled (discharge over weirs, over and under gates etc.).

Concerning the discharge characteristics of a control section with free surface flow, there is already a great complexity: three flow regimes are distinguished. Later this will be illustrated in Figures 3 and 4, in which configurations with openings and overtopping are introduced.

- a. free flow (or modular flow), where the discharge is related to the upstream head only; $Q = f(h_0)$. Because the upstream energy head H_0 (being $(h_0 + V_0^2/2g)$) is related to h_0 and Q , also $Q = f(H_0)$ is a unique relation. In the design it is of interest to know how low the downstream water level must be to guarantee modular flow.
- b. fully submerged flow, here "fully" means with small head differences. Fully submerged flow is comparable with internal flow because the nearly horizontal water level is a boundary which remains independent of the flow velocity (as long as this velocity is small), so the loss and the discharge relation are also $\Delta H = \xi V^2/2g$, and $Q = C_d A \sqrt{2g\Delta H}$, with the loss coefficient ξ and the discharge coefficient C_d being independent of ΔH . ΔH is the loss of energy head from up- to downstream of the control section. When the flow is overtopping a sill or a gate, then the flow section "A" depends on the water level.
- c. intermediate flow, in between the two former regimes; this is the most complicated one; the discharge depends on both energy levels H_0 and H_1 (or on both heads h_0 and h_1). It comprises the situation of what is called submerged weir flow, wherein ΔH determines the discharge but where the flow section is mainly determined by the downstream level instead of the upstream level (like Figure 4b). It comprises also the situation of semi-submerged gate outflow with an eddy on top of the jet (with thickness d_j) with super-critical flow (Froude number > 1 or $V > \sqrt{g d_j}$). And as will shown in section 1.7 (Figure 5) there can also be mixed flow, where the upper part of the weir flow behaves like free flow and the lower part like submerged flow.

The transition between the free flow and fully submerged regimes and the intermediate regime cannot precisely be predicted.

In Figure 1, a picture is shown of the generalized discharge/water-level relation, where the three flow regimes are presented. Such a presentation is valid for the control section, but can also be drawn up for the complete structure.

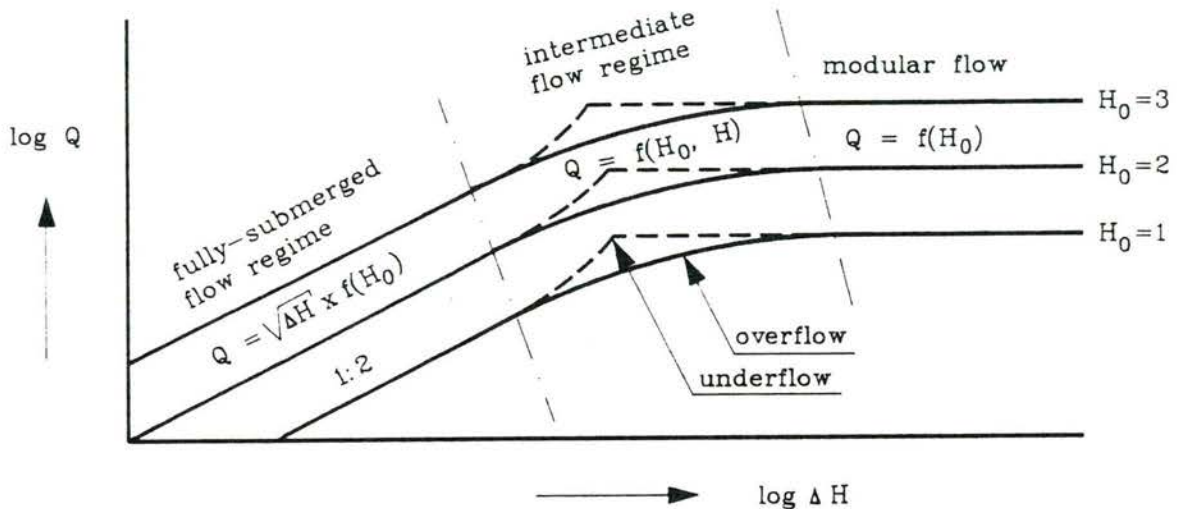


Figure 1 Generalized discharge/water-level relation for one geometry (and also one gate position).

In case the complete structure is considered, the characteristic property of the fully submerged flow regime remains that discharge Q increases in proportion to the square root of the head difference. At overflow the control opening and the discharge vary also with the waterlevel h_0 . The characteristic property of the free (or modular) flow is again that (at a given upstream water level h_0) the discharge Q is completely independent of the head difference. The relation with the upstream water level can be in proportion with $H^{3/2}$ (overflow) but also with $H^{1/2}$ (underflow or a horizontal slit halfway) or a combination of both.

At intermediate flow the characteristics of the total structure are more variable than the one of the control section.

When the head difference increases, a dip is seen in the water level just downstream of the control section. This is related to the recovery of potential energy further downstream. So the head difference over the control section is greater than the global head difference.

Therefore, if the flow opening remains constant, the discharge increases more than proportional with the square root of the head difference. This for instance is observed in Figure 42.

At overflow the flow section decreases with a lower downstream water level and this effect will generally be stronger than the effect of the increased head difference as was mentioned above.

The intermediate flow regime can also show a mixed flow condition at a number of openings, where some of them have modular flow and some submerged flow.

Figure 1 applies to one geometry only: at a structure with a gate such a set of curves should be set up for each gate position. Generally, this is not done but the result is that simplified presentations show scattered data!

Results of computation of losses in free-surface flow at hydraulic structures are less precise than those for internal flow. The number of parameters requires schematizations and often a scale model is used for final calibration.

Computations serve mainly for dimensioning the structure in the pre-design stage. When the structure is meant for discharge metering it has to be specially designed for that purpose (standard design weir), or the structure must have a reference section with a good flow distribution, where the discharge is calibrated with measurements of velocities at different points. With an acoustic discharge meter the flow distribution can be uneven and, depending on the type of equipment, streamlines need not be parallel.

In Section 2 is introduced a computer algorithm which can be used to handle the type of equations for free surface flow in the intermediate flow regime. For free or fully-submerged flow, data can be used which are presented in part II and part I in this manual (measuring weirs and internal flow respectively). Left out are special situations with, for instance, mixed air/water flow, and the transition of roofed culvert parts with submerged and with free flow.

1.2 Discharge relations of hydraulic structures introduced in far-field computations

In one-dimensional far-field computational models (networks), and in two-dimensional tidal and flow models, the discharge relation of structures, dikes, and so on needs to be represented.

Suppose that the type of curves of Figure 1 are determined either from scale-model measurements or from computations. In both cases there is some difficulty in incorporating the results in network or in tidal computation schemes. The nature of the curves is for each upper water level:

If Δh (or ΔH) $> P$, with $P = f(h_0)$ then modular flow: $Q = f_1(h_0)$ (or $f(H_0)$)

If $\Delta h < R$, with $R = f(h_0)$ then submerged flow: $Q = f_2(h_0) \sqrt{2g\Delta h}$

In dynamic networks or tidal computations one prefers to use discharge relations for a barrier or a closure gap, which can be differentiated continuously. Expressions with "if" statements (Boolean variables) are less suitable. The discharge relation can be replaced by an empirical expression approaching reality in a limited range of hydraulic conditions.

The following type of expression might be suitable to represent the complete weir flow-discharge relations (which at their turn are obtained by empiry or by computation) in a versatile way:

$$Q = \left[\frac{1}{\{f_2(h_0) \sqrt{2g\Delta h}\}^n} + \frac{1}{\{f_1(h_0)\}^n} \right]^{-1/n} \quad (3)$$

f_2 is representative for the fully submerged flow condition (where Δh is small) and f_1 for the modular flow.

In this expression f_1 , f_2 and n can still be functions of h_0 or Δh . It can be seen that, for one h_0 value, the left term dominates when Δh is small and the right one dominates when Δh is great, so similar lines as in Figure 1 are obtained.

The power n is introduced to describe the curvature between the modular flow and the submerged flow line in Figure 1.

At gate underflow the intermediate flow does not show a simple sharp transition between the submerged and modular flow regimes, for which a not-too-small n must be chosen, but the relation $Q \approx \sqrt{\Delta H}$ which is valid for the

fully submerged regime, gets steeper in the intermediate flow regime. So a function as

$$Q = \alpha \sqrt{\Delta H} + \beta \Delta H^a + \gamma \Delta H^b \text{ (with } b > a > 0.5)$$

should replace the former relation $Q \approx \sqrt{\Delta h}$. The power n in Equation 3 must be higher than a or b .

In two-dimensional far-field flow calculations the skew overflow over dikes causes a modification in the direction of momentum. This is discussed by Schönfeld [35]. When the dike is supposed to be smooth, the momentum in the direction of the width (say "perpendicular to the flow") does not change. The momentum in flow direction modifies according to what is found for two-dimensional flow. Now the initial upstream velocity (to be used for obtaining the energy head) must only be the velocity component in longitudinal direction of the crest.

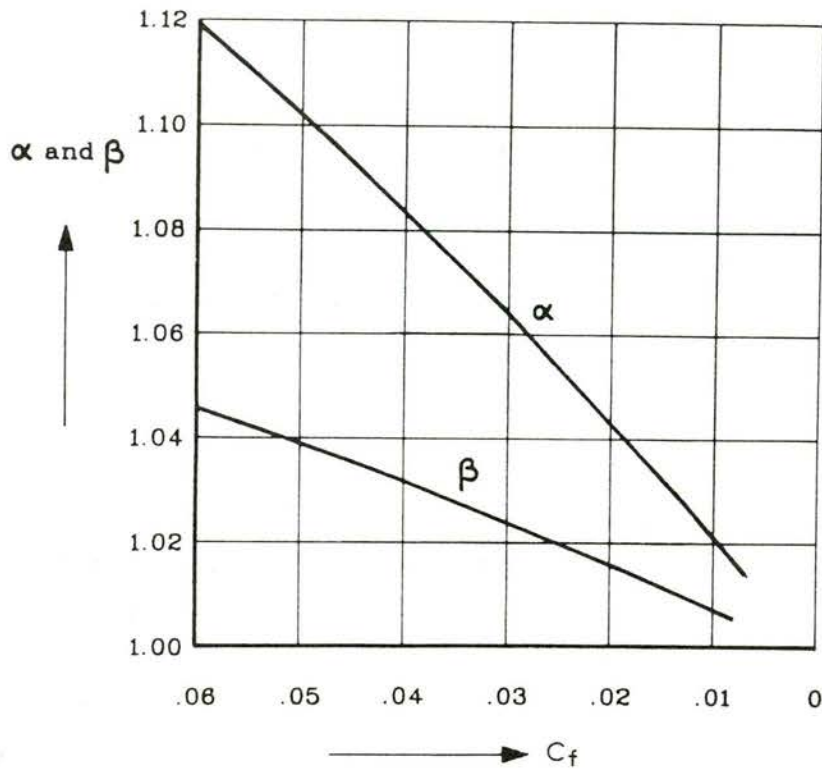
1.3 The use of the Bernoulli-, the momentum- and the Carnot equations

For free-surface flow the Bernoulli- and momentum equations can be applied in the same way as for internal flow. The Bernoulli equation applies only when the flow converges (accelerates).

The momentum equation can be applied when the pressure distribution is known. The momentum equation is then suited to calculate the losses in the zone of decelerating flow. The application of the momentum equation is of great value in all those cases where the flow profile is suddenly widening and where in zone of the separated jet and the eddy on top or underneath reigns a nearly hydrostatic pressure.

As for the momentum equation: for internal flow (pipe flow) it is common to use the Carnot equation at abrupt expansions with cylindrical or rectangular culverts. This equation, which is derived from the momentum equation, is easier to handle than the momentum equation itself. With free-surface flow, however, the Carnot equation only applies at low velocity conditions where the water level is almost straight and parallel to the bottom. Therefore, in general, with currents having free water surface the momentum equation must be applied directly.

Most computations of pressures and losses are based on one-dimensional considerations, where discharge is supposed to be evenly distributed over the flow section.



Bernoulli in 1-d computations

$$h_1 + \alpha_1 \frac{\bar{v}_{A1}^2}{2g} = h_2 + \alpha_2 \frac{\bar{v}_{A2}^2}{2g}$$

$$\alpha = \frac{1}{A} \int \frac{v^3 dA}{\bar{v}_A^3}$$

Momentum eq

$$\Sigma \text{ Force} = \rho Q (\beta_2 \bar{v}_{A2} - \beta_1 \bar{v}_{A1})$$

$$\beta = \frac{1}{A} \int \frac{v^2 dA}{\bar{v}_A^2}$$

definitions:

\bar{v}_A = average velocity over section A

$C_f (\frac{1}{2} \rho \bar{v}_A^2)$ = shear stress

Figure 2 Correction coefficient α and β for a fully developed velocity distribution as function of wall-friction factor; from Naudascher [24]

But when the velocity profile is non-uniform the Bernoulli equation cannot be applied automatically. The transport of energy, proportional to ρV^3 , must be expressed correctly in the energy balance.

A (sometimes necessary) refinement can be obtained when in the Bernoulli equation a factor α is introduced into the $\bar{v}_A^2/2g$ term. The \bar{v}_A now refers to the average velocity over the Section A. The α factor is always greater than 1. A similar procedure is used in the momentum equation (a factor β applies).

In Figure 2 α and β factors and their definitions are presented (from Naudascher [24], but referring to the work of Rouse) for those conditions where the velocity distribution is fully developed and adapted to the wall friction c_f .

In a streamlined flow contraction of short length one should apply $\alpha = \beta = 1$ because the boundary layers have not yet developed and the flow is still evenly distributed.

1.4 Some general remarks before starting the calculation of losses

- A. In general an outlet work or a sluice must be approached as if they were a chain of hydraulic losses. A dominant element is the discharge relation of the control section. This control section is a sill for instance, or an opening or a narrow flow section. First the discharge relation of the control section must be found.
- B. When first the modular flow is considered, then only the extra losses at the upstream canal section play a role, resulting in an additional rise of the upstream level.
- C. There is a maximum downstream level (close to the control section) where the modular flow is not affected. Naturally the corresponding water level farther away depends on losses, change in flow section, and so on. It is important to consider separately the water level just downstream of the structure and the water level farther away where the flow is distributed over the whole flow section.
- D. Discharge-regulating structures are relatively short. The losses due to the inlet, slots, shafts, and so on and, in fact, are therefore not independent of each other. In computation these interactions are neglected, and hence only a limited accuracy of computed results is obtained. The importance of interaction effects at non-modular flow increases when modular flow is nearly reached: diving jets and other phenomena cause deviations from the one-dimensional flow.
- E. For submerged flow or for the intermediate flow regime, first the discharge/water-level relation should also be established for the control section. Then the additional losses up- and downstream must be added. The momentum equation can be applied just downstream of this section, but only for abrupt expansions where sufficient information about the pressure distribution is available. For other configurations (scarcely available) empirical data have to be used.

Complicating factors in the analysis can be points F and G:

- F. There can exist conditions at which it is not clear where with modular flow the control section is located. A flow contraction at a gate recess can suddenly create a control section, and even situations where several critical sections occur are possible. The trash-rack can create such a flow contraction that at that location a control section will be formed resulting in extremely high (and often unexpected) losses.

- G. Near the modular flow condition hysteresis effects can occur; another discharge is found depending on whether a certain downstream water level is reached by raising or by lowering. With an overflow condition starting at a low downstream level the free-falling jet dives and causes a local dip in the downstream water level, which in turn results in sustaining the modular flow condition with a diving jet. However, starting at a high downstream water level the submerged jet does not tend to dive and hence no local dip in the downstream water level occurs.

The size of hydraulic structures is large, so that the influence of the water viscosity (Reynolds number) is negligible. This does not apply for the scale-model results.

1.5 Modular flow equations

Figure 3 shows examples of modular flow conditions and their discharge equations. Approximate atmospheric pressure will reign in the whole flow section of the vena contracta when sufficient side- and/or under-aeration occurs. Reality is somewhat different but in the applied equations an empirical coefficient will incorporate these deviations. Near-hydrostatic pressure occurs in the vena contracta with two-dimensional flow above a horizontal bottom or a long-crested sill.

In the case of the vertical partial slit the conditions of atmospheric pressure and the (assumed) horizontal outflow in the vena contracta lead to the following expression for the discharge relation (see Figure 3 case a)

$$Q = C_c w (2/3)(\sqrt{2g}) \{H_o^3/2 - (H_o - a)^3/2\} \quad (4)$$

and when the slit is elongated till the upstream water level (case b) this equation transforms into

$$Q = C_c w (2/3)(\sqrt{2g}) H_o^3/2 \quad (5)$$

Here the contraction coefficient is introduced as C_c , the slit width as w , the slit height as a , while H_o presents the upstream energy head in relation to the bottom of the slit.

In reality the contraction coefficient has to be replaced by a discharge coefficient C_d now also including the disturbing effects of vertical velocity components of vertical contraction.

For the overflow nappe (Figure 3 case c) which is fully aerated, a similar expression applies but although at the top and bottom atmospheric conditions exist, the pressure inside of Section A-A will deviate, the velocities will vary in direction and the effective flow section is evidently less than the overflow height.

In this case the discharge coefficient C_d , still related to Equation 5, is an empirical one and no relation is derived from an estimated contraction coefficient.

At the broad-crested weir or sill (symbols, see Figure 4b) streamlines are straight and thus there is hydrostatic pressure. Application of the Bernoulli equation for the broad-crested sill results in:

$$q = h_1 \sqrt{2g (H_0 - h_1)} \quad (6a)$$

q gets maximal when $h_1 = 2/3 H_0$, and for modular flow one gets the equation presented in Figure 3d:

$$q_0 = (2/3) H_0 \sqrt{(2gH_0/3)} \quad (6b)$$

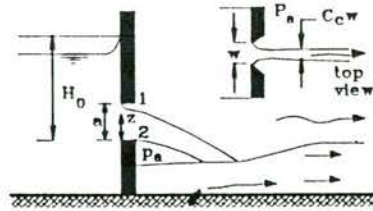
(H_0 is again the upstream energy-head level above the sill level and q_0 the discharge of modular flow per unit width). The critical waterdepth d_c above the sill (being $(2/3) H_0$) is the one where application of the Bernoulli equation (see also Figure 4b) leads to the maximum discharge, which remains when the downstream level is further lowered.

For flow under a gate with a contraction coefficient C_c see Figure 3e) the Bernoulli equation, also based on a hydrostatic pressure distribution, results in a velocity proportional to $\sqrt{2g (H_{upstr} - h_{downstr})}$, giving:

$$q = C_c a \sqrt{2g(H_0 - C_c a)} \quad (7)$$

(here a is the height of the opening under the gate)

P_a = atmospheric pressure

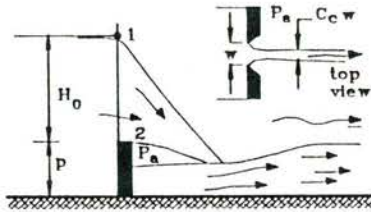


$$Q = C_c w \int_0^a \sqrt{2g(H_0 - z)} dz =$$

$$= C_c w \frac{2}{3} \sqrt{2g} \left[H_0^{3/2} - (H_0 - a)^{3/2} \right]$$

(a) ATMOSPHERIC PRESSURE OVER SECTION 1-2 (VERTICAL PARTIAL SLIT)

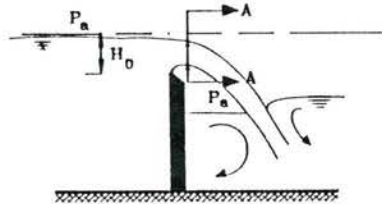
P_a = atmospheric pressure



$$Q = C_c w \frac{2}{3} \sqrt{2g} H_0^{3/2}$$

$$C_c = f(H_0/p)$$

(b) ATMOSPHERIC PRESSURE OVER SECTION 1-2 (vertical slit)

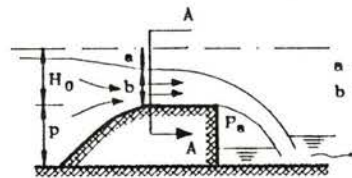


nearly atm. pressure and more or less horizontal velocity in A-A

$$q = C_d \frac{2}{3} \sqrt{2g} H_0^{3/2}$$

(similar to case b)

(c) NEARLY ATMOSPHERIC PRESSURE IN CONTROL SECTION A-A (2 dim.)



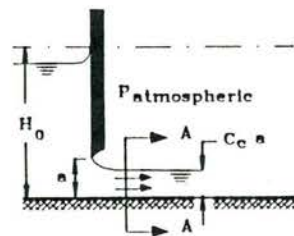
$$a = 1/3 H_0$$

$$b = 2/3 H_0$$

$$q = 2/3 H_0 \sqrt{2g(H_0/3)}$$

(A-A = control section)

(d) HYDROSTATIC PRESSURE IN CONTROL SECTION A-A (2 dim.)



$$q = C_c a \sqrt{2g(H_0 - C_c a)}$$

(e) HYDROSTATIC PRESSURE IN A-A (2 DIM.)

Figure 3 Modular flow conditions with atmospheric pressure and with hydrostatic pressure in the control section

A variant for the discharge relation under the gate can be derived directly from Eq. 7 when instead of the upstream energy level H_0 the upstream water level h_0 is introduced as reference for the upstream condition.

$$q = C_c a \sqrt{2gh_0} / \sqrt{1 + C_c a/h_0} \quad (8)$$

Remark:

This can be proved as follows:

Equation 7 can be written as $q^2 = C_c^2 a^2 2g (h_0 + (q^2/h_0^2 2g) - C_c a)$

or: $q^2 (1 - C_c^2 a^2/h_0^2) = C_c^2 a^2 2g h_0 (1 - C_c a/h_0)$ and after division of both terms by $(1 - C_c a/h_0)$ and taking the square root Equation 8 is obtained.

It is important to establish the maximum water level downstream of the control section for which no reduction of flow occurs. This downstream water level is different for the case that at modular flow the control section has a hydrostatic pressure distribution or that there is atmospheric pressure over the whole section:

- at atmospheric pressure any pressure higher than atmospheric pressure reduces the discharge, therefore any water level above the crest or the bottom has an effect.
- at hydrostatic pressure a downstream water level lower than the one at the control section, has no effect on the discharge, so in the case of Eq. 6 a downstream water level just downstream of the control section lower than $2/3 H_0$, gives no discharge reduction.

1.6 Fully submerged flow

The "fully submerged" flow regime as it is indicated in Figure 1 is related to the limit case of a (nearly) horizontal water level and very low velocities (low Froude number). Because the flow boundaries are now fully defined, the data of internal flow losses can be used when these are available for similar geometries. The plane water level can be seen as a flow boundary or as a line of symmetry of a mirrored situation, so still more comparable situations might be found.

The losses at internal flow are expressed in terms of

$$\Delta H = \xi V^2/2g \quad (9)$$

and this also applies for the fully submerged flow. The influence of ΔH on the losses ξ is negligible now. The total loss ξ is built up by a series of local losses (inlet, gate, outlet, friction). The final result can now be transformed as follows:

$$\Delta H_{\text{tot}} = \Delta H_{\text{inlet}} + \Delta H_{\text{gate}} + \Delta H_{\text{friction}} + \Delta H_{\text{outlet}} \text{ etc.} \quad (9a)$$

$$\Delta H_{\text{tot}} = \frac{V^2}{2g} (\xi_{\text{inlet}} + \xi_{\text{gate}} + \xi_{\text{friction}} + \xi_{\text{outlet}} \text{ etc.}) \quad (9b)$$

$$V = \xi^{-0.5} \sqrt{2g\Delta H} \quad (9c)$$

$$Q = C_d A \sqrt{2g\Delta H} \quad (9d)$$

At overflow the flow section A varies with the water level. Due to a variation in flow geometry ξ and C_d do not remain fully constant either.

The friction losses are calculated in a similar way as found for internal flow. The Moody diagram, as is commonly used for internal flow in circular pipes, can be used but the "hydraulic diameter" D_h in this diagram has to be replaced by the hydraulic radius R_h which is defined as the sectional area divided by the wetted perimeter.

For a pipe with circular section this gives:

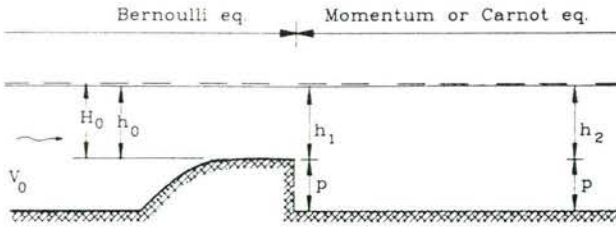
$$R_h = D/4 \quad (10)$$

A problem with the calculation of the friction is that the structure is not always long enough for getting the fully developed flow distribution, hence friction can be smaller or larger.

At weir flow, starting with fully submerged flow and gradually lowering of the downstream water level, the intermediate flow condition starts already at relatively small head differences. This is observed especially at weir flow (Figure 4b) where the flow section, being the water depth h_1 over the crest, varies with the downstream head h_2 . As has been indicated before, this condition is mentioned "submerged flow" (in contrast to modular flow and also in contrast to fully submerged flow where the water level is approximately horizontal).

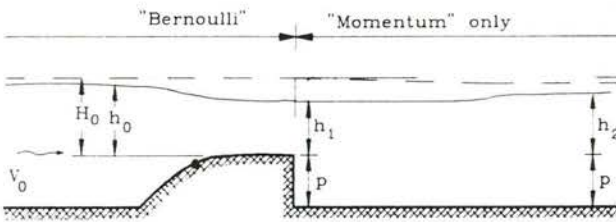
An example of the loss coefficient of a sill in the fully submerged condition is shown in Figure 4a. The water level being nearly horizontal and the downstream face being vertical, the pressure distribution is a hydrostatic one and thus the momentum equation can be applied. But because of the water level being nearly horizontal also the Carnot equation can be applied and this lead to an analytical expression for the discharge q as function of h_0 and ΔH . This can also be done for flow under a gate, Figure 4c.

The calculation for the losses is for the submerged condition, although here the flow section varies with the downstream water level, quite similarly as for the fully submerged condition.



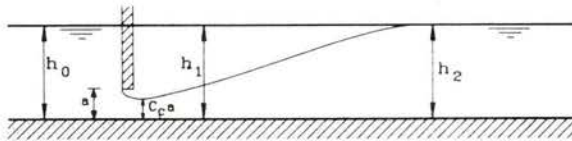
(a) FULLY-SUBMERGED FLOW REGIME (small ΔH)

$\Delta H = \text{loss of energy head}$
 $h_2 \approx h_0$ and $h_1 \approx h_0$
 $2g \Delta H = \left\{ \frac{q}{h_1} - \frac{q}{(h_2+p)} \right\}^2$ (Carnot)
 $q = h_0 \sqrt{2g H (h_0+p) / p}$



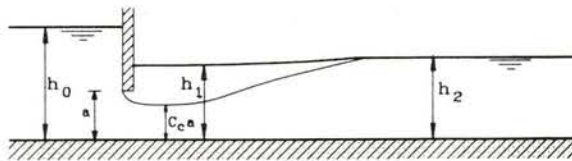
(b) INTERMEDIATE FLOW REGIME

ΔH Bernoulli equation:
 $h_0 + \alpha_0 q^2 / (h_0+p)^2 2g = h_1 + \alpha_1 q^2 / h_1^2 2g$
 $(\alpha_1 \approx 1)$
 Momentum equation:
 $\frac{1}{2} \rho g (h_1+p)^2 + \beta_1 \rho q^2 / h_1 = \frac{1}{2} \rho g (h_2+p)^2 + \beta_2 \rho q^2 / (h_2+p)$
 $(\beta_1 \approx 1)$



(c) FULLY-SUBMERGED FLOW REGIME

$h_1 \approx h_0$ and $h_2 \approx h_0$
 $2g \Delta H = \left\{ \frac{q}{c_c a} - \frac{q}{h_2} \right\}^2$ (Carnot)
 $q = c_c a \sqrt{2g \Delta H / (1 - c_c a / h_0)}$



(d) INTERMEDIATE FLOW REGIME

Bernoulli equation:
 $h_0 + \alpha_0 q^2 / h_0^2 2g = h_1 + \alpha_1 q^2 / c_c a^2 2g$
 $(\alpha_1 \approx 1)$
 Momentum equation:
 $\frac{1}{2} \rho g h_1^2 + \beta_1 \rho q^2 / c_c a = \frac{1}{2} \rho g h_2^2 + \beta_2 \rho q^2 / h_2$

Figure 4 Long-crested weir and gate flow under fully submerged condition and in the intermediate flow regime

1.7 The intermediate-flow relations at control sections

In the intermediate-flow conditions direct application of the Bernoulli equation (from h_0 to h_1) and the momentum equation (from h_1 to h_2) leads to a feasible result for the flow over a long sill (Figure 4b) and for flow under a gate (Figure 4d). But a discharge relation like Equation 1 cannot be found directly. Starting with h_0 , q and h_1 , the h_2 can be found through an iterative search or by solving a third-order equation. With the intermediate flow regime there are certain cases where mixed-flow can be assumed. A part of the discharge is related to free flow and a part to submerged flow. These cases are illustrated in Figure 5. When using these mixed flow equations with constant C_c coefficients results may not be very accurate but certainly useful for a first estimate of the discharge. The procedure is fairly evident for the case of a half submerged narrow vertical slit, where the horizontal flow contraction will not vary strongly and where one can clearly distinguish a free-flow part and a submerged part. At a nappe or at flow through a horizontal slit the pressure in the control section is also nearly atmospheric but the (vertical) flow contraction is more variable.

A usual way of expressing the weir flow discharge in the intermediate flow regime is to start with the modular flow discharge Q_0 and then apply a reduction factor C_S which is a function of the dimensionless submergence factor S .

$$S = h_2/h_0 \text{ or } h_2/H_0 \quad (11)$$

$$Q = C_S Q_0 \quad (12)$$

where Q_0 is the discharge at modular flow.

$$Q_0 = f(H_0) \quad (13)$$

By introducing a number of simplifications the reduction factor C_S due to submergence can be expressed analytically for both a short-crested and a long-crested weir.

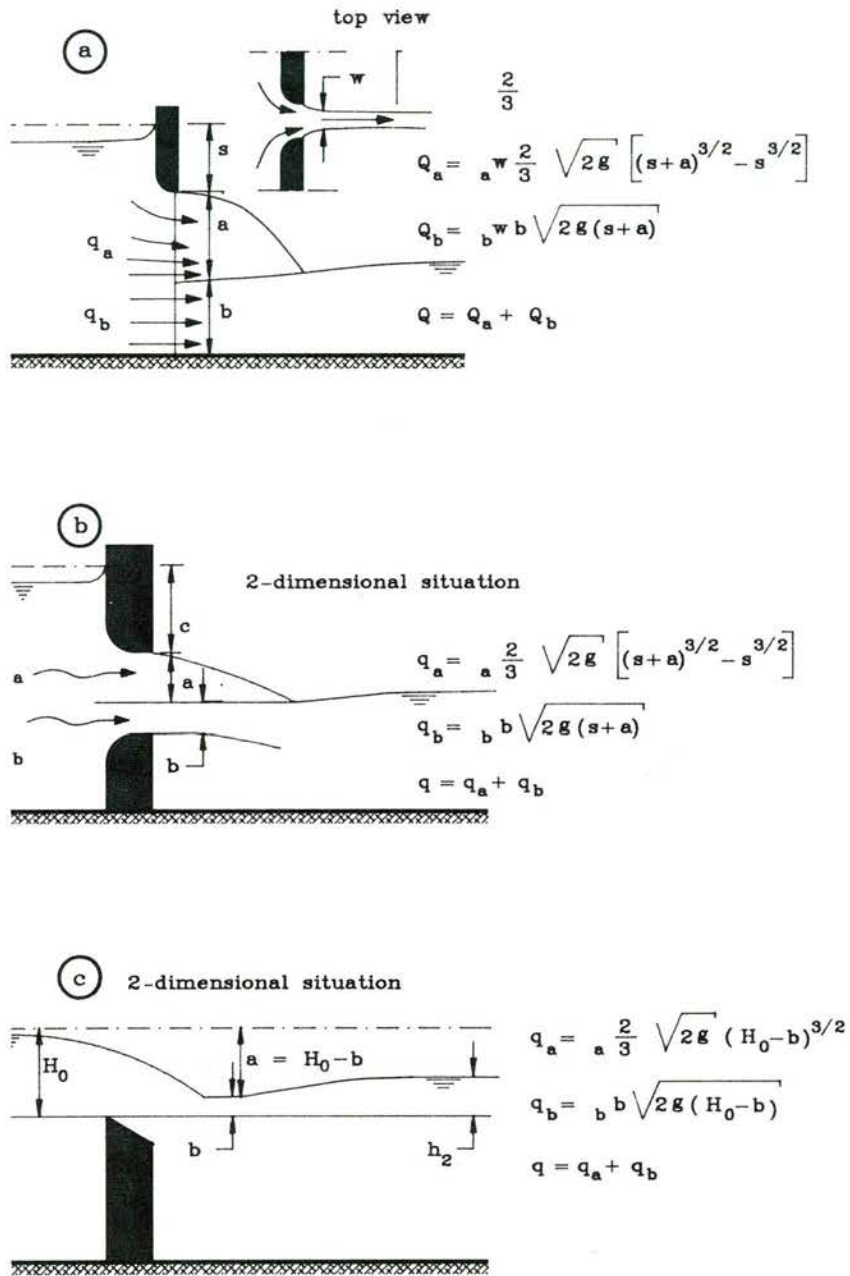


Figure 5 Vertical slit and horizontal nappe with mixed flow conditions

A: Short-crested weir (Figure 5c):

q_0 is found from the equation shown in the figure when $b = 0$ is introduced:

$$q_0 = C_d (2/3) (\sqrt{2g}) H_0^{3/2} \quad (14)$$

Then we introduce for the fully submerged condition $b = h_2$ (this is only true when the sill is relatively high) and we assume for the discharge coefficients $C_{d_a} = C_{d_b} = C_d$

The height b in Figure 5c can be expressed as $H_0 S$, and the discharge relation of Figure 5c becomes:

$$q = q_a + q_b = C_d (2/3) (\sqrt{2g}) (1-S)^{3/2} H_0^{3/2} + C_d S H_0 \sqrt{2g} H_0 (1-S)$$

So:

$$C_S = q/q_0 = (1-S)^{3/2} + (3/2) S \sqrt{1-S}$$

or:

$$C_S = (1 + \frac{1}{2}S) \sqrt{(1-S)} \quad (15)$$

This analytical expression was compared by Abou Seida and Quarashi [2] with experiments, see Figure 6.

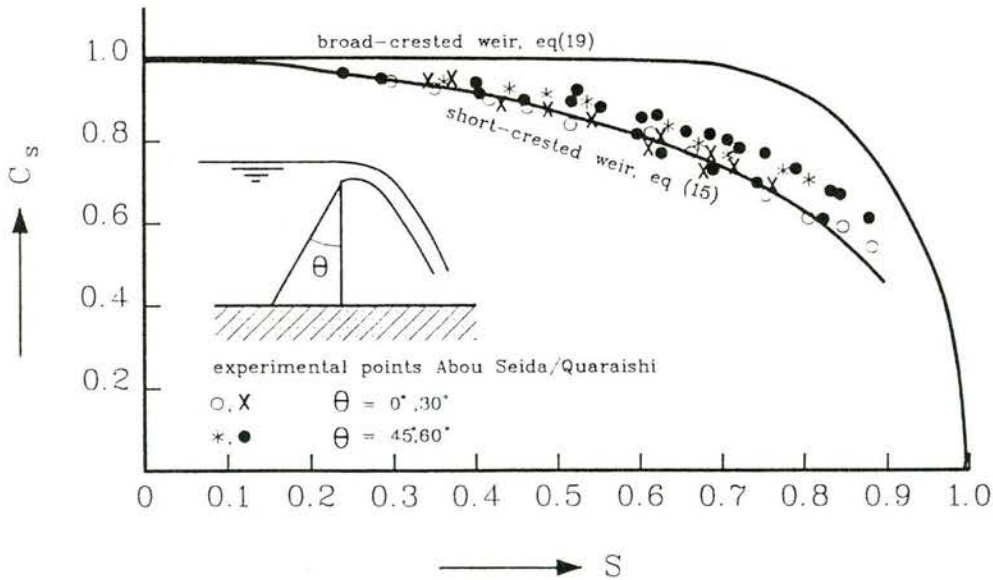


Figure 6 Discharge reduction by submergence

B: Broad-crested weir

Equation 6 was:

$$q_0 = (2/3) H_0 (\sqrt{2g H_0/3}) \quad (16)$$

When the weir height p is large compared to the overflow depth, then in the situation of Figure 4b the water level above the crest gets equal to the downstream water level. "Bernoulli" then results in:

$$q = h_2 \sqrt{2g (H_0 - h_2)}$$

and, introducing $S = h_2/H_0 \approx h_2/H_0$ one obtains:

$$q = S H_0 \sqrt{2g H_0 (1-S)} \quad (17)$$

$$(17) \text{ holds for } S > 2/3, \text{ otherwise } q = q_0 \quad (18)$$

This results in:

$$C_S = 1 \text{ for } S < 2/3 \text{ and}$$

$$C_S = (3/2) S \sqrt{3 (1-S)} \text{ for } 2/3 < S < 1 \quad (19)$$

Figure 6 shows the verification of Equation 15 with experiments on the sharp-crested weir in vertical and in 30° inclined position, and with a triangular sloping filling block at the upstream face on 45° and 60° (from Abou-Seida and Quaraishi [2]).

Again, the above relations for the control section must be extended to the water level further upstream and downstream for obtaining the discharge relation for the whole structure. The extra losses upstream will not cause problems but for calculation of the water level further downstream where the flow diverges, one could try to apply the momentum equation. However, when the downstream canal has diverging walls or when there is a sloping bottom, not all the forces which need be introduced are known; this in contrast to the sill with vertical back wall. What might be feasible, but this is not sufficiently verified, is that the rise in water level (by recovery of potential energy) with a certain slope (estimated to be somewhere in between 1:5 and 1:7) is used to introduce an extra horizontal

force in the momentum equation. Assuming a hydrostatic pressure distribution, the longitudinal force component acting at the diverging walls or sloping bottom can then be calculated; this force indeed gives a reduction in energy head losses at diverging walls. This procedure has originally been suggested by Kooman [21].

It can be seen that the calculations in the intermediate flow regime do not contain new elements, but computations should be done carefully. The steps or slopes in the water level do change the flow geometry so that the losses cannot be found so easily from literature data. The proposed computer program of Chapter 2 is suitable to handle the trial-and-error procedure which is related to the water-level computations in the intermediate flow regime.

1.8 Remarks about entrance losses

At the entrance of a sluice or a culvert the pressure lowers due to the velocity head $V_c^2/2g$ (wherein V_c is the culvert velocity). However, there is the "normal" flow convergence which depends only on the culvert section, and there is an extra contraction which depends on the mouth shape. The extra contraction will disappear further downstream but the result is an extra loss (similar to Carnot losses at a suddenly widened flow section).

Per definition:

$$H_0 = H_c + \xi_e (V_c^2/2g) \quad (20)$$

or

$$h_0 + V_0^2/2g = h_c + (1 + \xi_e) V_c^2/2g \quad (21)$$

h_0 and H_0 are pressure head, respectively energy head upstream from the culvert, and h_c and H_c are related to the ones in the culvert $V_c =$ culvert velocity.

ξ_e is determined from pressure and discharge measurements.

$$\xi_e = \{(h_0 + V_0^2/2g - h_c)/(V_c^2/2g)\} - 1 \quad (22)$$

In general it is assumed that the velocities are evenly distributed over the culvert section.

However, it has been discussed in section 1.3 that in reality an α factor should be introduced to take into account the uneven velocity distribution (Figure 2). Because inlet losses of nicely shaped mouths are small (in the order of 0.15 to 0.3 in prototype and still smaller in model, see section 4.1) a few percent greater $(V_c^2/2g)$ will also result in a in reality smaller ξ_e value (a few time 0.01 less).

In the total analysis of a structure the neglect of α is generally not important, because at the outlet the extra kinetic energy which initially is neglected is lost anyhow.

In par 4.1 the relation between the flow contraction coefficient C_c and the entrance loss ξ_e is discussed.

In a closed culvert or at lower water velocities the condition is comparable with a condition with a sudden flow expansion and hence "Carnot" can be applied to the entrance losses.

Using the symbols of Figure 7,

$$\Delta H = (V_m - V_c)^2 / 2g = (C_c^{-1} - 1)^2 V_c^2 / 2g$$

and hence

$$\xi_e = (C_c^{-1} - 1)^2 \quad (23)$$

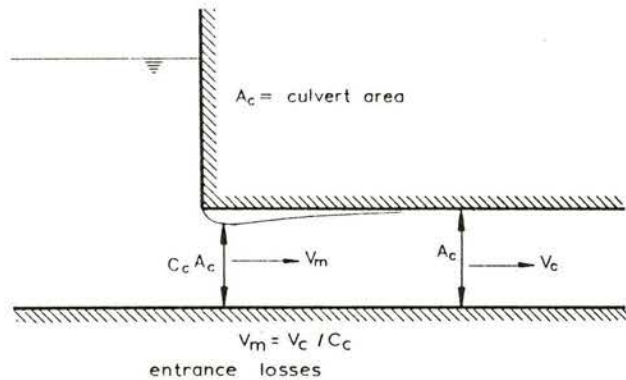


Figure 7 Entrance conditions.

C_c varies from about 0.55 (at a an all-sided sharp-edged entrance) till about 0.85 for an elliptically shaped entrance, which should result in ξ_e values from 0.03 to 0.67. The low values, however, are never reached in reality (see Figure 65).

1.9 Remarks about trash-rack and bridge-pier losses

Data about trash-racks found in literature refer to one-dimensional flow without influence of the free water surface. But these data can also be applied at lower water velocities with a nearly horizontal water level at free surface flow. In other conditions these data give losses which are too small. Even modular flow can occur in the flow contraction.

This is the reason why bridge-pier data are also related to the Froude number V/\sqrt{gd} , where V is related to velocity and d to water depth of the undisturbed condition.

There is a direct relation between the losses of trash-racks and the hydrodynamic forces exerted on the bars. This relation follows from the application of the momentum equation. When the rack is fully submerged then the inflow momentum equals the outflow momentum and the momentum equation results in:

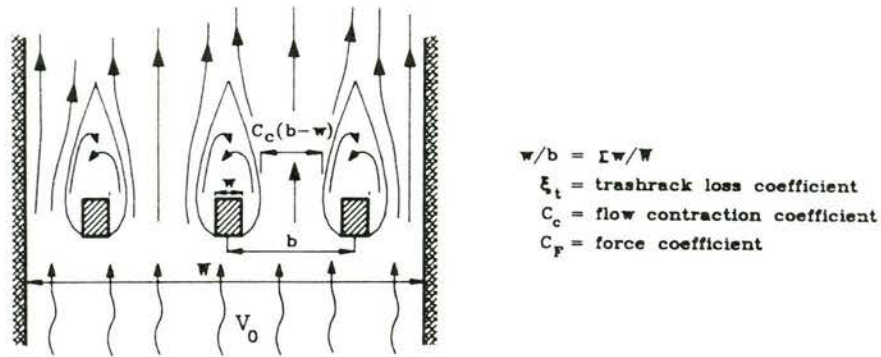
$$\rho g \Delta H = \text{rack resistance force per unit area of the culvert} \quad (24)$$

(ΔH = loss of energy head, ρ = fluid density)

and when free surface flow is involved one can derive from the momentum equation per unit width:

$$\frac{1}{2}\rho g h_1^2 + \rho q V_1 = \text{Force} + \frac{1}{2}\rho g h_2^2 + \rho q V_2 \quad (25)$$

There are three types of approach to establish the trash-rack losses (see Figure 8):



$$A: \Delta H = \left(\frac{V_0^2}{2g} \right) \left(\frac{W}{C_c(W - \Gamma w)} - 1 \right)^2 \text{ (Carnot)}$$

$$B: \text{force (per meter}^2) = C_F (\Gamma w / W) \frac{1}{2} \rho V_0^2 = \rho g \Delta H$$

with $C_F = f$ (bar-shape, and $\Gamma w / W$)

$$C: \Delta H = \xi_t V_0^2 / 2g \quad \text{with } \xi_t = f \text{ (bar-shape, and } \Gamma w / W)$$

Figure 8 Flow conditions at trash-rack and different types of approach for calculation of losses

- A. Estimation of the flow contraction and establishment of the losses by applying the momentum equation. The assumption is that in the whole flow-contraction section an equal pressure exists. (For small blockage ratios this does not need to be true!) Without any influence of the free surface (in a culvert or at a horizontal free water surface) the Carnot equation can be applied.
- B. Estimating the drag coefficient of the bars and transferring the total force into a hydraulic loss.
- C. Using direct data of trashrack tests where losses are presented as function of shape and density of the bars.

Mostly the third method is used, but it is advisable to apply also method A so as to regard the consequences of extra blockage by trash and for checking the possible effect of the modular or intermediate flow regimes.

1.10 Required and obtainable accuracies

In ISO 1438, included in the ISO handbook [18] are discussed the accuracies of discharge relations in prototype; the accuracy of hydraulic models are discussed by Kolkman [20]. One of the conclusions is that accuracy considerations must be set up separately for each specific case. The possibility of systematic errors and scatter in model results must be considered both. The definition of error can be related to the actual discharge or to the maximum discharge.

Even when a scale-model investigation is considered, in the pre-design stage it is important that a good estimate can already be made about the discharge capacity of the structure. For this case it is important to know how much one can rely upon data from literature.

The necessary accuracy is at the pre-design stage, say 5 to 15%; this percentage is related to other inaccuracies of the design input (water level, the once-in-a-hundred-years river discharge, etc.), and to construction costs when for instance too-large gated openings are designed.

Especially in the United States a large number of investigations have been carried out to establish systematic design data of free (modular) flow constructions.

For these modular flow conditions it is certainly possible to obtain an accuracy in discharge between 3 and 8% of the actual discharge. For discharge sluices in tidal areas the intermediate flow regime occurs frequently and here the accuracy of estimated losses is less (up to 20% errors is the experience).

There are structures with a diffusor-shaped outlet resulting in a high discharge capacity, but systematic data for the functioning of such diffusors at free surface flow are missing.

When using the structure for water-discharge control the required accuracy will be within 3 to 10% of the actual discharge. If a greater accuracy is required than 10 to 15%, a specific scale-model study should be set up and/or a separate discharge meter has to be installed.

In certain cases the structure can be calibrated with the use of propeller velocity meters, acoustic flow meters or with tracer methods. In these circumstances the obtainable accuracy is variable and depends largely on the measuring section, the accessibility, the number of measuring points, the flow distribution and flow direction, turbulence and so on. When there

is a straight canal or culvert in the structure an accuracy of 2% to 5% can be reached. Again, a discussion about accuracy of measurements is found in the ISO handbook [18].

When a high accuracy is required in discharge metering with the structure, the design must be modified to that purpose. A scale-model investigation must include an extended up- and downstream basin, the water levels must be measured at points corresponding to the location in prototype, the scale must be adequately chosen in relation to the wanted accuracy and a correction procedure should be used to compensate for scale effects due to friction. Structures with trash-racks need special research procedures. In general a structure with a trash-rack is not well-suited for discharge metering.

In the presentation of discharge coefficients following here, the influence of the Reynolds' number (viscosity effects) is not included. For the prototype structures this is of minor importance, and hence in the pre-design of the structure it does not play any role. For the choice of the scale factor in hydraulic modelling and for the interpretation of scale-model results specialized knowledge is needed; this is beyond the scope of this manual.

2. NUMERICAL PROCEDURE FOR COMPUTATION OF WATER LEVEL/DISCHARGE RELATIONS

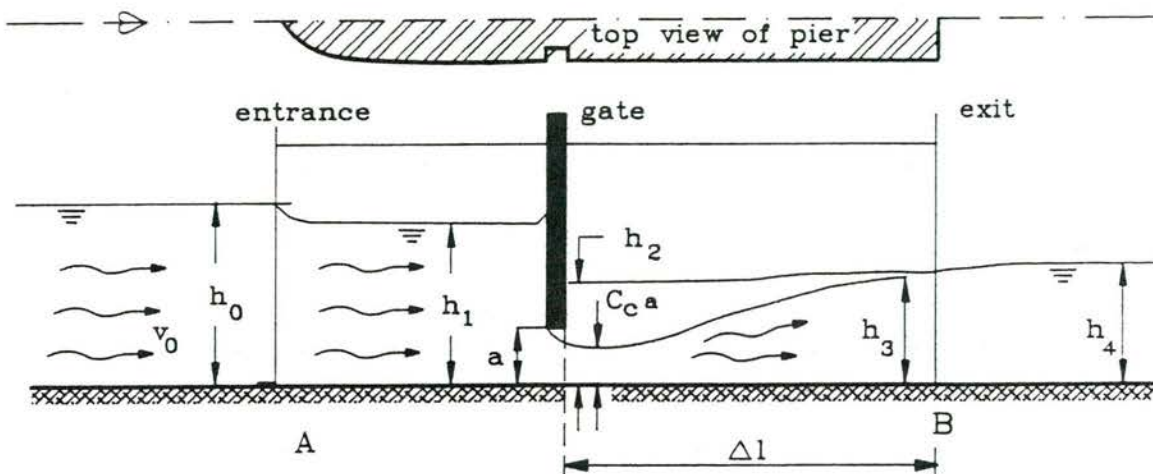
2.1 Introduction

Figure 9 Water levels in a discharge sluice

In Figure 9 a sluice with free-surface flow is schematized throughout as a chain of discontinuities for each of which an equation can be set up relating water levels and discharge. In this schematisation no interactions between the sections are introduced.

A is the inlet of the sluice. Sluice width is introduced as w . The inlet loss coefficient is ξ_1 . The relation between h_0 , h_1 and Q can be written as:

$$h_0 + \alpha_0 (Q/w_0 h_0)^2 / 2g = h_1 + \alpha_1 (1 + \xi_1) (Q/w h_1)^2 / 2g \quad (26)$$

(w_0 is the width upstream of the sluice, w is the sluice width and ξ_1 is the entrance loss coefficient).

When the flow is supposed to be evenly distributed over the flow sections the gate-discharge relation becomes:

$$h_1 + (Q/h_1 w)^2 / 2g = h_2 + (Q/C_c a w)^2 / 2g \quad (27)$$

Here C_c is the flow contraction coefficient in opening a .

When the computation starts from upstream, there is a certain Q which cannot pass at the upstream water level which was introduced; one can now for instance by trial and error find the modular flow discharge (h_2 cannot be smaller than the contracted jet $C_c a$).

The gate loss is produced in the deceleration zone of the flow further downstream of the gate. This loss can be computed using the momentum equation, provided that Δl (in Figure 9) is sufficiently large:

$$\rho g w (0.5 h_2^2) + \rho Q^2 / (C_c a w) = \rho g w (0.5 h_3^2) + \rho Q^2 / (h_3 w) \quad (28)$$

The exit loss at B (a sudden widening) can also be determined with the momentum equation, assuming that the water level in the basin near the sluice is related to the water level h_3 , as follows:

$$\rho g w (0.5 h_3^2) + \rho Q^2 / (h_3 w) = \rho g w (0.5 h_4^2) + \rho Q^2 / (h_4 w) \quad (29)$$

At a gradual widening an empirical relation between h_3 , h_4 and Q has to be introduced.

When a hydraulic jump downstream of the gate is involved one obtains:

$$\rho g w \{0.5 (C_c a)^2\} + \rho Q^2 / w C_c a = \rho g w (0.5 h_3^2) + \rho Q^2 / (w h_3) \quad (30)$$

When refined calculations are needed, one can still introduce the α and β factors of Figure 1.3, the friction of the culvert walls, a varying C_c value of the gate opening, depending on gate position, and on the water level h_1 . All these equations are coupled. It is common to solve each equation separately, and the "next" water level (more up- or more downstream) is found, mostly by trial and error, from the calculated energy level.

Using a computer one can now solve these equations in a standardized way. For each of the formulas we index the water level of the left-hand section as h_1 and at the right hand as h_2 . In the case of a hydraulic jump computation downstream of a gate, we define $C_c a$ as being h_1 for instance.

Each of the formula which were discussed before can be written as follows:

$$f(h_1, h_2, Q) = 0 \quad (31)$$

Starting the calculations from upstream with a given h_0 and Q , the given water level h_0 serves as the h_1 of Eq. 31. When also the Q is introduced then Equation 31 can be written as

$$f(h_2) = 0 \quad (32)$$

For the search for this h_2 standard procedures are available. In section 2.2 a procedure will be presented, written for the ACORN-BBC or the Archimedes computer.

When Eq. 32 is solved for h_2 , this is the h_1 to be introduced in the second formula, and then the next h_2 can be found.

The iterative procedure for the determination of the modular flow conditions is relatively easy as well; when the discharge is too high in combination with the chosen upper-water level, then no value of h_2 is found. Hence the modular discharge is the maximum discharge which still can pass.

But a direct way of computation is to set up the equation for modular flow at the control section and do the same type of calculation in the upstream direction. Downstream of the control section one proceeds in the normal way.

In the search procedure for h_2 one has to define the h_2 range where the search takes place. One limit of this range can be $h_{2\min}$ near zero (not exactly zero because then certain terms of the equations tend to infinity). The $h_{2\max}$ can just be an arbitrarily large value of h_2 . Not an extremely large value, because then the search steps generally get large as well, and two solutions (critical flow and supercritical flow) can be surpassed in one step.

When one wants to find the subcritical flow, then the search for h_2 has to start at $h_{2\max}$ and one goes downward; for the supercritical flow it is the other way around, that is working upward from $h_{2\min}$.

2.2 The search procedure

Equation (32) is transformed into

$$f(h_2) = Z \quad (33)$$

in which Z has to become about zero, with a wanted accuracy of ϵ .

A simple but fool-proof procedure would be stepping through the h_2 range with steps Δh , thus obtaining Z_1 , Z_2 and so on.

When

$$(Z_{n-1}) Z_n \leq 0 \quad (34)$$

the search is stopped, and the procedure starts again with h_{n-1} and h_n as new limits of the search range. The Δh steps must be small enough for the first search, because near the critical waterdepth the two solutions (sub- and supercritical are near to each other). The simplest procedure is to stop the iteration when:

$$f\left(\frac{h_{n-1} + h_n}{2}\right) < \epsilon \quad (35)$$

The wanted h_2 value is then

$$h_2 = \frac{h_{n-1} + h_n}{2} \quad (36)$$

In the appendix to this chapter a much faster procedure is used, based upon the Newton-Raphson method^{*}). At an arbitrary begin-value of h_2 the derivative is computed

$$dZ/dh_2 = \Delta Z/\Delta h_2 \quad (37)$$

(Δh_2 has been chosen as 1/2000 for the h_2 search interval)

When from this begin-value of h_2 , with its corresponding Z value the tangent line is considered, the $Z = 0$ corresponds with a new h_2 value.

* At a suggestion from H.K.T. Kuijper, Delft University of Technology.

It is checked whether

$$|Z = f(h_{2\text{-new}})| < \text{wanted accuracy}$$

When $|Z|$ is still too large, $h_{2\text{-new}}$ replaces the value of h_2 and the procedure is repeated.

This procedure is incorporated in a new-defined function, FNfast-implicit' with the following variables:

M = the number out of a series of self-defined functions of the type

$$f(h_1, h_2, Q) = 0 \text{ (like Eq. 31).}$$

h_1 (defined as in Eq. 31).

Begin- h_2 End- h_2	these values determine the search range of h_2
----------------------------	--

Q (discharge, see Eq. 31)

This procedure is fully adequate to solve h_2 from the Bernoulli or the momentum equation, but when using other types of equations, this procedure can evoke problems.

APPENDIX of CHAPTER 2 page 1

With the ACORN-BBC computer the following function "FNfast_implicit" has been developed which produces the waterlevel h2 when one introduces the discharge Q, the waterlevel h1 and the self-defined relation $F(h1, h2, Q) = 0$. The h2 value is found when the function is called for in the following way:

$$h2 = \text{FNfast_implicit}(M, h1, \text{begin_h2}, \text{end_h2}, Q)$$

The number M is the number of a series of self-defined functions which is referred to. The begin_h2 and end_h2 values define the range in which h2 has to be found. With a low value of begin_h2 the supercritical solution is found and with a high value the subcritical one.

As an example the sequent depth of a hydraulic jump is produced.

The momentum equation is as follows:

$$.5 \cdot \rho \cdot g \cdot (h1^2) + \rho \cdot (q^2) / h1 = .5 \cdot \rho \cdot g \cdot (h2^2) + \rho \cdot (q^2) / h2$$

This equation is transformed, putting all terms in the left hand:

$$.5 \cdot \rho \cdot g \cdot (h1^2) + \rho \cdot (q^2) / h1 - .5 \cdot \rho \cdot g \cdot (h2^2) - \rho \cdot (q^2) / h2 = Z$$

and Z has to be zero!

The input in the form of a program is as follows:

```
REMEMBER program starts here.
PRINT "OUTPRINT"
h1=1: q=15: g=9.81: rho=1000
begin_h2=40: REM this means that the subcritical solution is found.
end_h2= .01: REM the small begin_h2 or end_h2 should be greater than zero
M=1: REM this means that the first self-defined function is used.
h2= FNfast_implicit(M, h1, begin_h2, end_h2, q)
PRINT "begin_h2= "; begin_h2; " end_h2= "; end_h2; " h2= "; h2
END
```

REMARK in the following function the momentum equation is represented.

```
DEFN selfdefined_1(h1,h2,q)
Z= .5*rho*g*(h1^2)+ rho*(q^2)/h1- .5*rho*g*(h2^2)- rho*(q^2)/h2
=Z
```

```
OUTPRINT
begin_h2= 40 end_h2= 1E-2 h2= 6.29128557
```

```
,
Other begin and end values of h2 result in:
,
```

```
OUTPRINT
begin_h2= 1E-2 end_h2= 40 h2= 0.999999999
```

```
OUTPRINT
begin_h2= 10 end_h2= 40 h2= -99.99
```

Appendix of Chapter 2: Iterative search procedure for h_2 using the ACORN-BBC computer.

Appendix of Chapter 2: Iterative search procedure for h_2 using the ACORN-BBC computer.

APPENDIX of CHAPTER 2 page 2

REMARK the following contains the essential additional functions

```

DEF FNfast_implicit(M%,h1,begin_h2,end_h2,0):REM*****
REM h2 has to be found
LOCAL endh2, beginh2, wanted_precision, precision, steph2, P%, beginZ, endZ
LOCAL tangent_alpha, former_tangent_alpha
endh2= end_h2: beginh2= begin_h2
wanted_precision=ABS((end_h2-begin_h2)/5000)
P%=0: out_of_range=FALSE: stop=FALSE
REPEAT
  P%=P%+1
  steph2=(endh2-beginh2)/2000
  endh2= beginh2+steph2
  h2=beginh2: beginZ=FNadditional(M%,h1,h2,0)
  h2= endh2: endZ=FNadditional(M%,h1,h2,0)
  IF P%>=2 THEN former_tangent_alpha= tangent_alpha
  tangent_alpha=(endZ-beginZ)/(endh2- beginh2)
  IF tangent_alpha <>0 THEN trial_h2= beginh2- (beginZ/tangent_alpha)
  IF P%>=2 AND tangent_alpha*former_tangent_alpha<=0 THEN out_of_range=TRUE
  IF (trial_h2-begin_h2)/(end_h2-begin_h2)<0 THEN out_of_range=TRUE
  IF (trial_h2-begin_h2)/(end_h2-begin_h2)>1 THEN out_of_range=TRUE
  endh2=beginh2: beginh2= trial_h2
  h2= trial_h2: Z= FNadditional(M%,h1,h2,0): precision=ABS(Z)
  IF precision <= wanted_precision OR out_of_range THEN stop= TRUE
UNTIL stop
IF out_of_range THEN result=-99.99 ELSE result =trial_h2
= result:*****

DEF FNadditional(M%,h1,h2,0): LOCAL Z
IF M%=1 THEN Z= FNselfdefined_1(h1,h2,0)
IF M%=2 THEN Z= FNselfdefined_2(h1,h2,0)
IF M%=3 THEN Z= FNselfdefined_3(h1,h2,0)
=Z: REMARK indicates that Z is the output of the selfdefined function.

```

Appendix of Chapter 2; (continued).

3. DISCHARGE RELATIONS FOR CONTROL SECTIONS

Remark:

As noted before h is used for the water level and H for the energy head. When only the upstream water level is involved then h and H refer to the upstream conditions. Otherwise index 0 refers to the conditions upstream of the control section, 1 to the conditions in or just downstream, 2 to the condition further downstream. In U.S. reference like [38], [40] and [43], H_e (the real or the effective energy head) is used in contrast to the design head H_d which is a reference size whereupon the shape of a nappe-shaped crest is based.

3.1 The sharp-crested weir

Discharge relations for modular flow and the submerged flow are discussed separately.

A. Modular flow

Still in use and best-known is the weir-formula developed, and extensively tested between 1925 and 1930 by Rehbock [30], at the of the Karlsruhe University. The sharp-crested full-width weir has since then also been widely applied as a measuring weir in laboratories. In Figure 10 a section of the weir is presented. When installed precisely, obtainable accuracies are within 1% [18]. The weir is sensitive to roughness of the upstream face and at an imprecise installation 5 to 7% inaccuracies can occur (according to Bos [7]). Therefore its application as a discharge measurement structure in the field is less suitable.

The formula is based on a two-dimensional flow pattern and presents as:

$$Q = w (1.78 + 0.24 * h/p) (h + 1.1 \cdot 10^{-3})^{3/2} \quad (39)$$

The equation is not dimensionless, and the dimensions of the parameters are: discharge Q is in m^3/s , the width w , the weir height p , and h are all in metres; h is the upstream water level above the crest.

The flume width upstream of the weir equals the weir width w .

The correction of 1.1 mm in h caused some problems when it was tried to transform Equation 39 into a dimensionless form. It certainly contains a mixture of viscosity and surface-tension effects.

For a measuring weir the crest shape has, according to ISO [18], to be designed as indicated in Figure 10.

Special care is required for the upstream face to be vertical and smooth, and to get a complete aeration under the nappe.

Sarginson [34] proposed to replace the value 1.1 mm by a factor representing the influence of the surface tension (σ) by the Weber number. He defined this number We as:

$$We = \rho g h^2 / \sigma \quad (40)$$

After analyzing theoretically the possible effect of surface tension, he proposes the following discharge formula:

$$Q = w(1.81 + 0.22 h/p + 4.22/We) h^{1.5} \quad (41)$$

Also this expression is not dimensionless.

The expression by Sarginson deviates up to 1.5 % from the Rehbock values.

Accepted by the ISO committee on water-flow measurements [18], are nowadays the experimental results of Kinsvater and Carter [19]. They investigated the discharge over a sharp-crested weir at different ratios between crest width (w) and flume width (W). They proposed the following discharge formula:

$$Q = C_e (2/3) (\sqrt{2g}) w_e h_e^{3/2} \quad (43)$$

This formula resulted from investigations for a wide range of W/w and h/p ratios. C_e is presented in Figure 11. w_e is defined as the effective breath which equals $(w + K_b)$; h_e is defined as the effective water-level height being $(h + K_h)$. The h correction K_h remains 1 mm for all situations, the K_b can be read in Figure 12. Again, the authors attribute the small K_h and K_b corrections to the viscosity and surface tension effects. The 1 mm correction means that the total weir formula is not completely correct in dimensions (according to the theory of dimensional analysis).

The differences between the results of Kinsvater et al. and Rehbock, are illustrated with the following results for $w/W = 1$. The conclusion is that, applied in practice, they both produce the same result.

h (m)	p (m)	b (m)	Q _{Rehb.} (m ³ /s)	Q _{Kinsv} (m ³ /s)	% difference
.05	.4	.5	.01045	.0104	+ 0.5
.1	.4	.5	.0296	.0296	0
.2	.4	.5	.0857	.0855	+ 0.2
.2	.6	.8	.1342	.1339	+ 0.2

A correction factor for the discharge, in case of insufficient aeration, is mentioned by Bos [7]. It relates to air pressure underneath of the nappe.

$$\Delta Q/Q = -0,2 (p_2/\rho gh) \cdot 0,92 \quad (43)$$

The author compared this theoretically with the results of Sarginson in relation to surface tension effect (which also leads to a pressure in the water which deviates from the atmospheric one); however, the latter leads to a 5 times greater correction than Eq. 43. It seems reasonable to apply Eq. 43, which is based on experiments.

B. Submerged flow

The ratio of submergence is defined as:

$$S = h_2/h_0 \quad (44)$$

Now h_0 is the definition for the height of the upstream water level above the crest, h_2 is the downstream water level, also above the crest. Several authors have presented a reduction coefficient for the discharge, where S is the only relevant parameter and where h_0/p is left out. The discharge is always compared to Q_0 , the modular discharge.

1) Villemonte [41] presents:

$$Q/Q_0 = (1 - S^{1.5}) \cdot 0,95 \quad (45)$$

2) Varshney and Mohanty [39] propose (for $.03 < S < 1.0$):

$$Q/Q_0 = \sqrt{(1.03 - 0.27S - S^2)} - .059 \quad (46)$$

- 3) As it is presented in Chapter 1, Figure 6 and equation 15, Abou-Seida and Quarashi [2] propose an analytical approach, resulting in

$$Q/Q_0 = (1 + \frac{1}{2}S) \sqrt{(1-S)} \quad (47)$$

It is remarkable that Eq. 46 does not reach $Q = Q_0$ when submergence is zero, but this is on purpose: Varshney and Mohanty present experiments where a kind of jump in the curve is observed between $S = 0$ and $S = .03$. Theoretically it might be imaginable that at zero submergence the discharge increases, because the last bit of air underneath is sucked out by the jet and a little underpressure occurs.

All three equations are presented in Figure 13. Because at the modular flow regime atmospheric pressure occurs under the nappe, any extra water pressure will reduce the discharge, so a downstream water level higher than the crest has a direct effect.

In the discussions presented by Villemonte [41] it is interesting to see that he also points to Eq. 47, while referring to the Frenchmen Dubuat (Principles d'Hydraulique, Vol. 1 p.203, 1816). Villemonte shows that his own experimental results are better (within + and - 5% of his formula). At his smallest investigated h/p value (p being the weir height) of 0.06, his experiments yield a higher discharge, especially so when the submergence is under 0.4. His higher h/p range (up to 0.25) results in a lower discharge compared to Equation 45, especially when $S > 0.4$.

For the moment one must conclude that the bundle of curves in Figure 13 shows the possible scatter in discharge relations of submerged conditions.

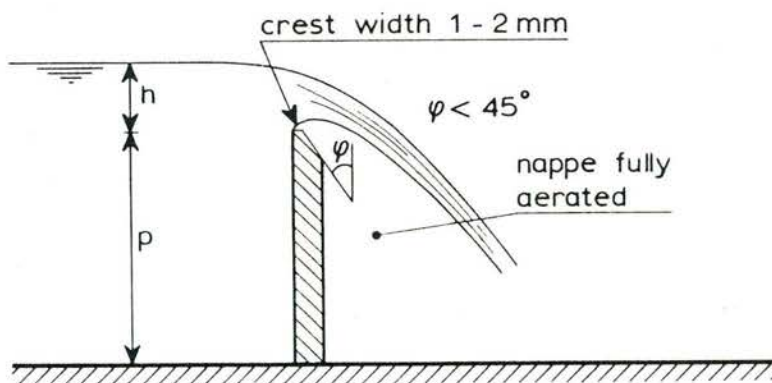


Figure 10 Section of the Rehbock standard weir.

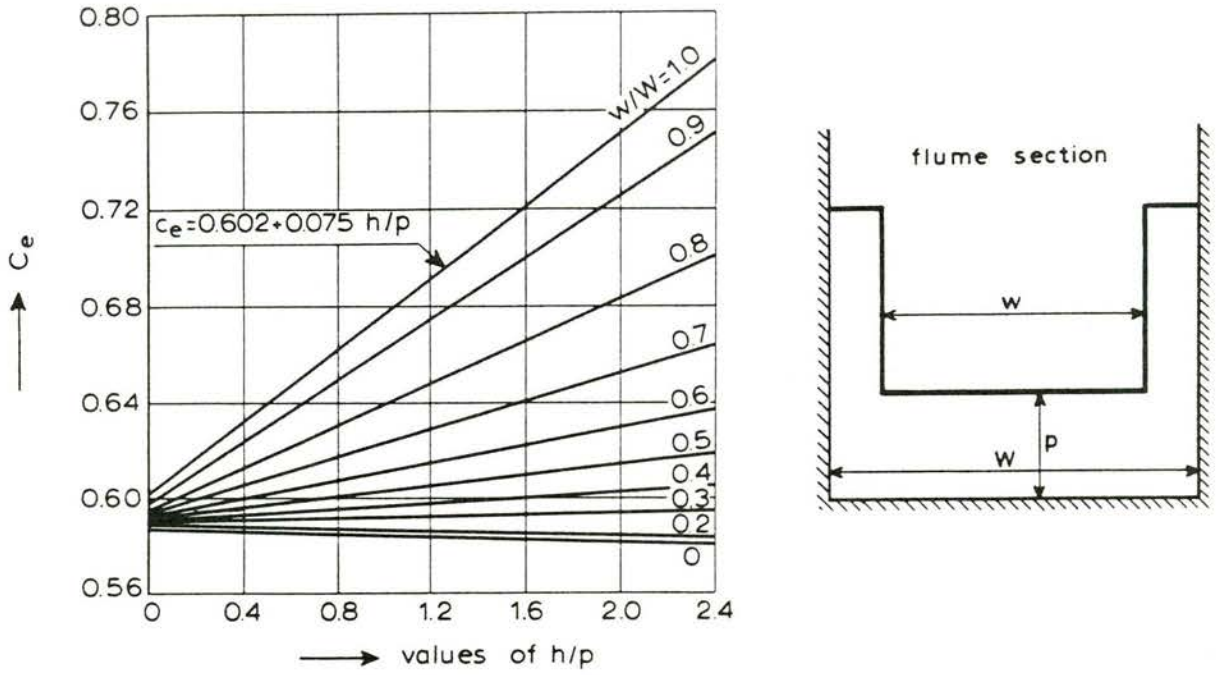


Figure 11 C_e factor as function of h/p and w/W , also after ISO 1438 [18]

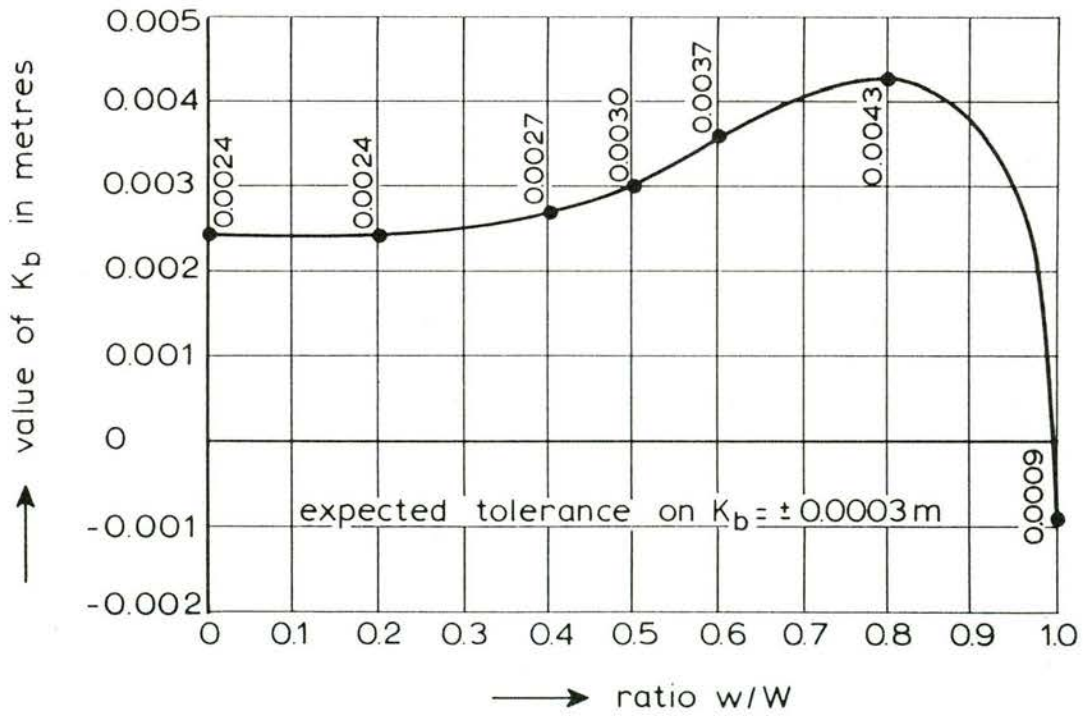


Figure 12 Values of K_b as function of w/W , from Kinsvater and Carter, after ISO [18]

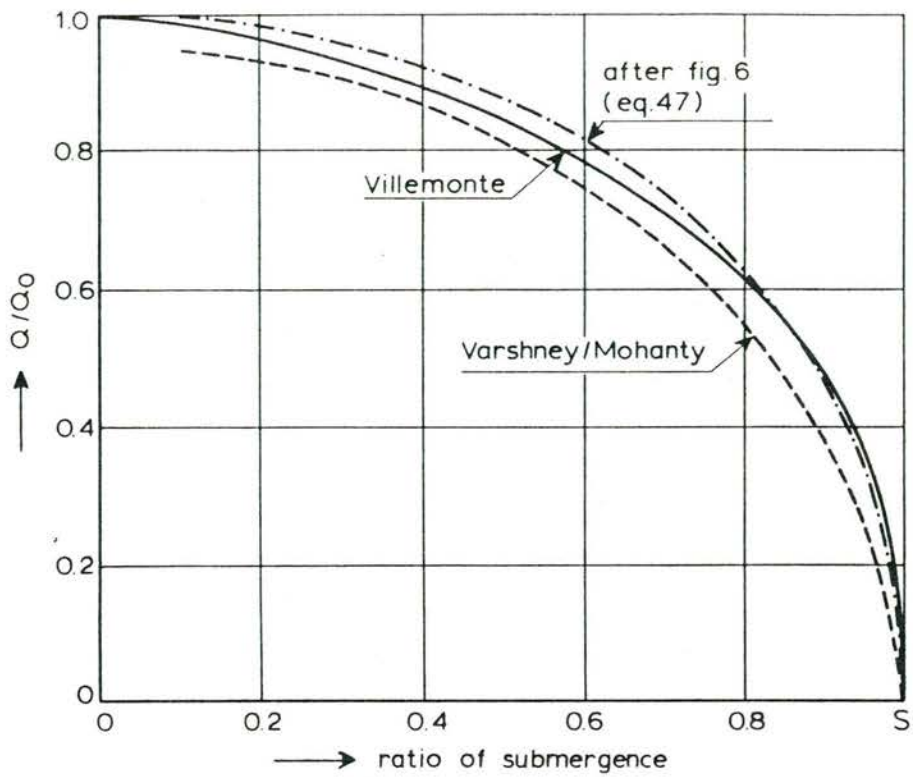


Figure 13 Flow reduction by submergence at a sharp-crested weir; different expressions.

3.2 The weir with circular crest section

In contrast to the sharp-crested weir, the semi-circular weir does not have a fixed point of flow separation. From a certain overfall height onward ($H/R = 1.5$ to 1.8) the pressure under the nappe becomes lower than atmospheric, and from this point on when H/R is increased, aeration can occur. When aerated the flow separation point shifts backwards, and comes below the crest level. Just upstream of the separation point the pressure is still lower than atmospheric (flow separation is retarded, particularly at the smaller diameters), and related to this retardation and to the low pressures at the crest, the nappe becomes more curved and the velocity becomes higher. For these reasons the discharge coefficient is greater than for the sharp-crested weir. In the region $1.5 < H/R < 2$ it is still difficult to obtain a good aeration in a natural way.

Thus, as a measuring device the semi-circular weir is only used from $H/R > 1.5$ on.

Rouvé/Indlekofer [32] performed tests on a weir with semi-circular crest (Figure 14) where, with some of the tests the air is sucked out, so as to obtain comparative tests with and without atmospheric pressure underneath. They also refer to a number of published data.

Figure 15 and 16 show the discharge coefficient C_d in the following discharge relation

$$Q = C_d w^{(2/3)} \sqrt{2g} H^{3/2} \quad (48)$$

The energy level H is introduced as the relevant parameter. Although a wide range of the radius (1-15cm) and the weir height (20-95cm) is investigated, the authors state that only the parameter H/R appeared to be relevant. The weir height had only an effect within 2%. The test values in Figure 15 are the average ones, obtained with a radius between 10 and 140 mm.

For small H/R values, where the nappe remains attached, the discharge coefficient is presented in Figure 16 in more detail. At a small radius C_d decreases and this must be attributed to viscosity effects.

Similar results are found by Sarginson [34] for the full-circle cylindrical crest. (In his definition of the discharge coefficient Sarginson uses the upper water level h and not the energy level H). From Figure 17 it can be observed that for diameters smaller than 86mm the discharge coefficient

decreases with the crest radius. This must be a viscosity effect related to the boundary layer which probably means that also the roughness of the cylinder surface can have a considerable influence. From $h/R=2$ (or greater) the flow separates from the highest crest point. The C_d does not grow and even tends to become lower for h/R , exceeding a value of about 4. The protrusion of the cylinder upstream from the weir plate, is causing the weir height p not having so much influence on C_d , because independent of the weir height the water is almost stagnant underneath.

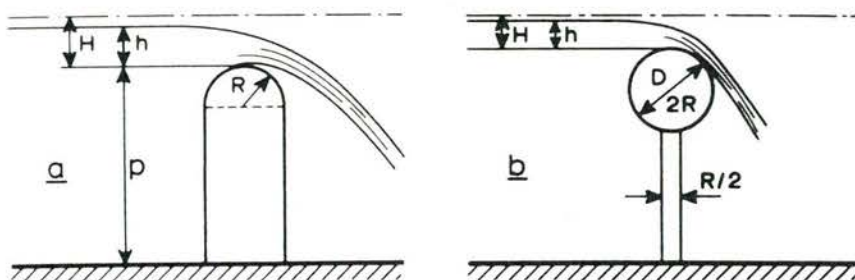


Figure 14 Weir section with semi-circular crest and with circular crest, a as investigated by Rouvé/Indlekofer [32] and b by Sarginson [34]

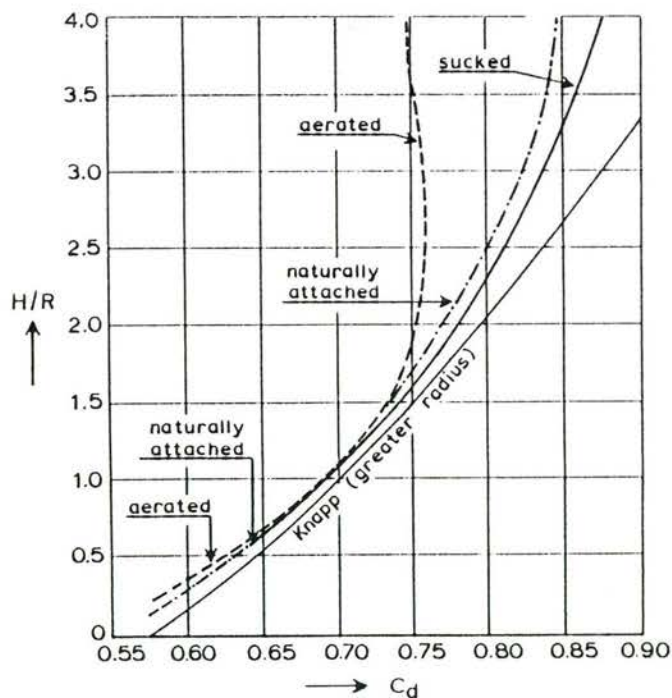


Figure 15 Discharge coefficients of semi-circular crest with and without sucking-out air (from Rouvé and Indlekofer [32] and cited authors)

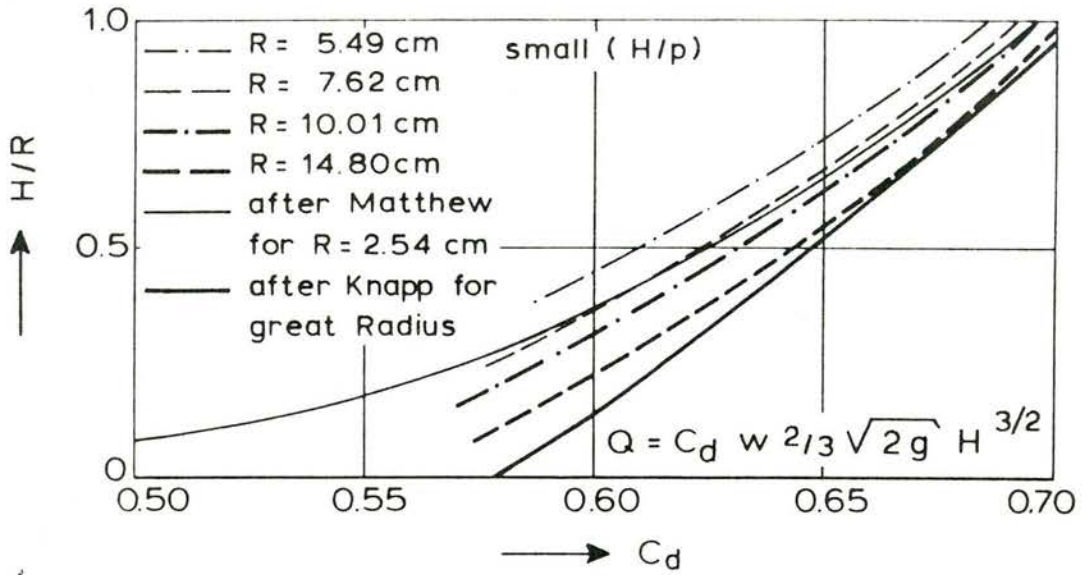


Figure 16 Discharge coefficient with attached nappe at varied crest radius, from Rouve and Indlekofer [32].

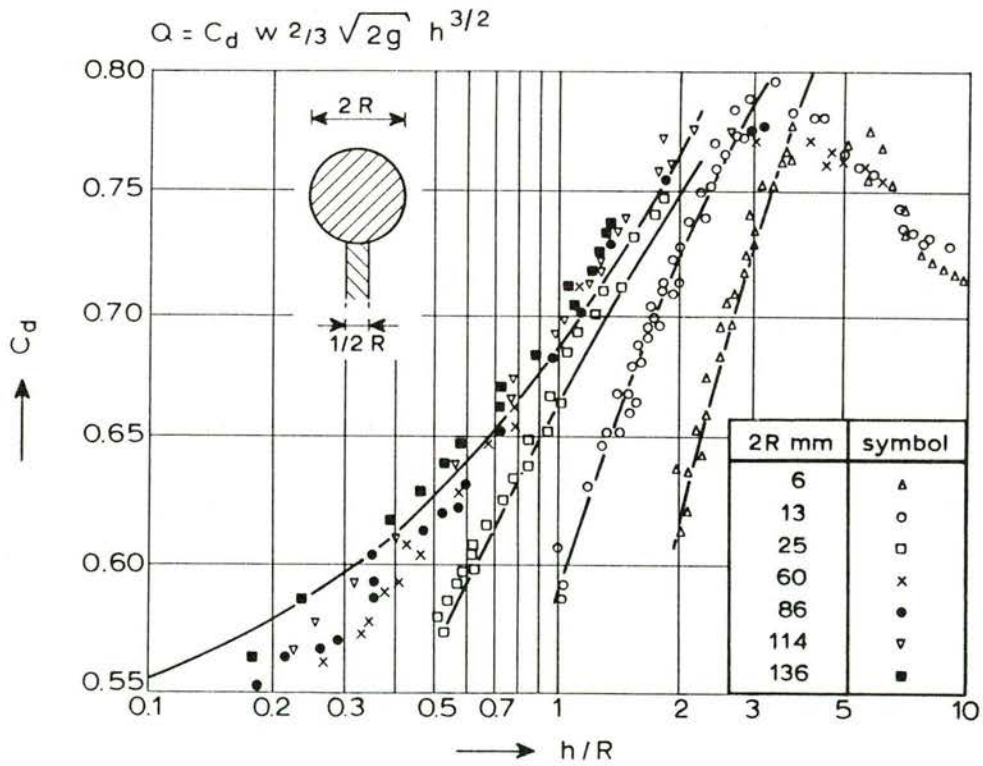


Figure 17 Discharge coefficient for the circular cylinder crest, after Sarginson [34]

3.3 The nappe-shaped overflow weir

A. Modular flow

The crest shape of the nappe-shaped overflow weir was developed by experiments in scale models where the location of the lower boundary of an overflow nappe over a sharp-crested weir was exactly measured. All the radii of the curvature are related to a reference length for which is chosen the "design head" H_d (in fact the design energy head). When the energy head of free overflow H_0 equals the design energy head H_d , then one would expect that on the whole crest pressure is exactly atmospheric. In reality small deviations occur. The weir height p is not introduced directly, but in the form of the influence of the velocity head h_a of the approach velocity in relation to H_d . The crest shape is found in Figures 18 and 19. All data are taken from USBR "Design of small dams", Ref. [38].

The nappe-shaped weir type has the property that when the real overflow height (H or H_0) equals H_d , the pressure at the crest and the downstream face equals the atmospheric pressure, and hence only small risk of unwanted aeration or cavitation occurs. When the real H value is smaller than H_d , then pressure is higher than atmospheric, and when H is greater than H_d the pressure is lower than atmospheric; the natural jet of the sharp-crested weir is thrown out farther when H increases. The advantage of this weir type is its high discharge coefficient. For instance, compared to the sharp-crested weir at the same discharge, the crest is now at the top level of the underside of the sharp-crested overflow nappe. This means that the equivalent crest height of the sharp crest lays 12.7% of H_d lower than the nappe-shaped profile. An additional safety exists for conditions at an extremely high flood, because then the discharge coefficient becomes still higher as a result of lower crest pressures (see also middle figure of Figure 20). This advantage, however, is paid for in the form of an additional risk of cavitation.

The very systematic investigations of this weir type (crest shape and discharge relations) have been performed by the US Bureau of Reclamation USBR and the Vicksburg Waterways Experiment Station of the US Army (WES) [43].

The upper graph of Figure 20 is a revised version from [33], applying the definition of C_d , similar as for the sharp-crested weir:

$$Q = C_d w (2/3) (\sqrt{2g}) H^{3/2} \quad (49)$$

A few exercises and checks:

It is observed in Figure 20, the upper graph, that with a small H the discharge coefficient reduces to 0.575. This case is comparable with the long-crested weir for which was derived the theoretical discharge relation of Eq. 6. This equation equals Eq. 49 when $C_d = 1/\sqrt{3} = 0.577$ is applied, which is well in agreement with the value of Figure 20.

Also one finds for a great weir height a discharge coefficient of 0.739. When this is combined with the reduction factor of 0.78 at small H_0/H_d (again a situation similar to the long-crested weir) then 0.739 times 0.78 is read in Figure 20 and this becomes 0.575 which is also in agreement with the aforementioned C_d of 0.577.

Also one can see that for $H_0 = H_d$ the discharge coefficient for a high weir is 0.739. Reading in Figure 19 that $Y_c/H_d = 0.127$ one can derive that the equivalent sharp-crested weir is $1.127 H_d$ below the water level. The discharge coefficient of the sharp-crested weir will be $0.739/(1.127^{3/2}) = 0.618$ while from the Rehbock formula (eq. 39) combined with Eq. 49 one can derive $C_0 = 1.78/\{(2/3\sqrt{2g})\} = 0.603$. The difference of 2½% might be explained by the correction in h of 1mm which is proposed by Rehbock and which for small scale tests results in a little higher value of C_d .

B. Submerged flow

Figure 21 shows the different types of flow which might occur at submerged flow and the decrease of discharge coefficient. This graph, to be found for instance in the USBR [38] was modified by Naudascher [24], who introduced p/H_e on the horizontal axis. H_e is the upstream energy head, which generally will be different from the design head (see in Figure 20 the central figure for the influence of H_e/H_d).

C. Modular flow with piers

When the weir has modular flow conditions also the effect of piers and abutments is found in the "Hydraulic Design Criteria" of WES [43].

The width w which has to be introduced in Eq. 49:

$$w = [L' - 2(NK_p + K_a) H_e] \quad (51)$$

L' = total crest length between abutments and piers

N = number of piers

K_p = pier contraction coefficient

K_a = abutment contraction coefficient

H_e = upstream energy level (above crest level)

K_p and K_a can be read from Figure 22 and 23.

To check the order of magnitude of such an correction:

when $K_p = .025$

and $K_a = .1$

and $N = 3$ and $H_e/L' = .1$

the correction in crest length becomes:

$$2(3 * 0.025 + 0.1) 0.1 = 0.035 \text{ (or 3.5 \%)}$$

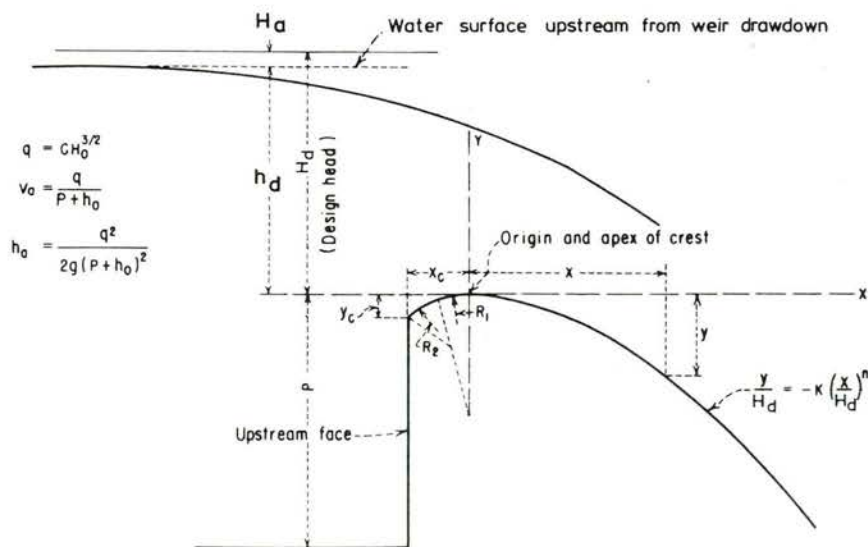


Figure 18 Crest shape: symbols and definitions, from [38]

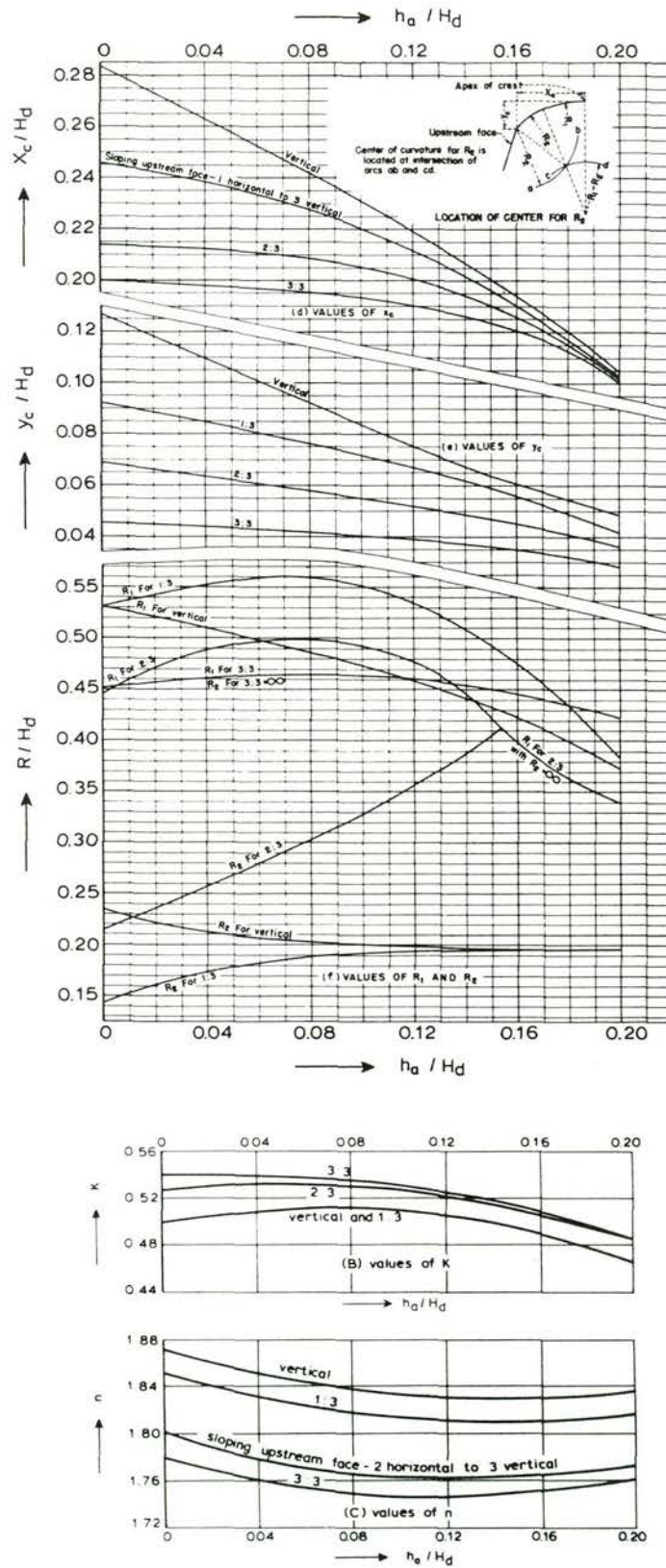


Figure 19 Crest shape at different slopes of the upstream face, from "Design of Small Dams USBR" [38].

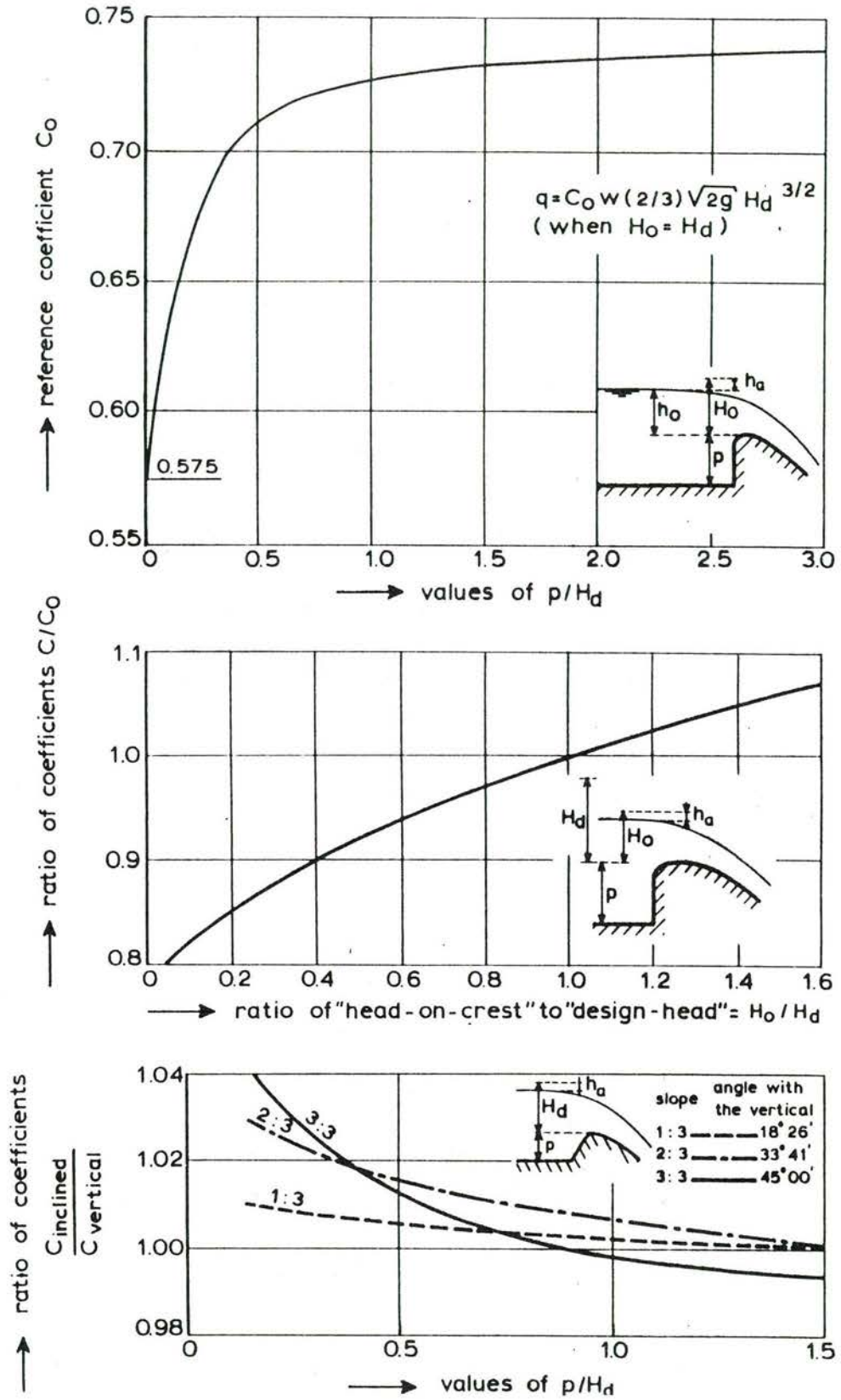


Figure 20 Discharge coefficients of nappe-shaped crests at different conditions and different upstream slopes, (USBR [38]).

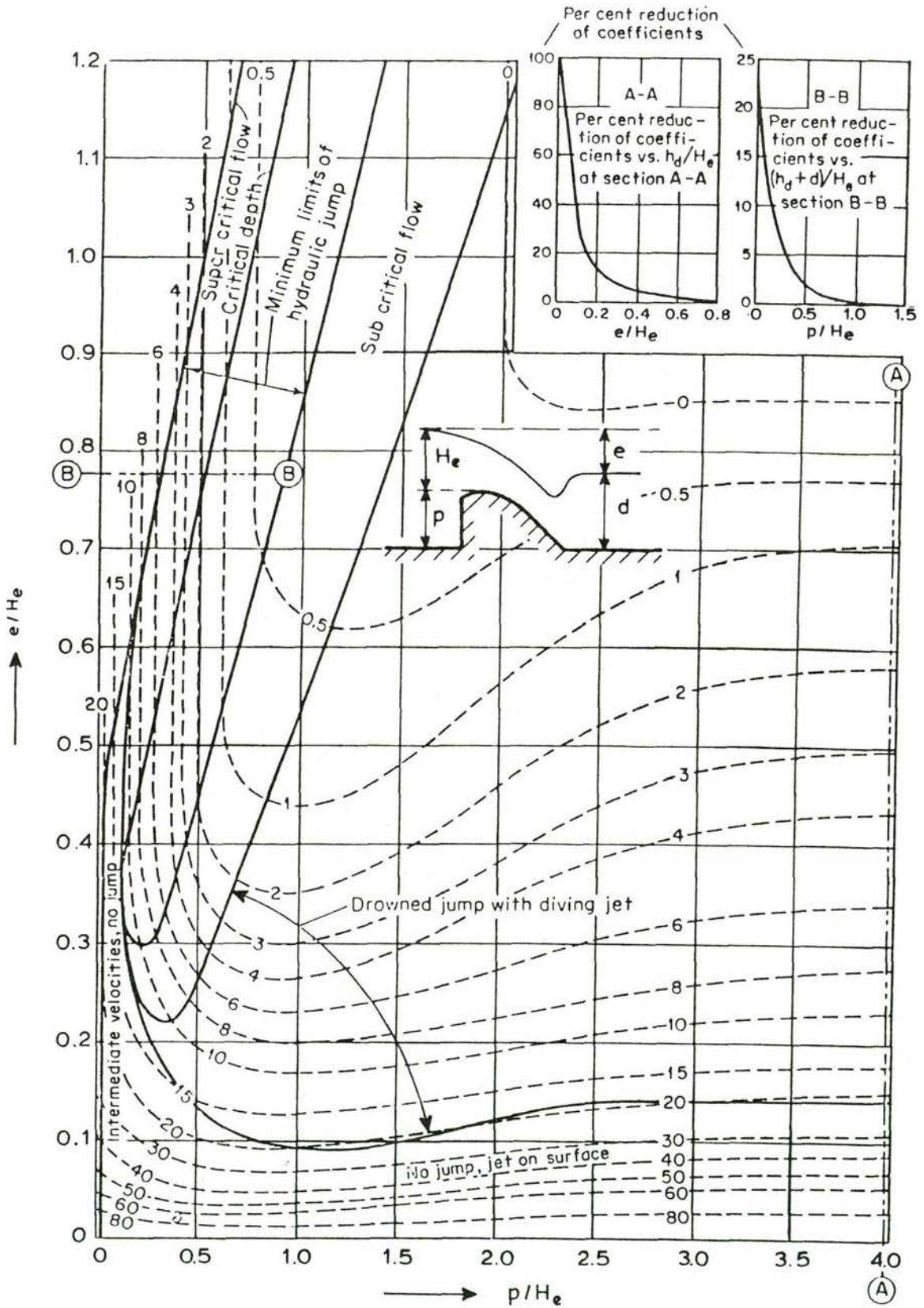
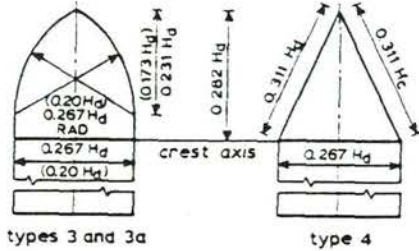
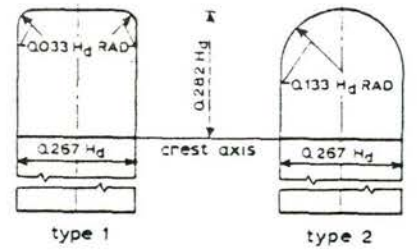
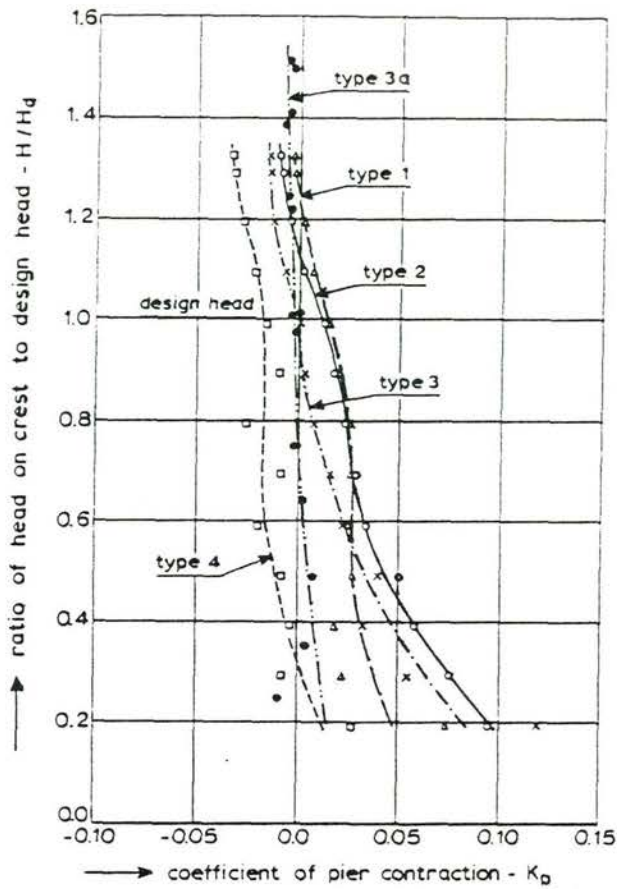


Figure 21 Flow reduction by submergence—corrected version from Naudascher [24], and originally taken from Ven Te Chow [40].



PIER NOSE SHAPES

note: pier nose located in same plane as upstream face of spillway
 dimensions in parentheses are for type 3a

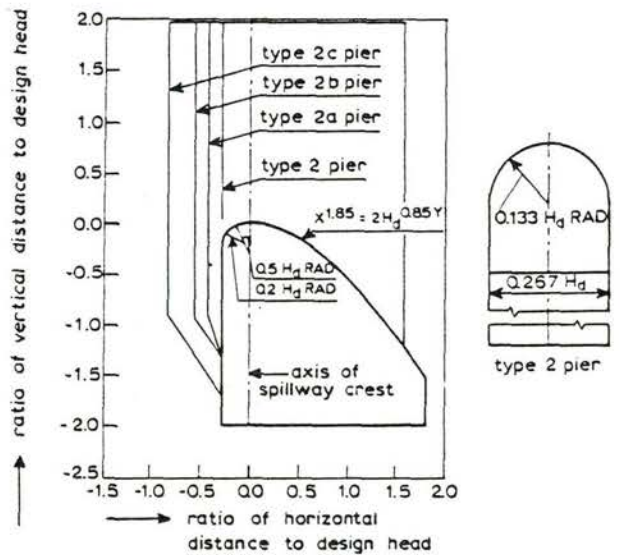
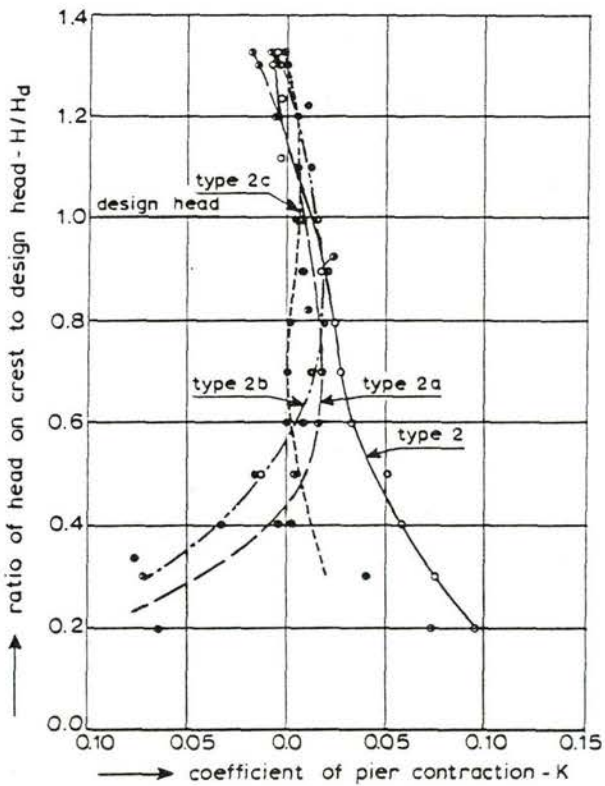
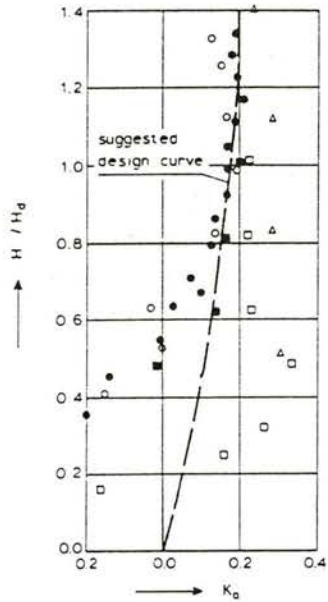


Figure 22 Pier-contraction coefficient, from WES [43]

Figure 23 Abutment-contraction coefficient, from WES [43]



basic equation

$$Q = C_d [L' - 2(NK_p + K_a) H_e]^{2/3} \sqrt{2g} H^{3/2}$$

where:

- Q = discharge - m³/s
- C_d = discharge coefficient
- L' = net length of crest - m
- N = number of piers
- K_p = pier contraction coefficient
- K_a = abutment contraction coefficient
- H = total head on crest - m

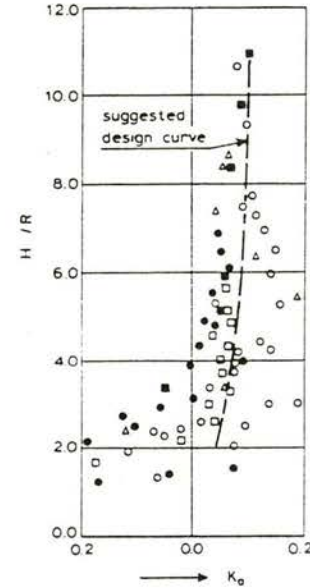
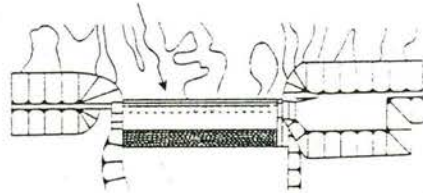
legend

symbol	project	R	W/L	W/H
□	dorena	1.2	1.55	0.96
■	oarena	2.4	2.10	3.77
○	red rock*	1.5	2.67	1.42
●	carlyle*	1.2	2.12	1.77
△	water f. george	1.5	3.83	9.48

* gated spillway with piers

note:

- R = radius of abutment - m
- W = width of approach reproduced in model - m
- L = gross width of spillway - m
- H = depth of approach in model - m
- H_d = design head on crest, m



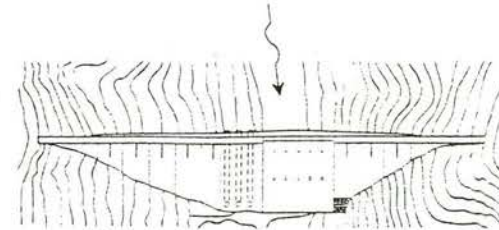
legend

symbol	project	R	W/L	W/H
□	CW 801	1.2	1.55	0.96
●	falsom	2.4	2.10	3.77
○	philpott	1.5	2.67	1.42
■	pine flat*	1.2	2.12	1.77
△	center hill*	1.5	3.83	9.48

* gated spillway with piers

note:

- R = radius of abutment - m
- W = width of approach reproduced in model - m
- L = gross width of spillway - m
- H = depth of approach in model - m



3.4 The nappe-shaped spillway with gate

For the weir profile of the former section, the discharge coefficient of a tainter gate can be read in Figure 24 and the one for a flat gate in Figure 25. The discharge coefficients are based on a pure two-dimensional situation.

The WES [43] presented the discharge coefficients for a sharp-edged tainter gate as C . The discharge equation reads:

$$Q = C G_o w \sqrt{2g H} \quad (51)$$

G_o is the gate net opening as indicated in Figure 24, w is the width of the gate opening and H is the energy head compared to the level of the centre of the gate opening.

For the flat gate on a spillway crest the equation of discharge starts with the free flow discharge Q_0 (see for the determination of Q_0 section 3.3) and then a reduction factor is applied. In Figure 25 it is indicated that the reduction factor can be written as

$$Q/Q_0 = (H_2^{3/2} - H_1^{3/2})/H_0^{3/2} \quad (52)$$

This equation is based upon a consideration presented in section 1.5, and on Equations 4 and 5. However, it seems illogical that the gate seat does not correspond to the spillway crest level, whereas in Eq. 4 the bottom level is the same as in Eq. 5.

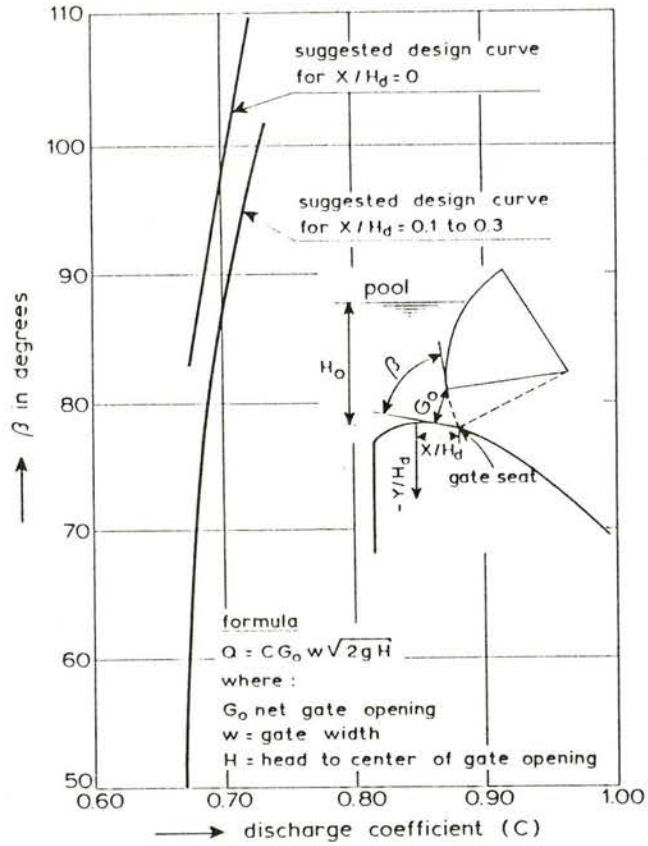


Figure 24 Discharge coefficient tainter gate on spillway crest, from WES [43]

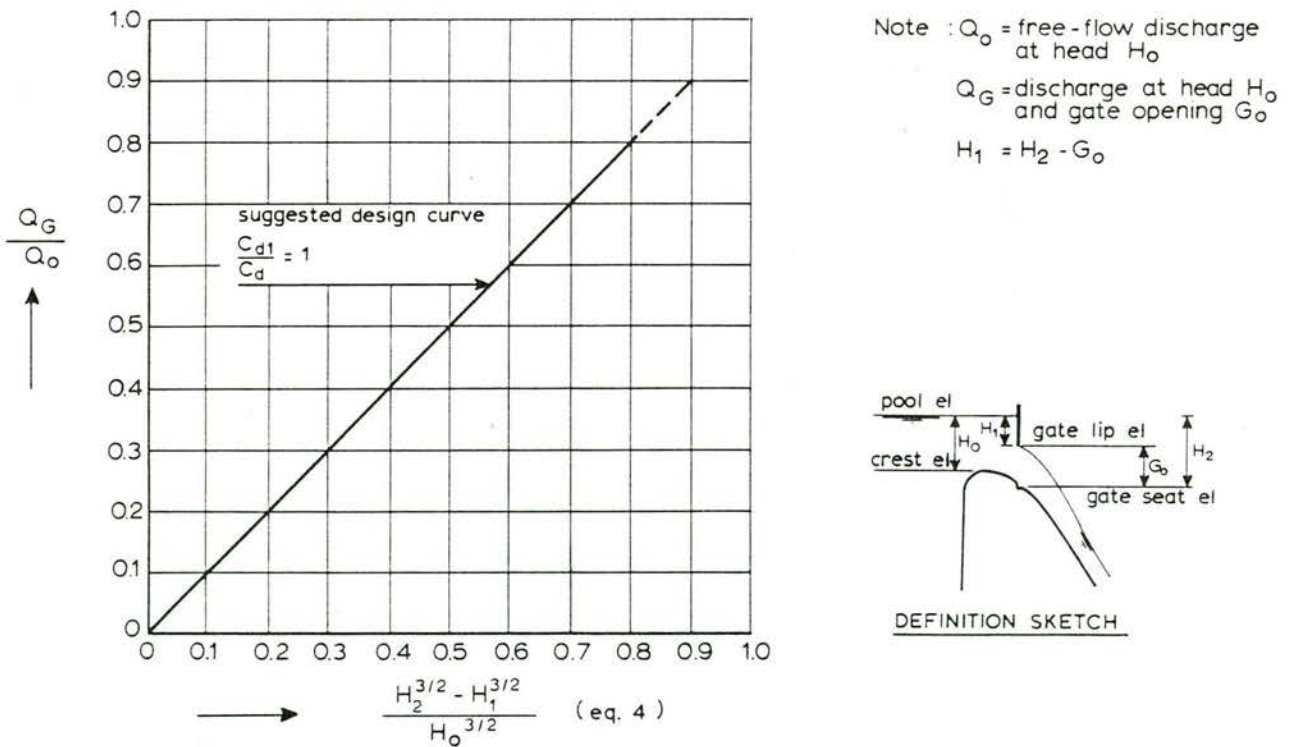


Figure 25 Discharge coefficient of a flat gate on spillway crest, from WES [43]

3.5 Broad-crested weirs and dikes

At broadcrested weirs the streamlines above the crest are approximately parallel and there is a hydrostatic pressure distribution. From the upstream water level to the level on the top of the crest the Bernoulli equation can be applied. Two elements cause that a correction coefficient need be introduced: there is an energy loss by friction and the boundary layer displacement thickness δ_d is a quasi-heightening of the crest.

The discharge equation for a broad-crested weir with a horizontal crest (sometimes called a long-crested weir) at modular (free) flow is found from section 1.5, Eq. 6a and 6b.

$$q = h_1 \sqrt{2g (H_0 - h_1)} \quad (53a)$$

For the condition of maximum discharge (equal to the conditions of free flow) holds also:

$$h_1 = (2/3) H_0 \quad (53b)$$

So the discharge equation becomes (introducing $(H_0 - h_1)$ equals the velocity head)

$$q = (2/3) H_0 \sqrt{2g H_0/3}$$

(At the crest the waterdepth h_1 equals also the critical depth $h_1 = d_c = \sqrt[3]{q^2/g}$.)

In practice also a correction factor C is introduced so that the discharge equation becomes:

$$Q = Cw (2/3) H_0 \sqrt{2g H_0/3} \quad (54)$$

(w = width)

The discharge equation 54 is a theoretical one; a small correction is needed due to the boundary layer effect.

Naudascher [24] gives the following theoretical corrections for a long-crested weir with adequate flow convergence, without extra flow contraction or other losses. It is based on a reduction of the net flow section by the displacement thickness δ_d of the boundary layer:

$$C = (1 - 2 \frac{\delta_d}{w}) (1 - \frac{\delta_d}{H_0})^{3/2} \quad (55)$$

The displacement thickness of the boundary layer depends on the crest length L and the Reynolds number (related to crest velocity and crest length).

$$\text{for } Re_L < 3 \cdot 10^5 \text{ the } \delta_d/L = 1.73 \cdot Re_L^{-0.5} \quad (56)$$

$$\text{for } Re_L > 3 \cdot 10^5 \text{ the } \delta_d/L = 0.037 Re_L^{-0.2} \quad (57)$$

To give an order of magnitude for the necessary correction for the last condition he presented the following table for C values, for the ratio $w/L = 0.2$.

	H/L				
L(m)	0.05	0.075	0.10	0.125	0.15
0.61	0.883	0.923	0.941	0.953	0.960
1.83	0.923	0.446	0.958	0.966	0.971
3.50	0.932	0.953	0.964	0.970	0.975
15.25	0.953	0.967	0.975	0.979	0.982

Table 3.5.1 Correction coefficient C in Eq. 54.

The downstream waterlevel has only effect when the induced pressure at the downstream crest edge is higher than the hydrostatic pressure belonging to the modular flow condition. This occurs when $h_2 > h_d$ (see Figure 26 for notations).

Only when the back face of the sill is vertical, the submerged-flow pressure conditions downstream of this face is assumed to be hydrostatic. The waterdepth h_2 can then be calculated with the momentum equation (see section 1). The effect of the downstream water level is expressed as a reduction which is a function of the submergence factor:

$$S = h_2 / h_0 \quad (58)$$

Here h_0 and h_2 are the up- and downstream water levels above the crest level. The downstream water level at which submergence has influence, is higher than the critical depth h_c , being 66% of H_0 , because of the recovery

of potential energy. This recovery is still more when the downstream sill face is sloped. In Figures 27 to 29 some data about discharge coefficients of broad-crested weirs and dikes are shown; they have been taken from DELFT HYDRAULICS [10], [11] and [12]. At the dike model where also skew conditions are tested (Figure 28) the downstream flume walls do not correspond with the natural direction of outflow, so the discharge reduction factor C_{RS} (by submergence and by the skew approach flow) in prototype might be somewhat greater than the measured one. The effect of the skewness in Figure 28 is also greater than what is expected from the considerations of Schönfeld [35] mentioned in section 1.2.

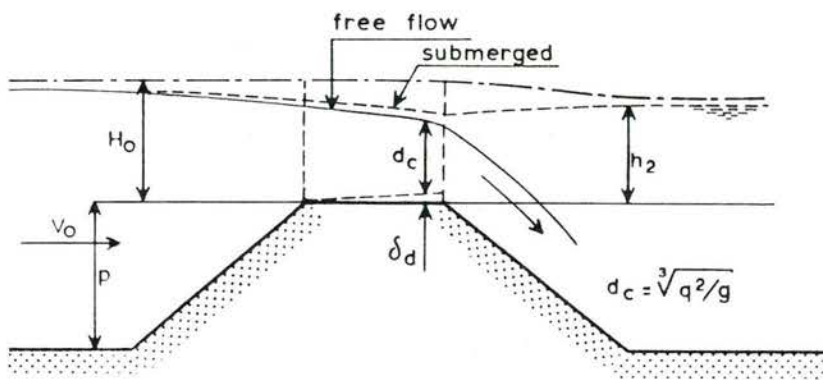
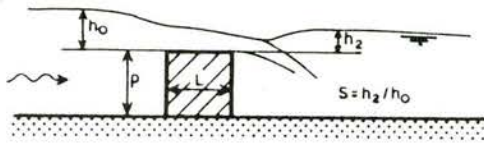
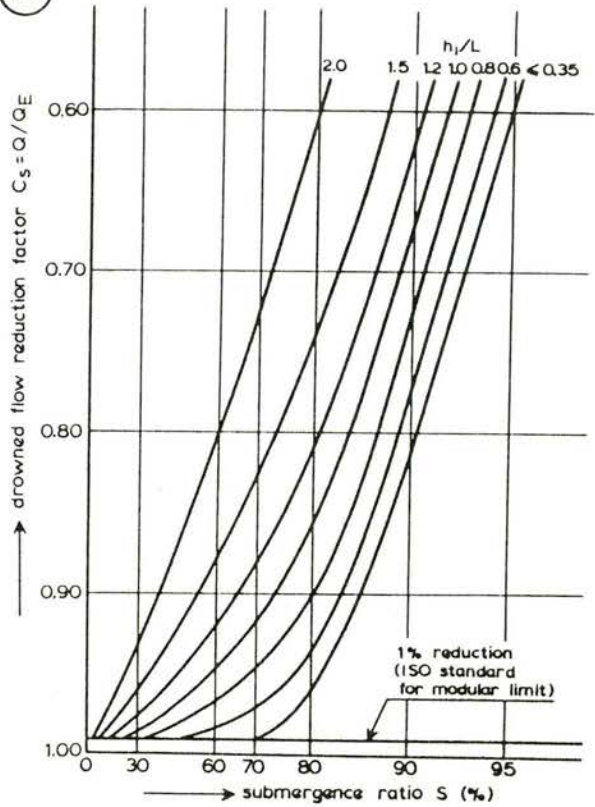


Figure 26 Notations: flow conditions at a broadcrested weir.

(B)



(A): free flow relations
 (B): reduction by submergence



DISCHARGE COEFFICIENT

$$C_D = \frac{2}{3} \cdot 1.5 \cdot g^{0.5} \cdot B \cdot H_0^{1.5}$$

and $Q = C_S Q_0$

(A)

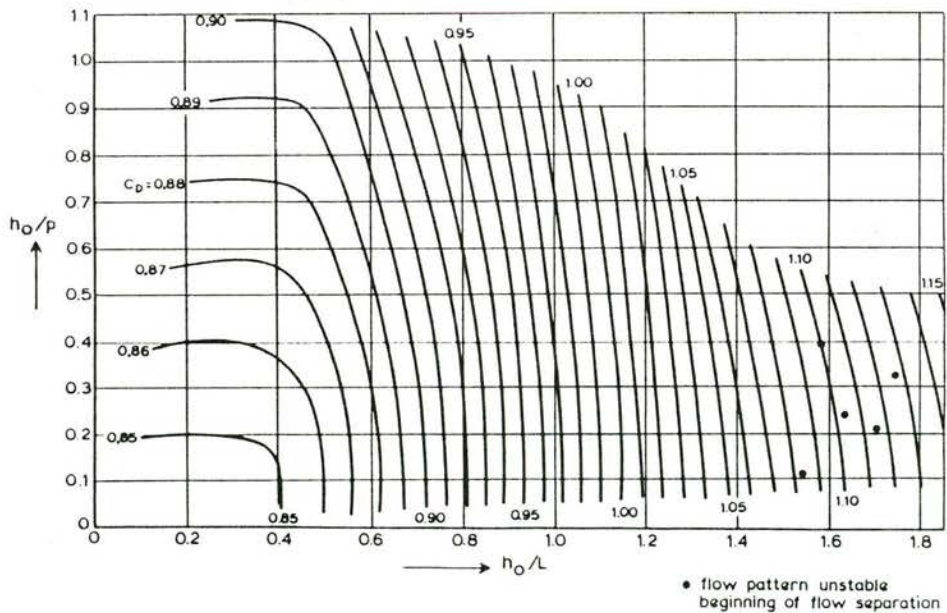
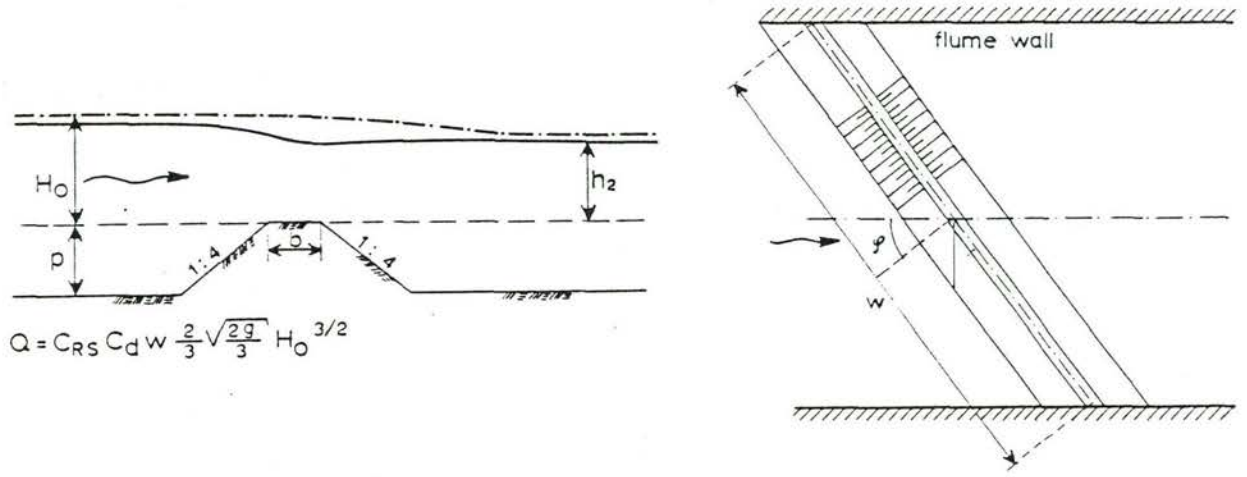


Figure 27 Discharge relations of broad-crested sills with variable sill length, from DELFT HYDRAULICS [11]



$$Q = C_{RS} C_d W \frac{2}{3} \sqrt{\frac{2g}{3}} H_0^{3/2}$$

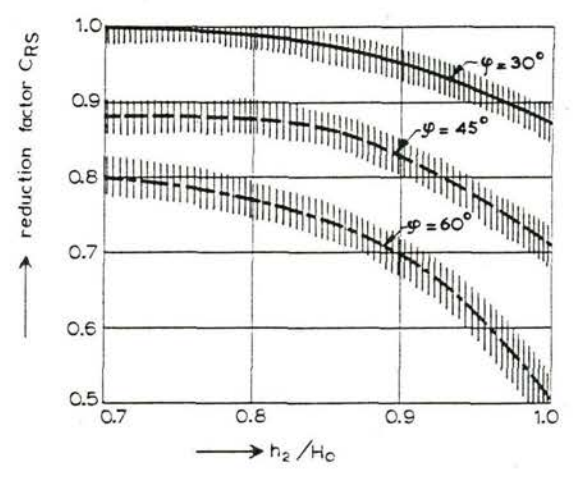
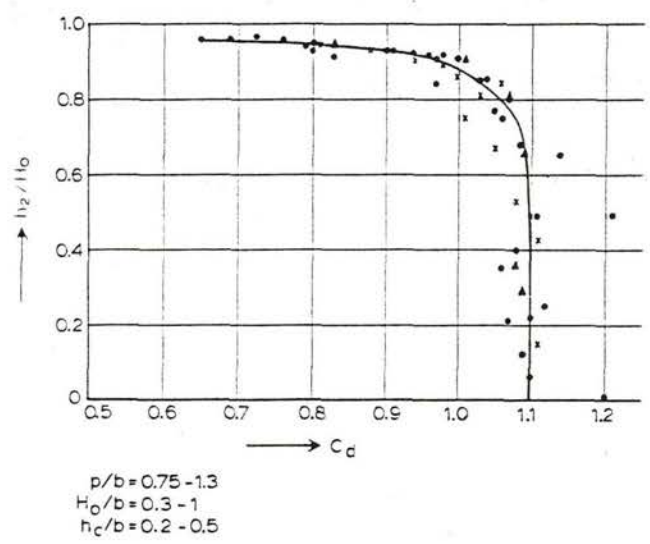


Figure 28 Discharge coefficients of dikes, (model on scale 1:25) from DELFT HYDRAULICS [10]

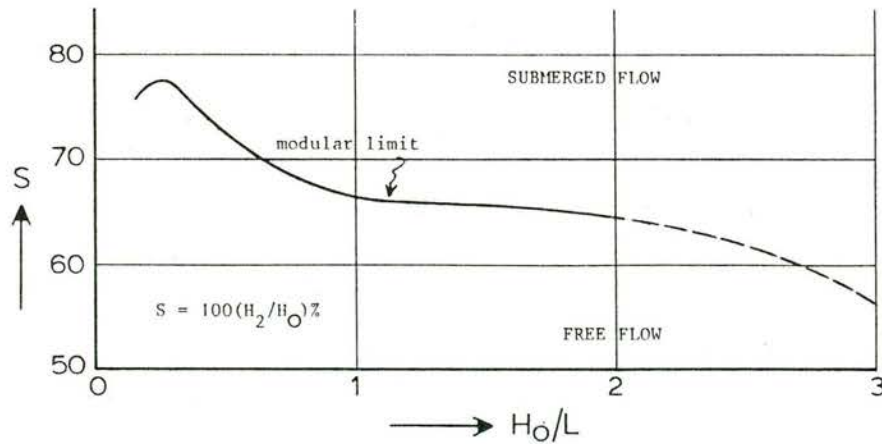
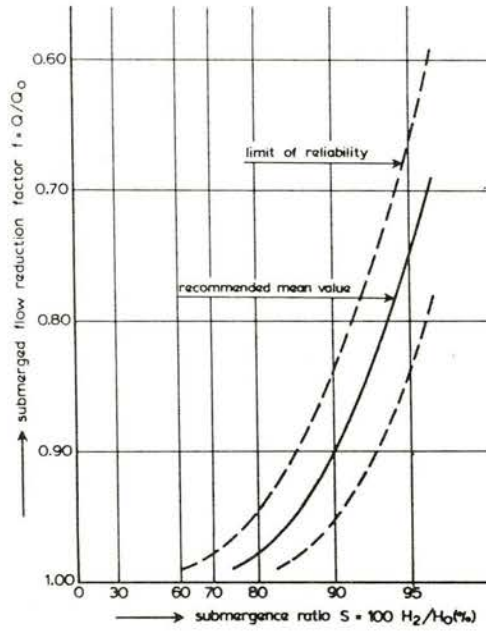
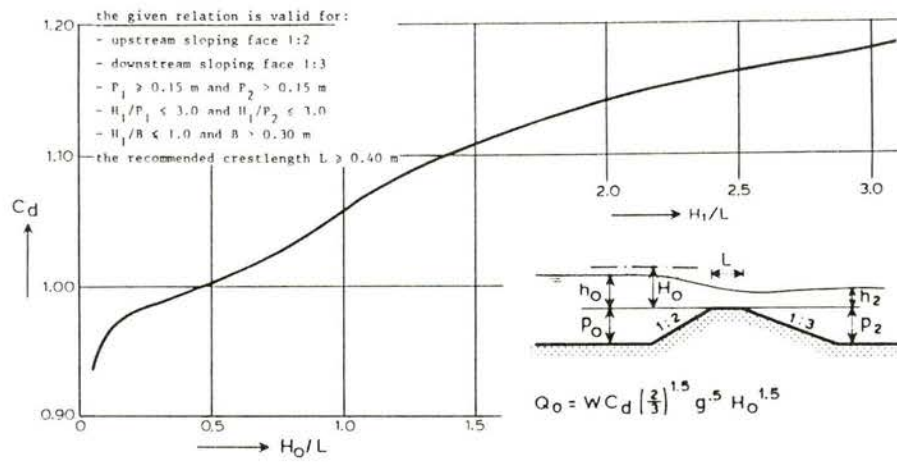


Figure 29 Discharge coefficients of different types of sills with sloping front and back face, from DELFT HYDRAULICS [12]

3.6 The morning glory spillway

The morning glory spillway is a spillway which is circular (or a part of a circle) in plan. It is an option when a tunnel is applied in whatever way, for instance a diversion tunnel left in place after the dam has been built. The compactness of its shape is favourable for its application. To prevent siphoning of the whole tunnel, which would cause a dangerous situation at extremely high discharges, a control section is created underneath the spillway with, for instance, a sudden widening of the tube section, or where air is let in to guarantee that atmospheric pressure occurs at that level. The level of this air inlet cuts off the discharge, and even when the inlet is fully submerged, velocities at the cut-off section are restricted to $\sqrt{2gh}$ where h is the difference in level between the upstream energy head and the cut-off section. Figure 31 shows an example of how a cut-off section is introduced.

It is not advised to apply the morning glory spillway for conditions where prediction of a maximum required discharge capacity is still very uncertain. At higher water levels Q increases with $\sqrt{2gh}$, whereas for a straight spillway the discharge increases with $H^{3/2}$. Therefore, the risk of overtopping the dam is smaller in the latter case. In Figure 30 is shown the different types of flow which can occur when no aeration is applied.

At condition 1, the discharge is determined by the overflow capacity of the crest.

At condition 3, at full siphoning, the total head difference H_T is determinative, $Q \approx \sqrt{2g H_T}$.

At condition 2 the level difference H_a determines the discharge. H_a is between the upstream level and the highest point where air at atmospheric pressure occurs. But when air pressure is lower than atmospheric, the effective H_a is greater.

At condition 2 the H_a moves downwards at greater discharge, because the air is sucked out gradually and the situation is very unstable.

Without the introduction of a control section by widening and/or aeration it is in fact the downstream tube-end which, in condition 3, is the control section, while with aeration at the point "orifice control" of condition 2 the situation is stabilized at that level. See further the discharge curve of Figure 31.

Like the nappe-shaped spillway of section 3.3 the design of the crest of the morning glory spillway is based upon the atmospheric wall pressure condition related to a design discharge. And as in the straight spillway, this condition is established by measuring the lower nappe profile of the free overfall nappe of a sharp-crested weir (in plan circular) with radius R_s , see [42].

In the design of the morning glory spillway the requirements lead to a compromise. This design process is an iterative one. In the final design stage model investigations are often applied. The following elements should be taken into account.

- a At the condition of submerged crest and discharge control at the control section, the discharge has to pass any section without a wall pressure lower than atmospheric, so the distance z below the upstream water level follows from the conditions that z equals also the velocity head; so

$$Q = \pi R^2 \sqrt{2gz} \quad (59)$$

hence at any level

$$R_{\min} = (Q/\pi)^{1/2} (2gz)^{-1/4} \quad (60)$$

- b As a first estimate in the iteration, the design head can be taken equal to the demand of the design water level departing from free flow and maximum discharge. With Figure 32 the outer radius R_s can be determined. As a next step H_s can be read in Figure 33. R_s and H_s are the values which were tested in the sharp-crested weir test of Ref. [42]. The discharge is free flow when $H_s/R_s \leq 0.45$, and is submerged when $H_s/R_s > 0.9$ to 1. From H_s and R_s the weir shape can be designed from Figure 33.

- c The location where the curves, discussed in a and b, meet can be a first choice for the level of the discharge cut-off (control) section, but due to a discharge coefficient smaller than one (0.9 is advised in [38]) the control section is a little wider than the corresponding section of the curve obtained in a. Then the transition between the curves a and b is smoothed. Condition a can lead to a local or to a total widening of the upper part of the bell mouth as found in b, but this is not so when H_d/R_s is smaller than 0.225 to 0.3.

The procedure does not lead straight forwardly to the final design, so other values of H_d and R_s have to be tried also.

The correspondance of the area of the control section with the tube section further downstream, is also a point of consideration.

However, when other H_d values are tried, the real energy head H_e is not equal anymore to the design head. Figure 34 gives the correction for the discharge (but only for $H_d/R_s = 0.3$). In [38] it is advised to use this curve for other H_d/R values also. But one should consider that at small H values the discharge relation approaches the one of the broad-crested weir. Therefore, in Figure 34 could also be completed with reduction factors (at a small head) for other H_d/R_s values than 0.3; they are calculated from Figure 32 in combination with the theoretical discharge equation for a broad-crested weir of Equation 54.

Another design element in the last stage of the design is related to cavitation. In contrast to a straight spillway the discharges smaller than the ones at the design head, cause wall pressures lower than atmospheric. Wagner [42] also performed tests with lower pressures than atmospheric underneath the nappe and these results could serve, by comparison with the designed shape, for estimation of the related pressures.

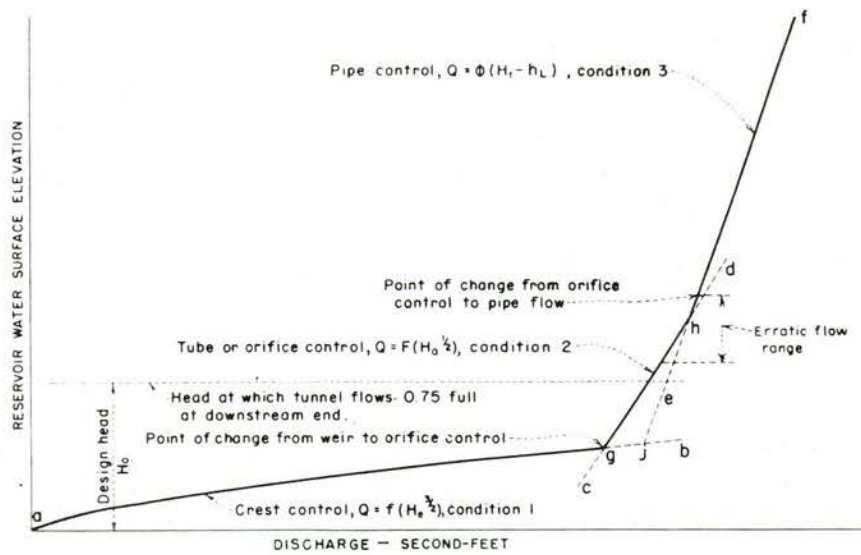
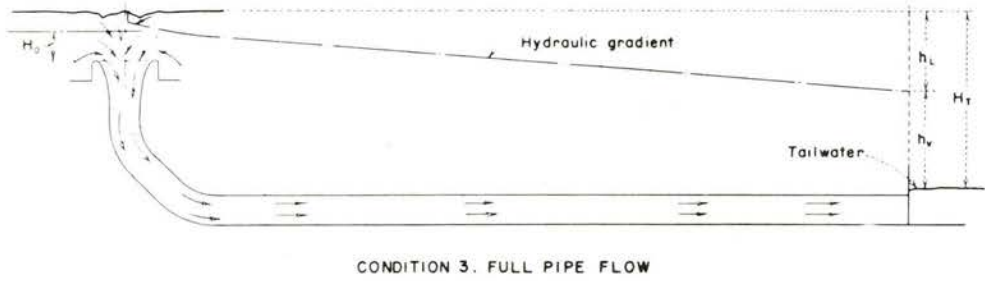
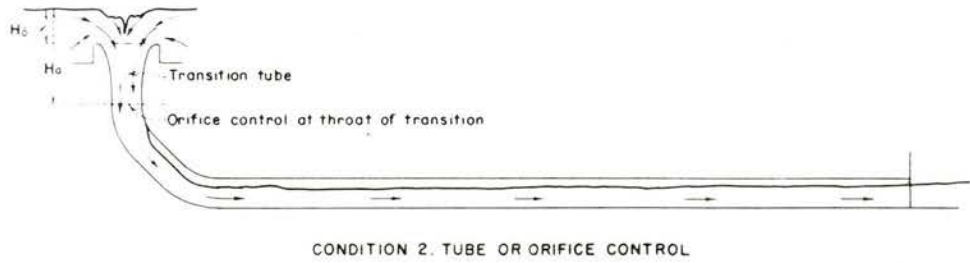
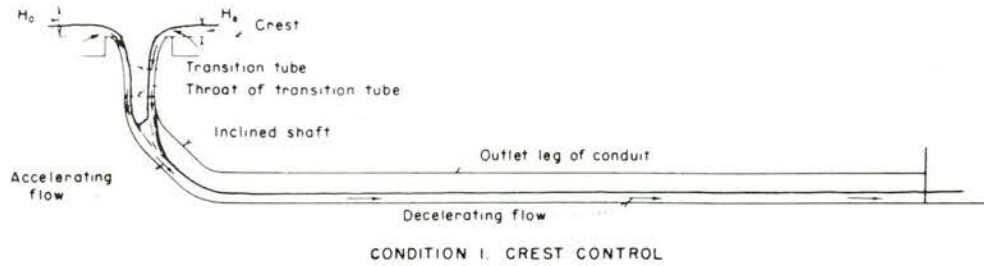


Figure 30 Nature of flow and discharge characteristics of a morning glory spillway, from USBR [38]

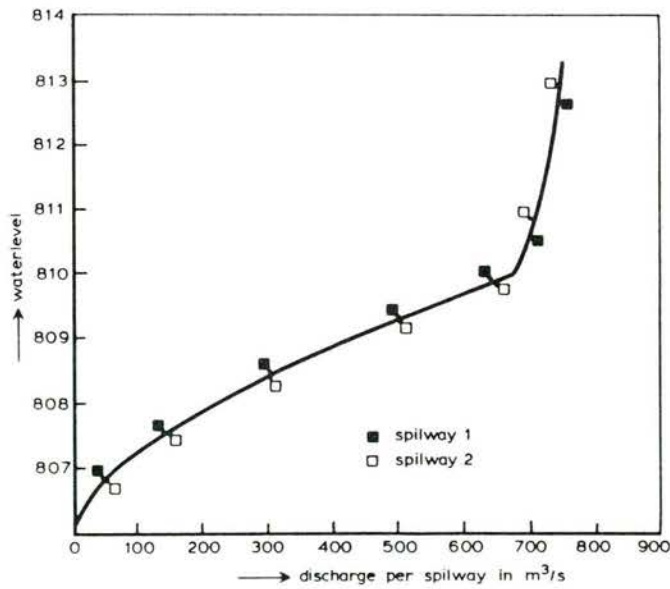
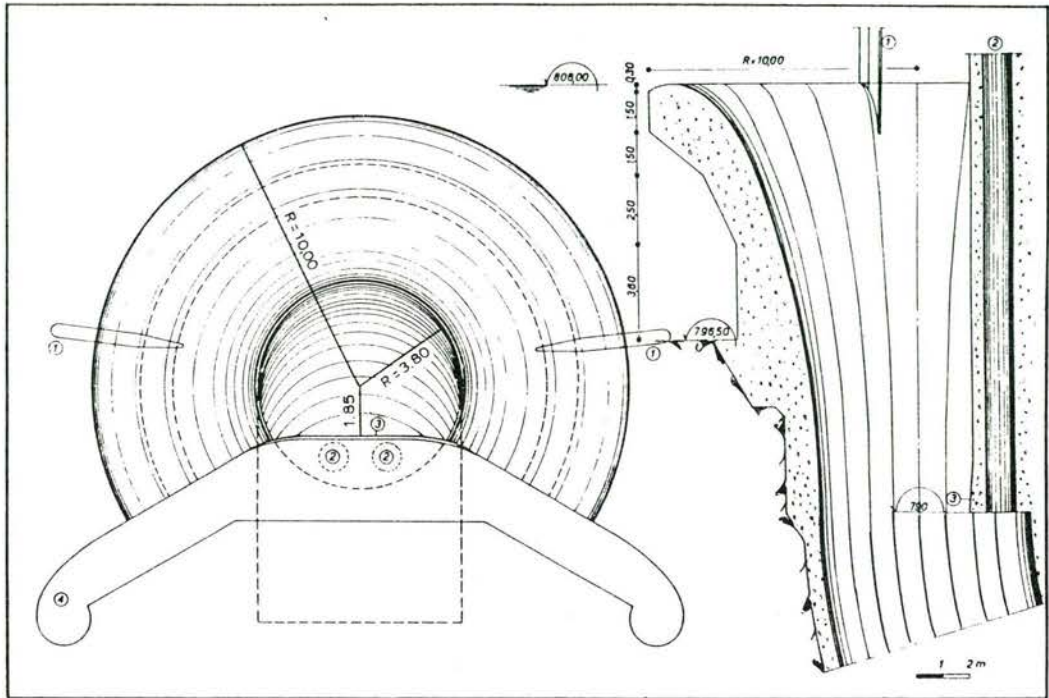


Figure 31 Control section introduced by aeration and enlarged pipe profile (design Coyne and Bellier, from [4])

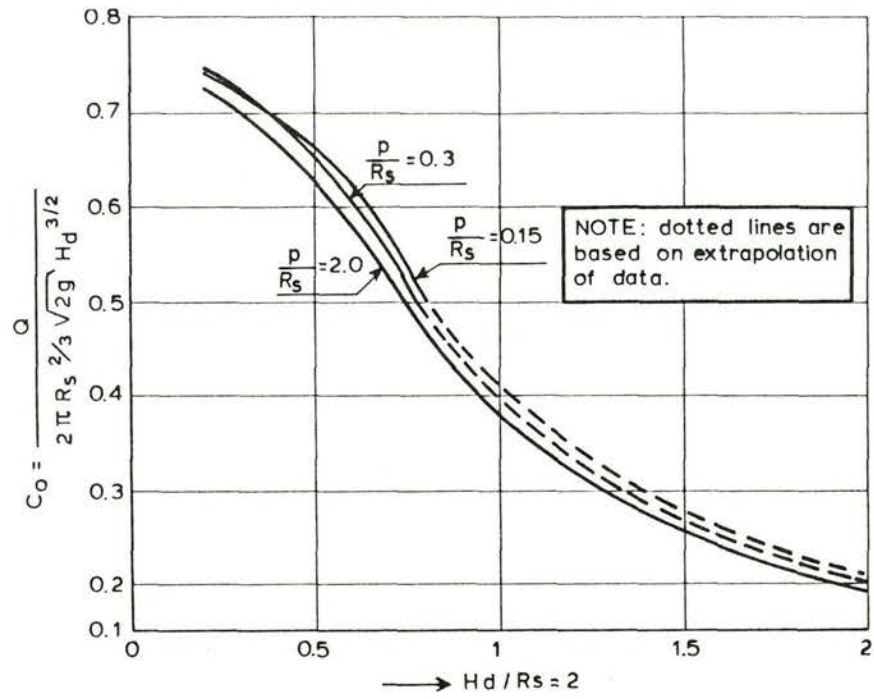
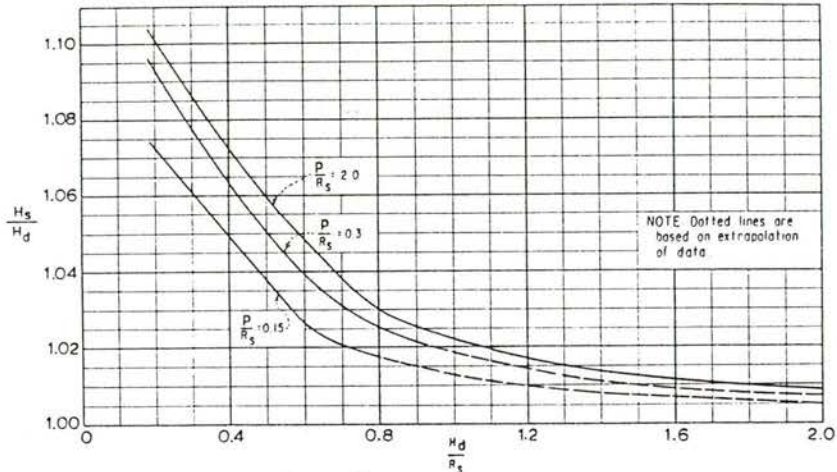
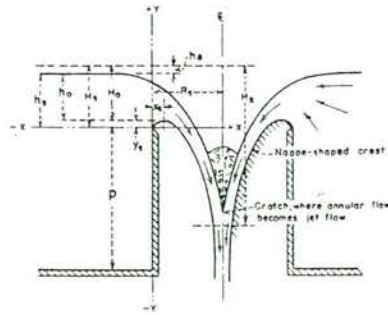
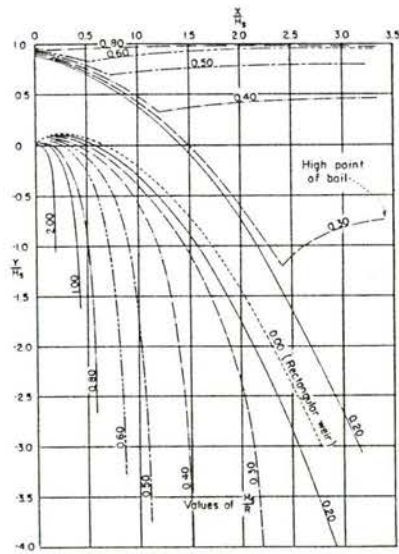


Figure 32 Discharge relation of the Morning Glory spillway at the design head, dimensionless redesign after USBR [38]



Relationship of $\frac{H_s}{H_d}$ to $\frac{H_d}{R_s}$ for circular sharp-crested weirs.



Upper and lower nappe profiles for circular weir (aerated nappe and negligible approach velocity).

Figure 33 Lower nappe profiles of the morning glory spillway, from USBR [38]

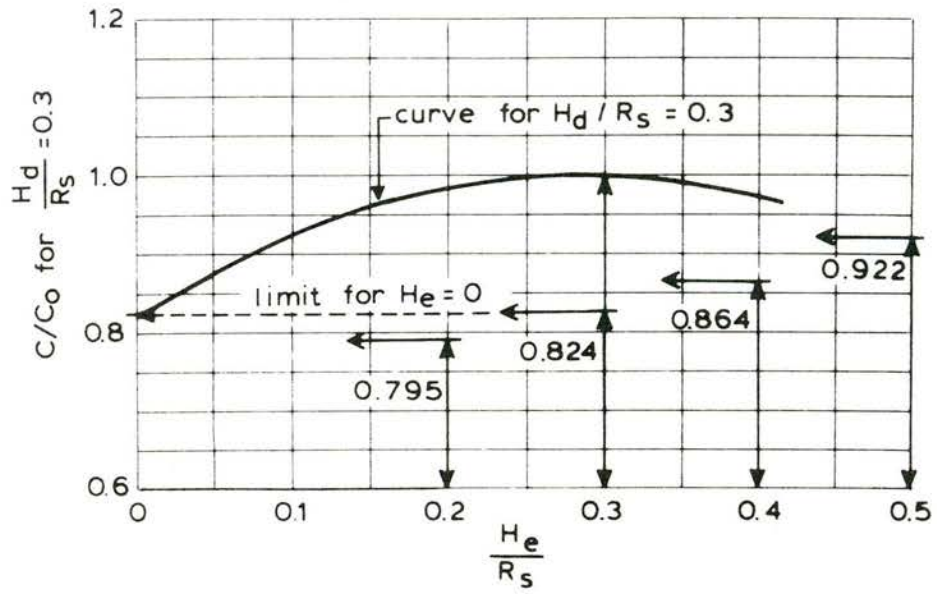


Figure 34 Reduction of crest-discharge coefficient for heads different from the design head; the curve is for $H_d/R = 0.3$ (from USBR [38])

3.7 Labyrinth weir

The labyrinth weir is used for increasing the weir length within a limited width of the opening. In the following the performance of the sharp-crested labyrinth weir is presented, following the recommendations of Hay and Taylor [16].

Figure 35 shows the Labyrinth weir in plan, and the applied symbols.

The following parameters are importance:

- L/w = Length magnification
- Q_N = Normal discharge of straight sharp-crested weir with width w
- Q_L = real discharge over labyrinth weir
- h_0 = upstream waterdepth + lmm (like eq. 43)
- p = weir height above (upstream) bottom
- α = angle of the flanks; α equals α_{\max} at a triangular shape
- S = submergence factor = h_2/h_0
- R = bottom step (downstream bottom lower)

When h_0/p is small, the extra weir length tends to be fully effective and globally $Q_L/Q_n = L/w$ within certain design limits.

The following recommendations are taken from Hay and Taylor:

- Crest-length magnification, L/w : If operation of higher head related to crest height is envisaged, then length magnification greater than 6 gives little return when designing for h_0/p ratios exceeding .25.
- Vertical aspect ratios, w/p : it is recommended that the adopted value of the vertical aspect ratio should not be less than 2 in the case of trapezoidal weirs (in plan) and not less than 2.5 in the case of triangular weirs. Nappe interference effects will be negligible on a weir designed in accordance with these recommandations. Where p is very high, the value of w/p ratio may be less than 2 providing the ratio on the head to the cycle pitch h_0/w does not exceed 0.25.
- Side-wall angle α : This factor is of primary importance in determining the performance of the labyrinth weir. Furthermore, the correct choice of the side-wall angle α does not affect the structural costs. For maximum performance, the greatest value of the side-wall angle should be adopted in the design, i.e. triangular plan-form weirs should be used wherever possible.

If the triangular plan-form is unacceptable for other reasons, a trapezoidal plan-form having a side-wall angle not less than .75 times the maximum value (given by the triangular plan form), may be used without incurring a large loss of performance.

- Channel-bed elevation differences: Downstream interference which has small detrimental effects on performance can be reduced by decreasing the elevation of the downstream channel bed, and can be completely eliminated for the operating range recommended here, if the difference in channel-bed elevation is equal to or greater than the maximum operating head.
- Aprons: Both upstream and downstream aprons are detrimental to performance. However, they may be necessary for structural reasons. In situations where a fall in the channel-bed elevation occurs on the downstream side of the weir, the size of the downstream aprons will not or nearly not affect performance, provided the channel depth at all points of the downstream channels is greater than the expected depth of flow in the upstream channel.
- Crest sections: Under high flow rates labyrinth weir discharge tends to be, to some extent, independent of the weir-crest coefficient; the use of complex, expensive crest sections is unnecessary from the hydraulic point of view.
- Submergence: Because labyrinth weirs operate under smaller head than a corresponding linear weir discharging the same quantity of water, in a situation which usually involves operations under drowned conditions the use of a labyrinth weir will increase the degree of submergence. It is not recommended that labyrinth weirs be used where they would usually be subject to operation under heavily drowned flow conditions^{*}).

It has been found by Hay and Taylor that the Villemonte equation for the effect of submergence (Eq. 45) can be applied here too:

$$Q = Q_0 [1 - (h_2/h_0)^{1.5}]^{.385}$$

Figure 36 and 37 give the discharge relations for the triangular-plan and the trapezoidal-plan labyrinth weir for horizontal bottom and for deepened downstream bottom.

* Authors comment: This is not literally true because at submerged flow a labyrinth weir placed over the whole canal width, downstream of a narrow sluice, can serve as discharge spreader.

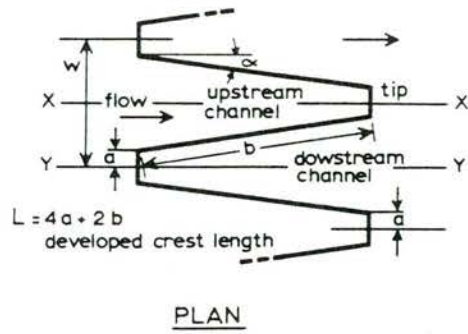


Figure 35 Labyrinth weir in plan and symbols.

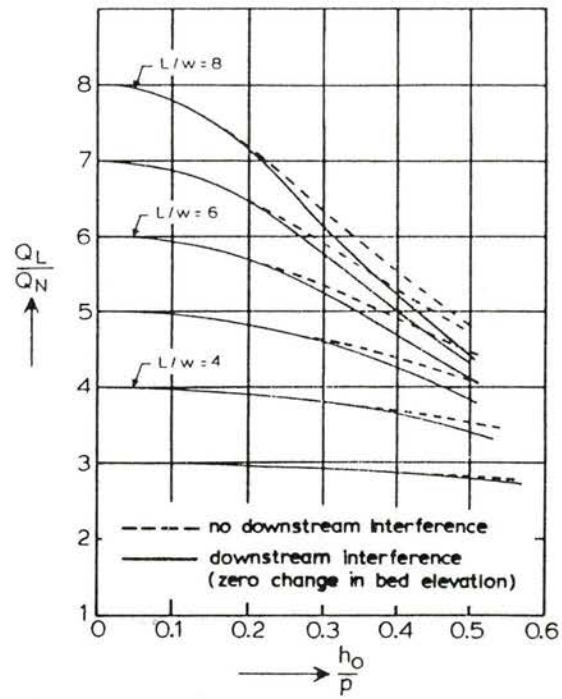


Figure 36 Discharge amplification for the triangular plan-form weirs without aprons with $w/p \geq 2.5$ and $\alpha = \alpha_{\max}$. From Hay and Taylor [16].

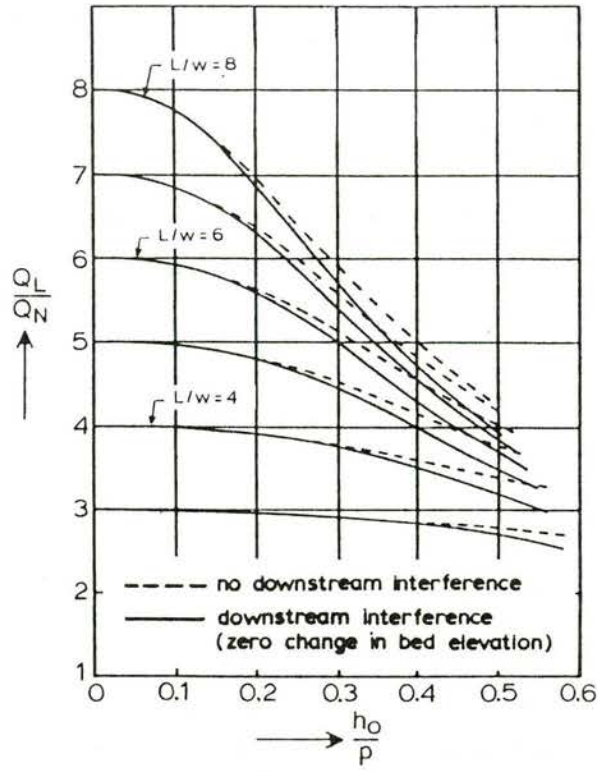


Figure 37 Discharge relation for the trapezoidal planform weirs without aprons with $w/p \geq 2$ and $\alpha = 75\alpha_{\max}$. From Hay and Taylor [16].

3.8 Gates with underflow

In this section only two-dimensional situations will be considered, without shafts and slots. In this section results from different authors duplicate, but the reason of referring to these (nearly equal) results is that they served for each of the authors as the basis for further analysis; therefore, it was considered only fair to present also the results from where they started.

When the upstream energy head is H_0 and the pressure head just downstream of the gate is h_1 , then the Bernoulli equation leads to the following discharge equation.

$$q = C_c a \sqrt{(2g (H_0 - h_1))} \quad (61)$$

C_c is the contraction coefficient of the jet, a is the gate opening. In the case of the free jet the downstream pressure head h_1 equals $C_c a$. The flow contraction depends on the geometry: this results in an influence of D/a in the case of a culvert with height D or, at free surface flow, of h_0/a (where h_0 is the upstream waterdepth). But the flow contraction also depends on the pressure distribution at the top of the jet contraction. When the jet is submerged the piezometric head there is constant; at a free jet the pressure itself is constant (atmospheric). The influence of the gravity can then be expressed in terms of the Froude number.

$$Fr = V_c / \sqrt{(g C_c a)} \quad (62)$$

(V_c is the velocity at the jet contraction)

When Fr is great enough the gravity influence disappears and the submerged and the free flow have the same contraction. This is found both in the theoretical study of Rouvé and Khader [33] and the experiments of Nago [23] presented hereafter.

When the upstream water has a free surface, the Froude number and the upstream waterdepth are coupled and C_c can then be expressed in terms of h_0/a only. At free outflow from a culvert C_c depends on both D/a and the Froude number, as shown in Figure 38.

The C_c can be derived theoretically, as for instance published by Rouvé and Khader [33]. Friction effects are neglected in the derivation. The interesting presentation of Figure 38 is not directly suitable for practical use

because the C_c value and the discharge are both needed to calculate the Froude number, and then C_c depends on this Froude number. In a design graph the relation a/D , a/d_c and a/H_0 should have been presented (d_c = critical depth, H_0 = energy upstream). A global check consists of recalculating at different points in Figure 39a the Froude number and the contraction coefficient C_c and comparing these results with Figure 38: no deviations were found.

When the contraction coefficient is known, the free flow discharge can be expressed theoretically by application of the Bernoulli equation as in Eq. 61.

From dimensional consideration it can be seen that Eq. 61 and the influence of the Froude number can be combined in a single presentation.

$$q = C_d a \sqrt{2gH_0} \quad (63)$$

C_d is a discharge coefficient.

But in general the following expression is used:

$$Q = C_d w a \sqrt{(2g h_0)} \quad (64)$$

It can be theoretically proved, see section 1.5 Eq. 8, that the discharge coefficient C_d of Eq. 64 equals:

$$C_d = C_c / \sqrt{(1 + C_c a/h_0)} \quad (65)$$

The advantage of the use of Eq. 64 and 65 over Eq. 61 is that no iterative procedure is needed; from C_c and a/h_0 the q can be computed.

Cozzo [9] investigated the contraction for sector gates and flat gates with free surface flow and found systematically that the angle near the edge was determinative for the discharge coefficient (Figure 39a). The flat gate and tainter gate show the same results. Figure 39b, derived from the curves of Figure 39a, shows the discharge related to the upstream energy head.

In Figure 40 the discharge relation for free flow is presented for a tainter gate located in a roofed culvert with free outflow, from WES [43]. The upstream pressure is expressed in terms of an energy head in the culvert. In fact, it is the contraction coefficient which is presented in Figure 40.

From the modular flow relations of Cozzo the limiting conditions for which the downstream water level does not affect the modular flow discharge is presented in Figure 41. This relation is found by calculating the contraction coefficient C_c from the discharge coefficient C_d (the inverse of Eq. 65), and then calculating the conjugate depth of the hydraulic jump. The C_c is from $h_0/a = 2$ on nearly constant.

In Figure 42 are presented calculations and measurements of the submerged discharge relations at a vertical sharp-edged gate plate. The measurements of Henry are found in Rouse [31], and are also discussed in Naudascher [24].

The results of the computations presented by Rouse/Naudascher [24, 31] were based upon the theoretical values of the contraction coefficient similar to the ones presented in Figure 38.

Discrepancies were found which were attributed to disturbances like uneven flow distribution, and so on. The author performed new computations, presented in Figure 42, based upon slightly smaller C_c values (see Figure 42 also), and he found a fairly good agreement with the measurements. The use of adapted C_c values is useful when the discharge relations of complete structures are performed with the computer program of Chapter 2.

There exist also measurements which are in agreement with these lower values. For instance, Naudascher [24] presents similar measurements as the ones of Cozzo, but then from Gentilini. These results have for great h_0/a (about 12) values a C_d of 0.585, corresponding with a C_c of about 0.6.

Nago [23] performed a very systematic research on the free flow characteristics of different types of gate edge. He distinguishes also, as it was presented by Rhov e and Khader in Figure 38, a flow contraction plus an effect induced by gravity. Because Nago only considered free surface flow the results are simpler. The contraction coefficient he obtained theoretically. He presents the effect of gravity as a correction which can be added to the contraction coefficient at submerged flow. The correction is a function of a/h_0 (Figure 44). The calculated discharge coefficients are compared with measurements, Figure 46.

The results for the three gate types of Figure 44 are presented in Figure 45.

Boiten [6] investigated vertical plates with round edges at underflow conditions. The shapes are presented in Figure 47. The discharge relations presented in Figure 48 show that all the circular shapes have the same

discharge coefficient. It is observed that from h_0/a being about 2.5 that this parameter has nearly no influence on the contraction coefficient of the investigated circular shapes. At smaller values this parameter has an important effect but measurements are then also scattered, due to air-entrainment.

The discharge coefficient can be much higher for the rounded edge than for the sharp-edged gate. It is remarkable that Boiten found a contraction coefficient for the sharp-edged gate which is higher when compared to the results presented above.

The results of a series of tests of reversed Tainter gates in completely submerged culverts (Pickering [27]) with and without divergence in the downstream culvert part, are presented in Figure 49 and 50. This is in this part of the manual one of the few cases which represents internal flow. But the reversed tainter valve is typically in use in a hydraulic structure (high head navigation lock) and nowhere else.

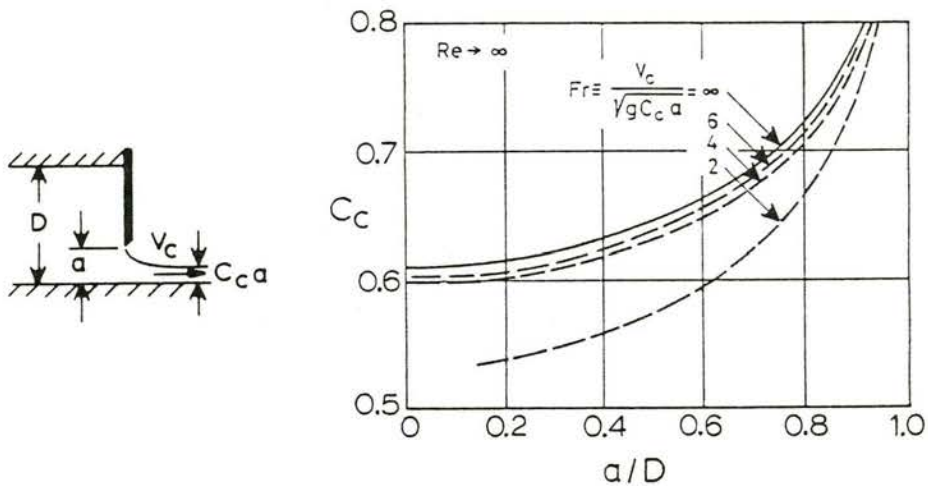


Figure 38 Contraction as function of Y_1/a and Froude number, from Naudascher [24] and after Rouve and Khader [33]

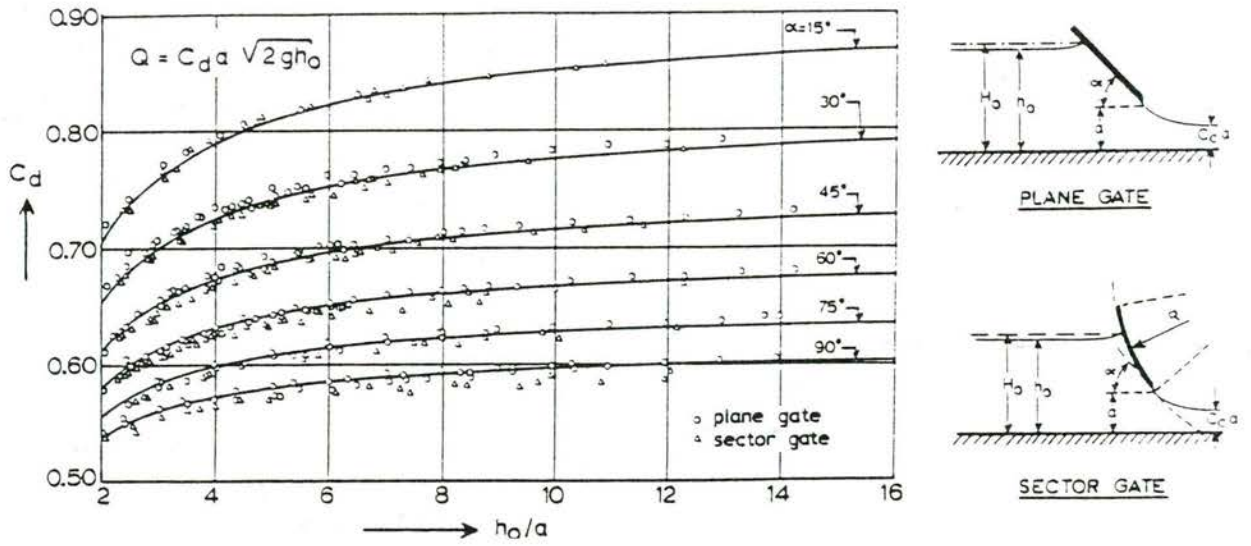


Figure 39a Discharge coefficient for free outflow as function of plate angle at the edge, from Cozzo [9]

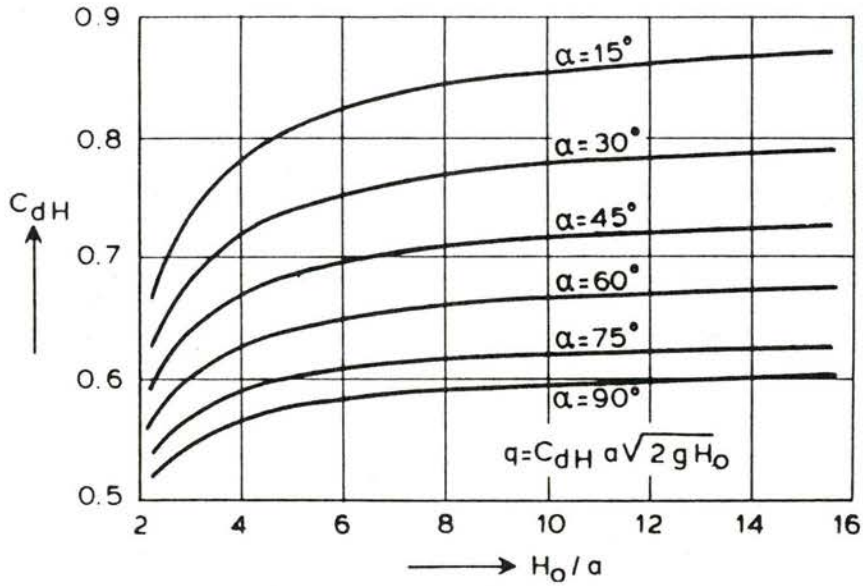


Figure 39b Discharge coefficient related to the upstream energy head, derived from Figure 39a

basic equation
 $Q = C_d G_0 B \sqrt{2gH}$

where:

- Q = discharge
- C_d = discharge coefficient
- G_0 = gate opening
- B = width of gate opening
- H = energy grad. elev.
 - (invert elev. + $C_d G_0$)

Remark: in this definition
 C_d equals the flow contraction coefficient in eq. 7 and 65

LEGEND

- von Mises (computed)
- Garrison model

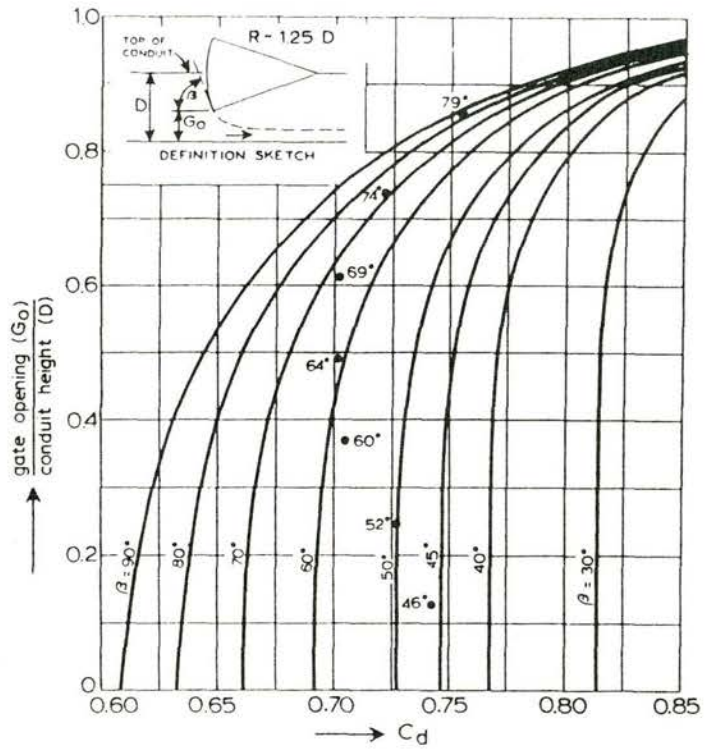


Figure 40 Discharge coefficient for free outflow of a tainter gate in a roofed culvert, after WES [43]

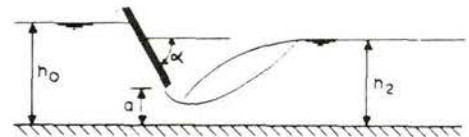
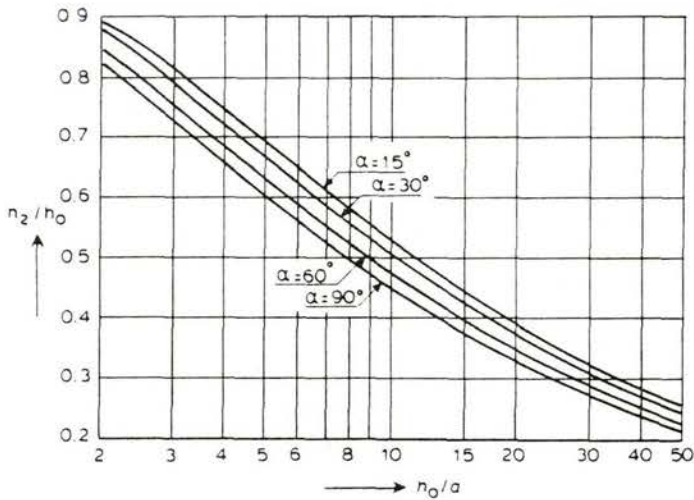


Figure 41 Limit condition of modular flow derived from the discharge relations of Cozzo (Figure 39a)

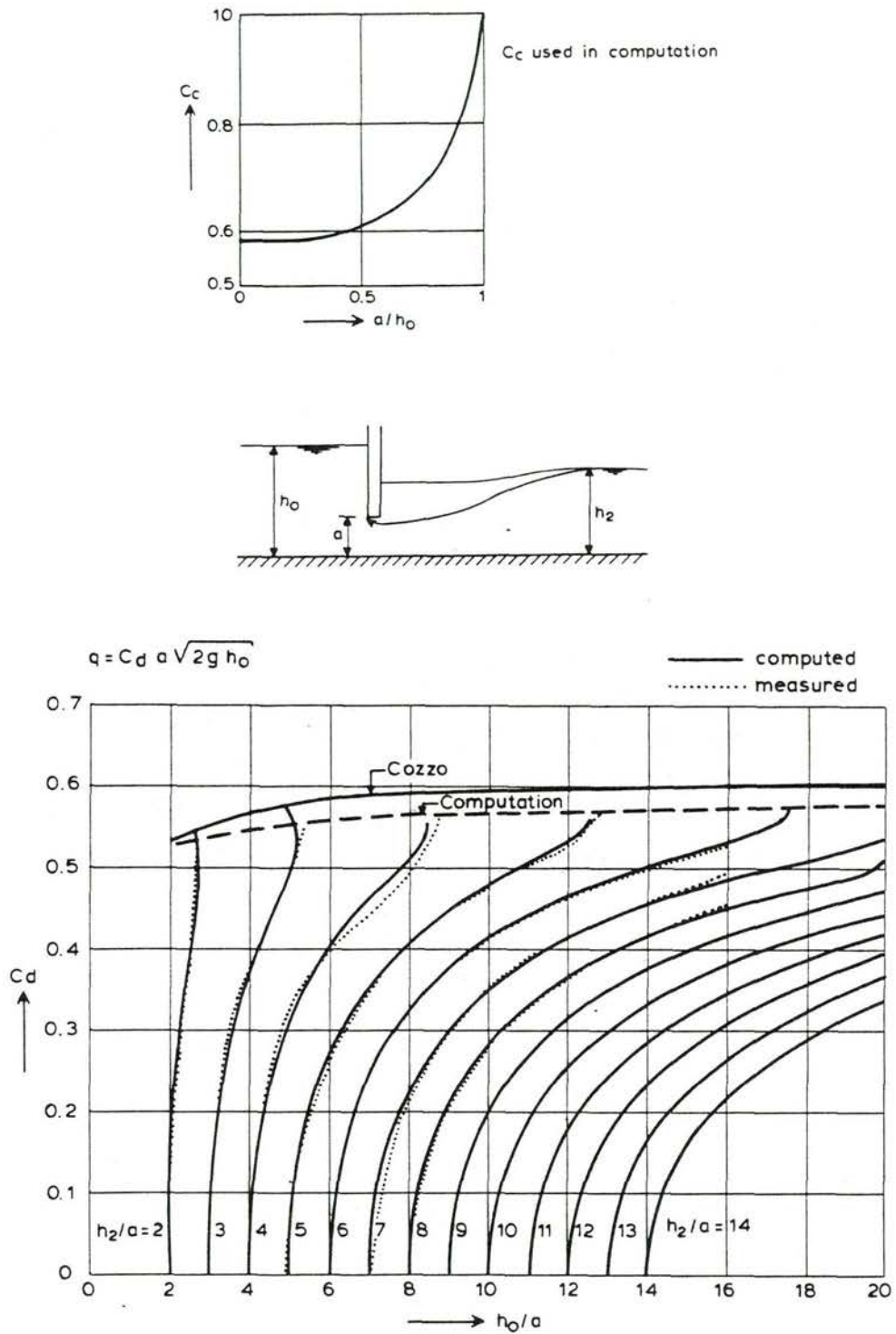


Figure 42 Discharge relation for submerged flow of a sharp-edged vertical plane gate, calculated with a best-fit relation for the contraction coefficient compared to measurements by Henry, as indicated in Rouse [31]

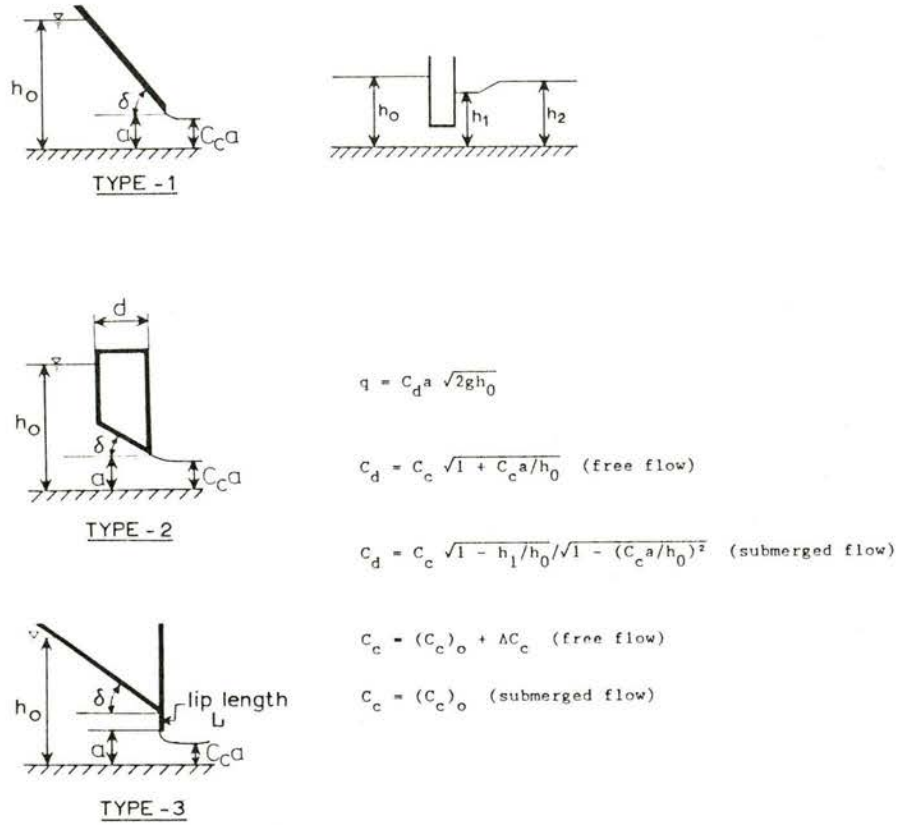


Figure 43 Type of gate edges investigated by Nago and notations [23]

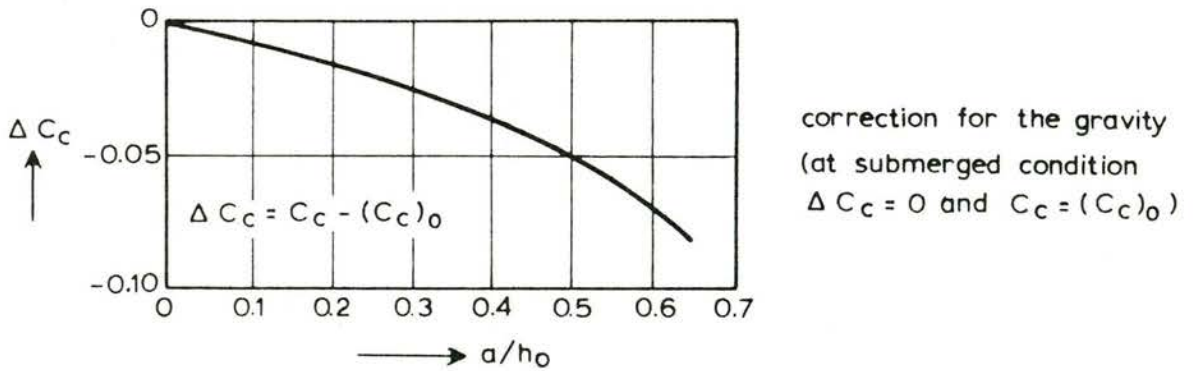


Figure 44 Correction coefficient for gravity effects on the contraction, from Nago [21]

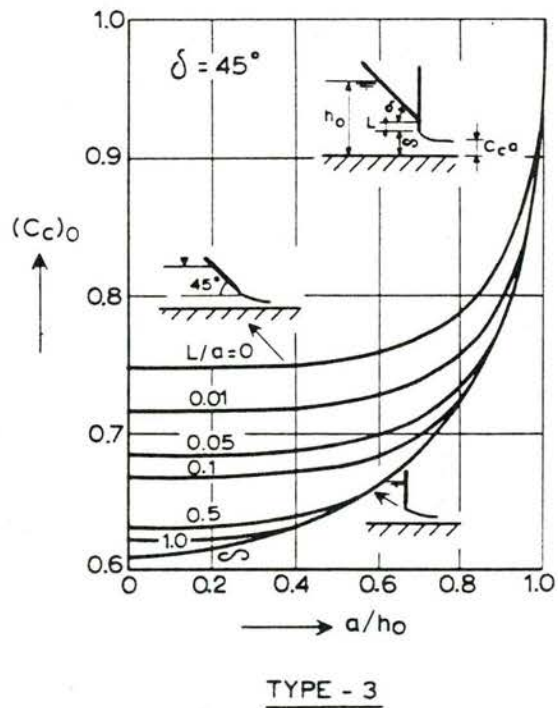
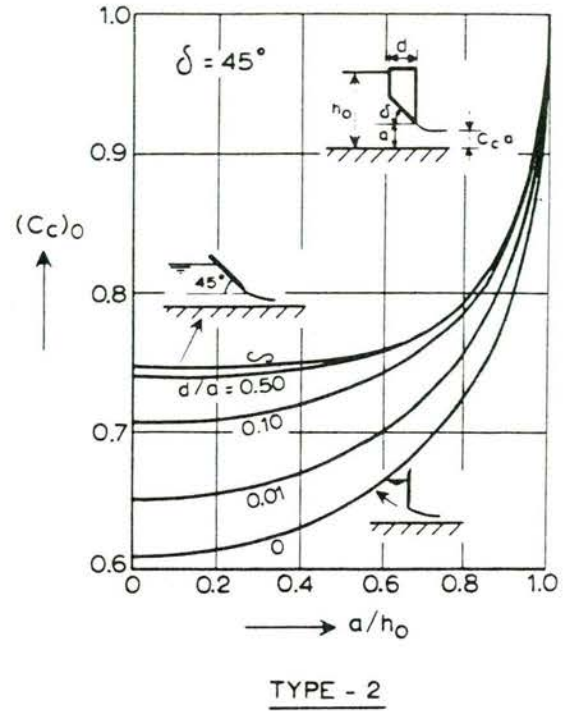
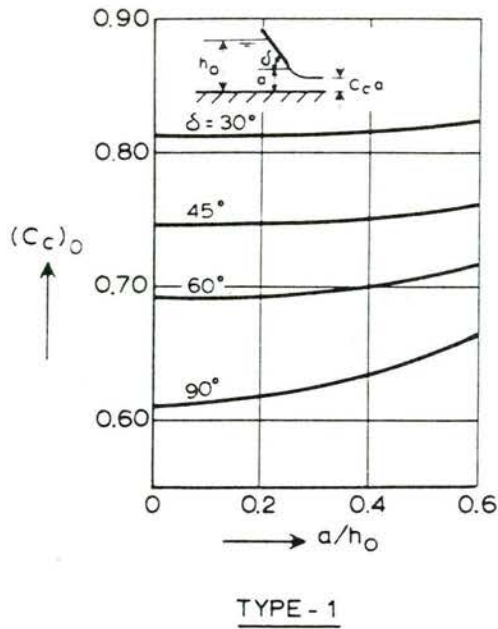
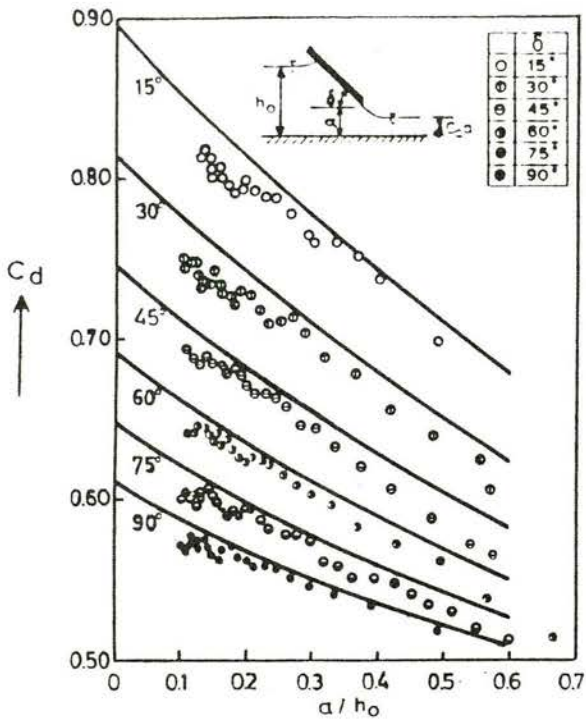
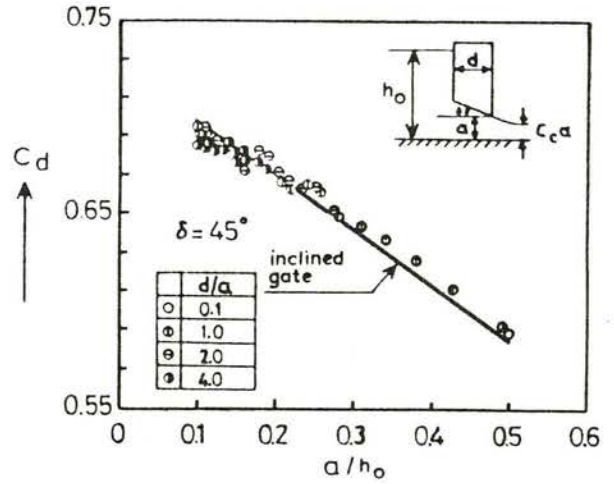


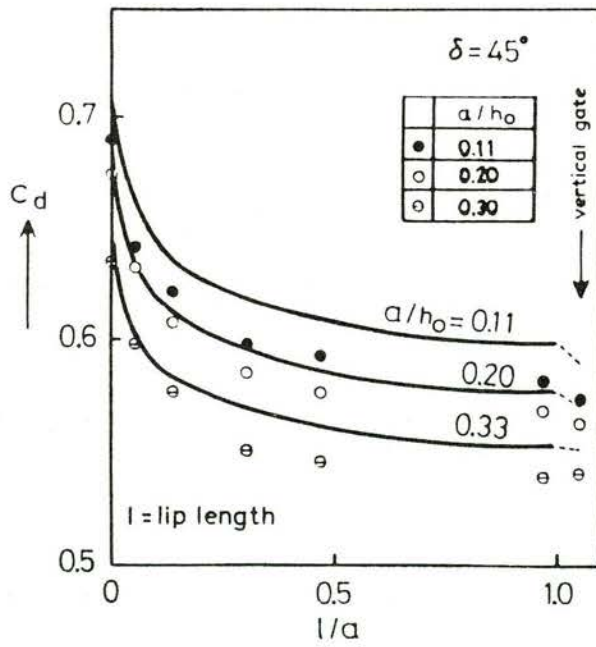
Figure 45 Contraction coefficients without gravity correction, from Nago [23]



TYPE - 1



TYPE - 2



TYPE - 3

Figure 46 Discharge coefficient compared with measurements, from Nago [23]

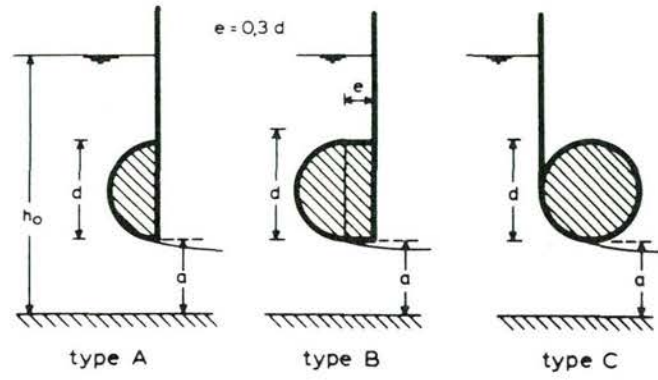
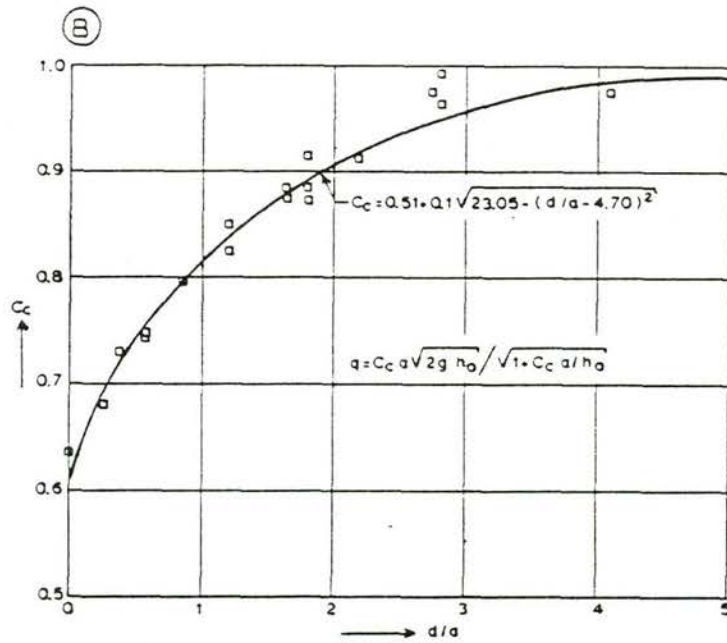
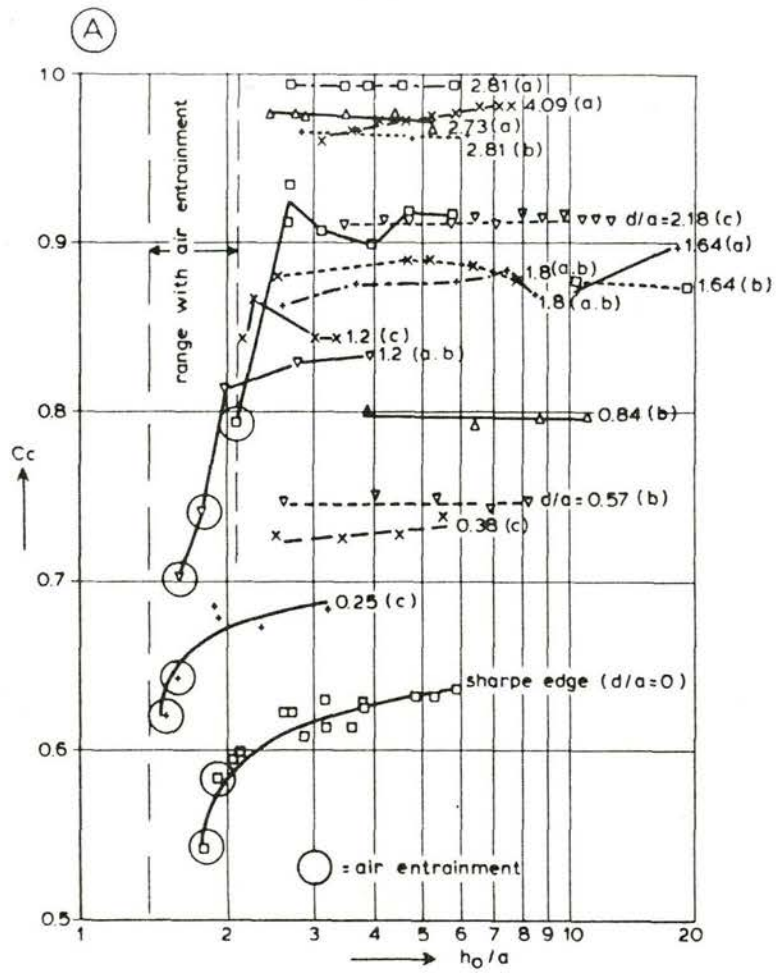


Figure 47 Shape of round edges as investigated by Boiten [6]



Limit values of C_c from Fig. A

Figure 48 Discharge relations for round-edged gates [6], A measurements and B the proposed relation

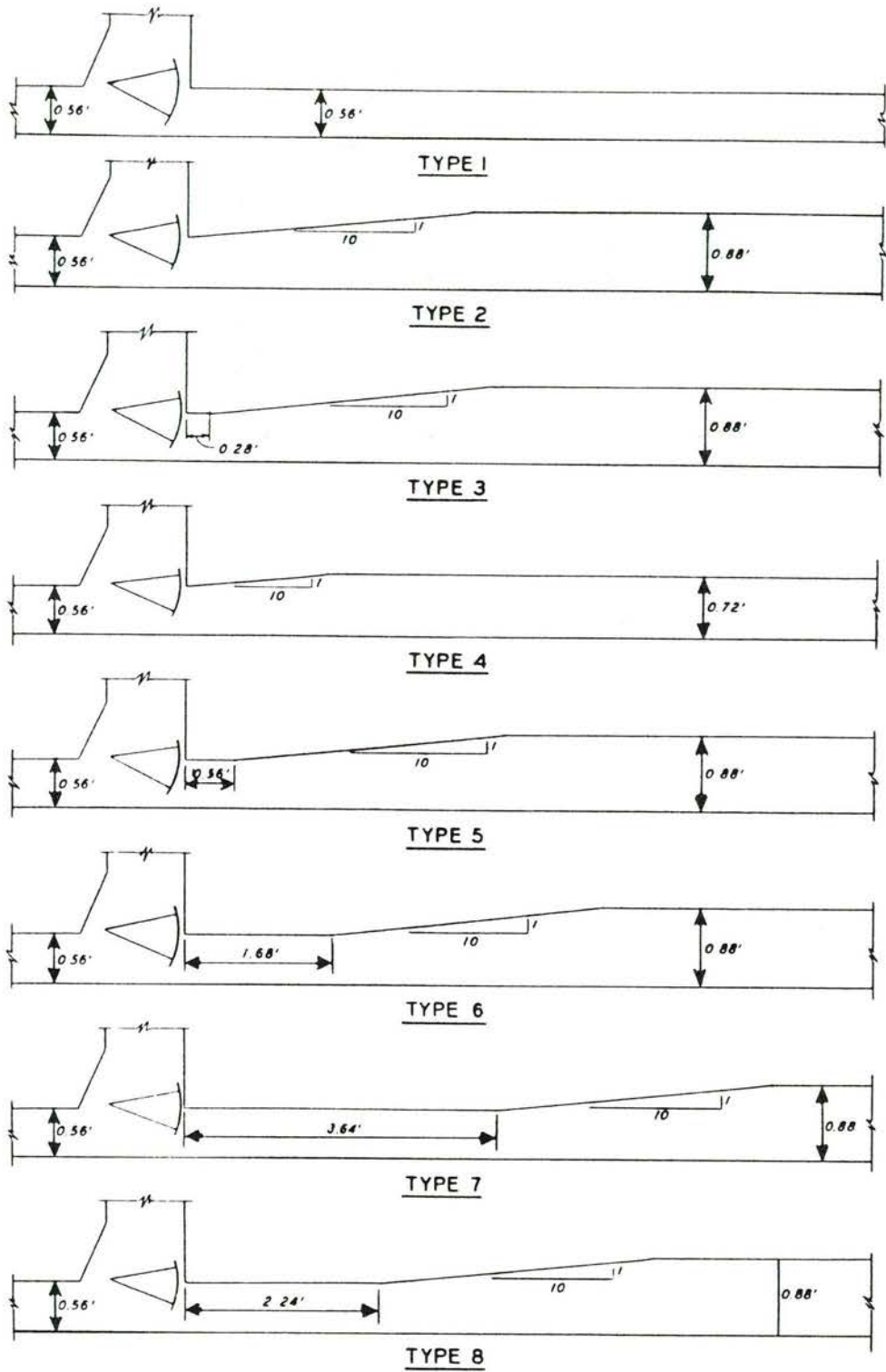


Figure 49 Culvert configurations with expansions and reversed tainter valve investigated by Pickering [27]

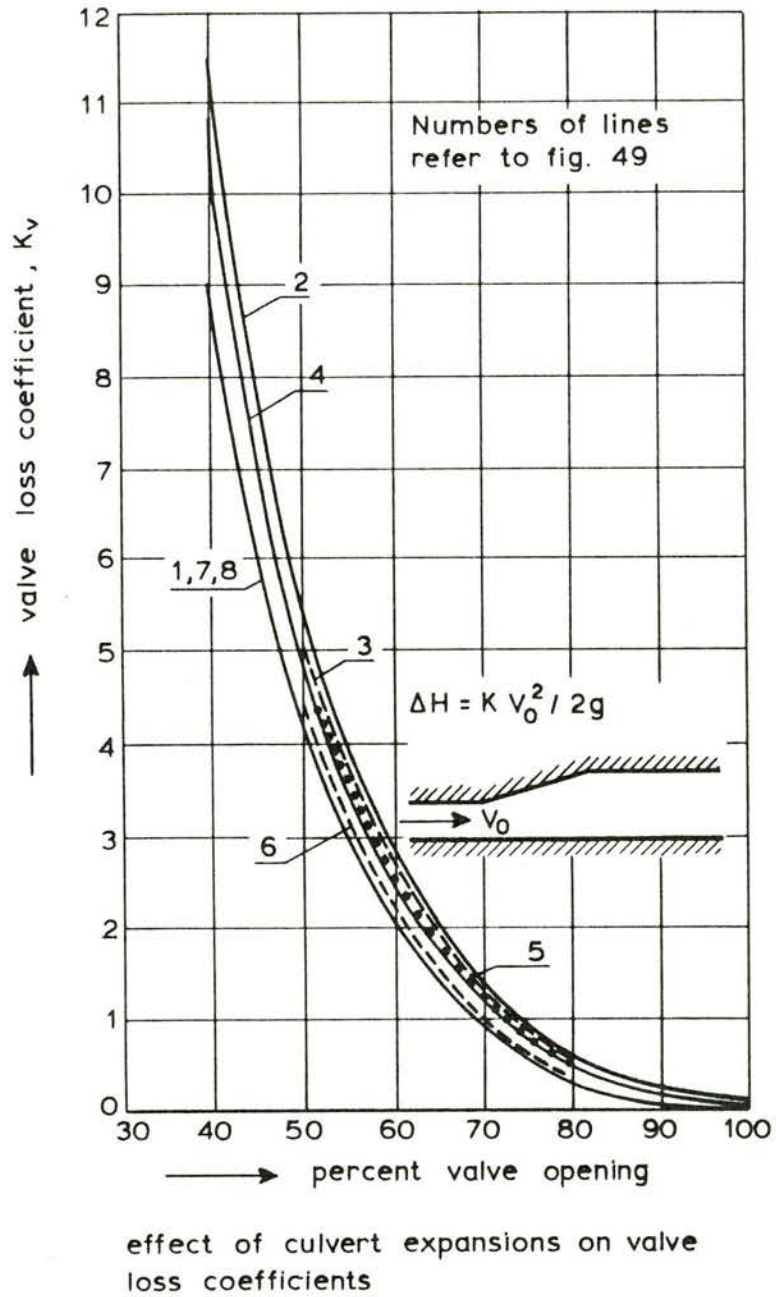


Figure 50 Energy loss of reversed tainter valve in culverts with and without divergence, with submerged flow, from Pickering [27]

3.9 Gates with overflow

Two examples of discharge relations of overflowing gates are presented, the drum gate in Figure 51 and the flap gate in Figure 52. The discharge coefficients refer to the following equation:

$$q = C_d (2/3) \sqrt{(2g)} H_o^{3/2} \quad (66)$$

Results of a model investigation of a flap gate on top of a vertical (Stoney) gate are presented in Figure 53. The angle α was varied between 27 and 68 degrees. As reference the results of Sarginson are also presented (see section 3.2).

As for other gate types it might be that, depending on the crest shape, some discharge data presented in section 3.1, 3.2 or 3.3 can also be used for overflowing gates.

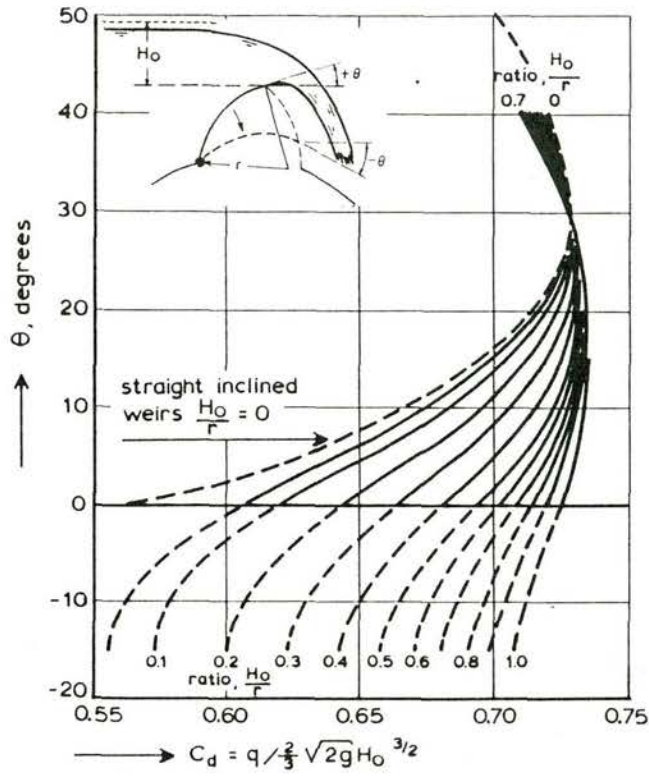


Figure 51 Discharge coefficient of a sector-shaped raising drum gate, from Ven Te Chow [40] referring to original work by Breadyly [8]

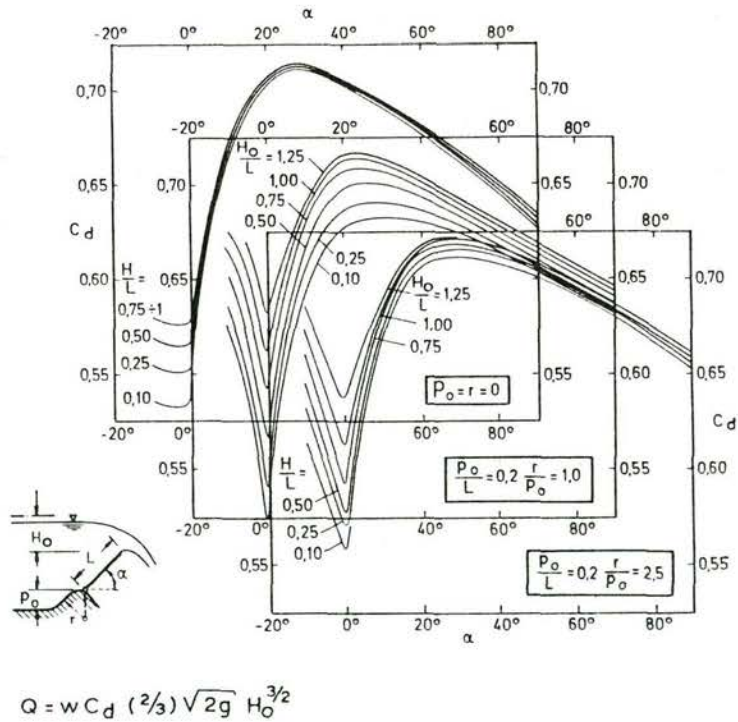


Figure 52 Discharge coefficient of a fully aerated flat-flap gate, from Naudascher [24] referring to original work by Böss.

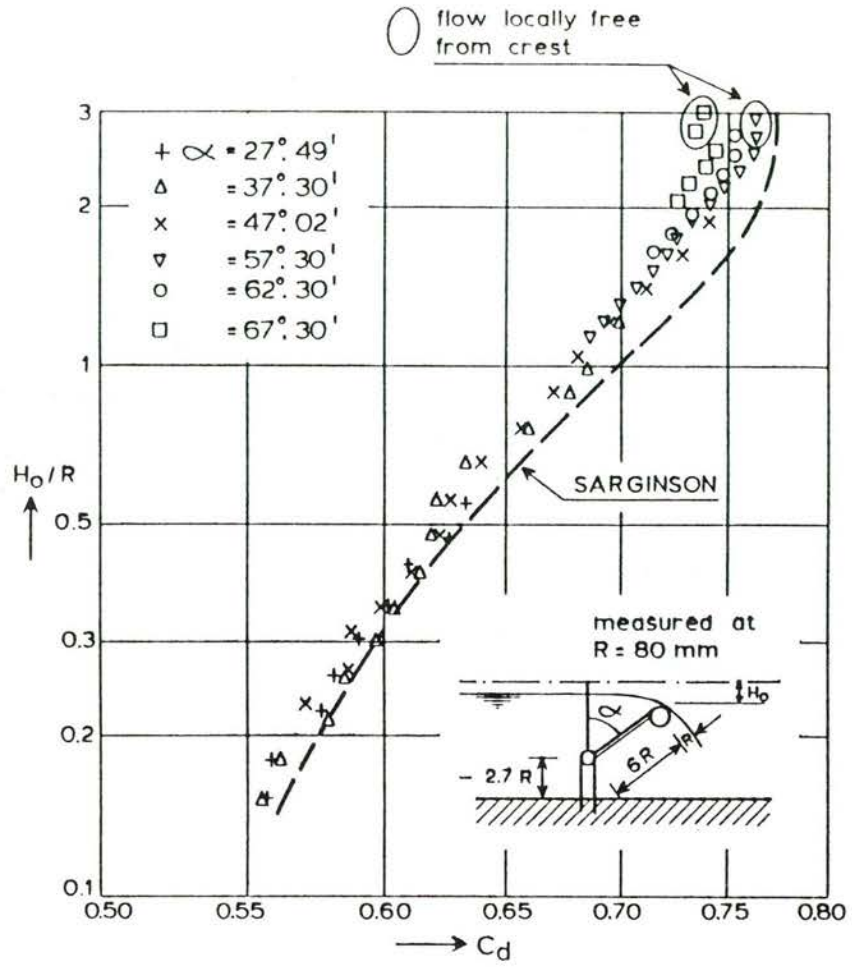


Figure 53 Discharge coefficient of a flat-flap gate with circular crest, from Boiten [5]

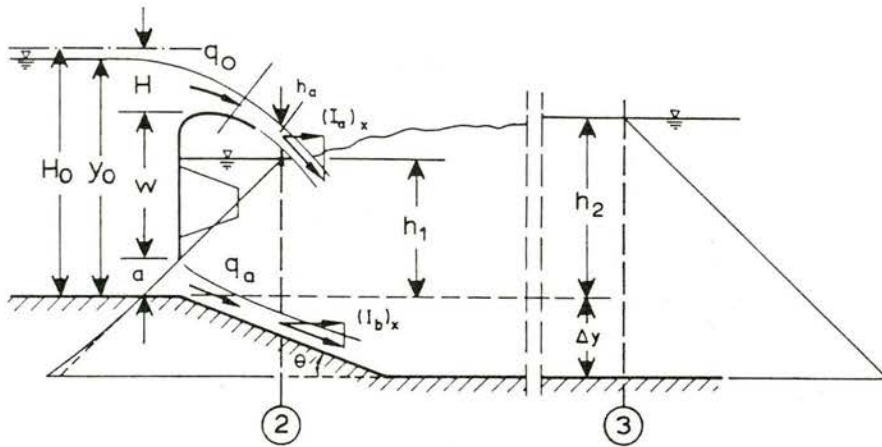
3.10 Gates with combined under- and overflow

The discharge relation of gates where simultaneously over- and underflow occurs, is not fundamentally different from the situation where only one of the two occurs. Whether the situation is suitable for an estimate of the discharge depends on how exactly the conditions just downstream of the gate are known. The overfall nappe should be fully aerated, but that is also the case for nappe flow without underflow.

Naudascher [24] discusses an example of a calculation where the momentum equation is applied downstream of the gate under the assumption that just downstream of the gate hydrostatic pressure occurs, even at the sloping bottom. This is only justified when no recovery of potential is to be expected.

Figure 54 shows the conditions, the symbols and the momentum equation as it was applied to compute the water-level difference ($h_2 - h_1$). The coefficients C_a and C_c related to the nappe and the jet respectively, follow from the nappe thickness (in vertical sense) at the end of the gate crest and the contracted jet thickness (contraction is about equal to the discharge coefficient).

Figure 55 shows the computed results compared to measurements.



$$\frac{\rho g}{2} (h_1 + \Delta y)^2 - \frac{\rho g}{2} (h_2 + \Delta y)^2 = \rho \frac{(q_0 + q_a)^2}{h_2 + \Delta y} - \rho \frac{q_0^2}{C_a H} - \rho \frac{q_a^2}{C_c a}$$

Figure 54 Application of momentum equation at combined overflow and underflow, from Naudascher [24]

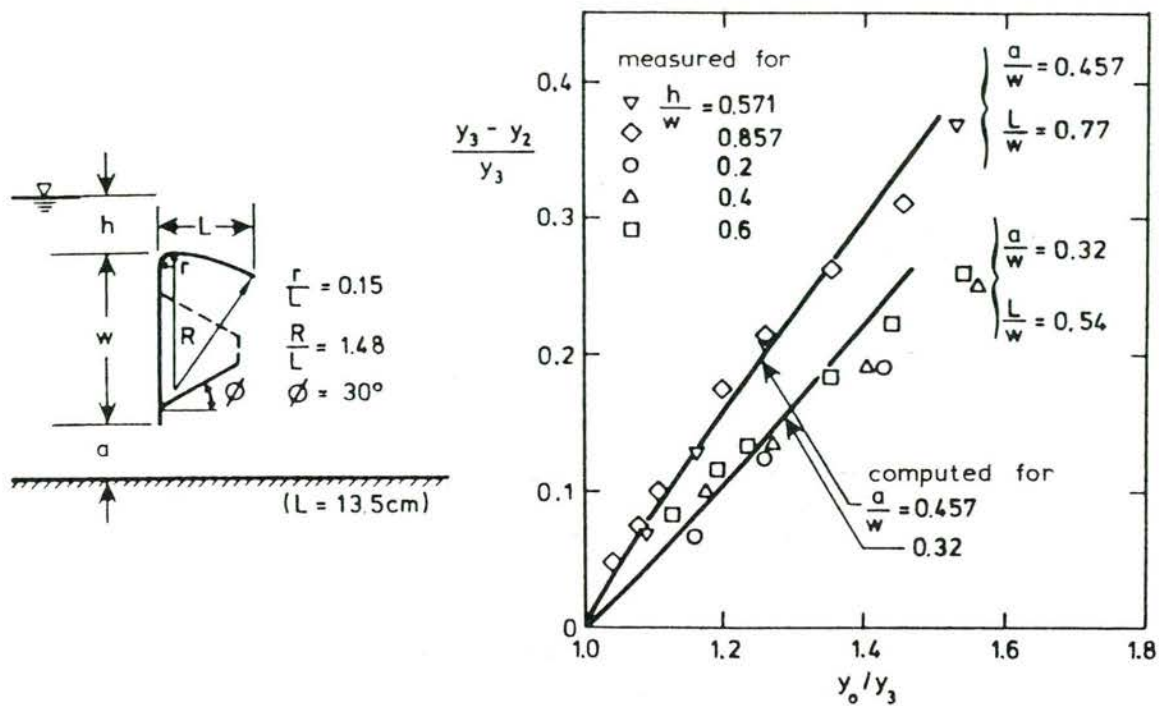


Figure 55 Difference in water level near the gate and further downstream; calculated and measured, from Naudascher [24]

3.11 The Howell Bunger valve

A Howell Bunger valve (also called hollow-jet valve or cone valve) is applied at the downstream end of a tunnel. It has the function of spreading the jet. There is also a very good aeration and hence the cavitation risk is reduced. The spreading of the jet is favourable for the stilling basin. The central cone is fixed to the pipe through supports which are internal vanes. The cylinder which moves around the pipe is the valve, see further Figure 56.

Gieseke [14] performed the theoretical study on the discharge relations of the Howell Bunger valves and compared the results with measurements. He applied potential flow theory and assumed radial symmetrical flow. The gate opening (S/D), the cone angle (2α) and the cone diameter ($D-2b$) was varied (see Figure 56).

For $\alpha = 45^\circ$ and $b = 0$ the computations were verified with different experiments, which showed a good agreement (Figure 58). Figure 57 shows the results of the computations with systematically varied parameters. The C_t values are discharge coefficients related to the tube section and not to the gate opening.

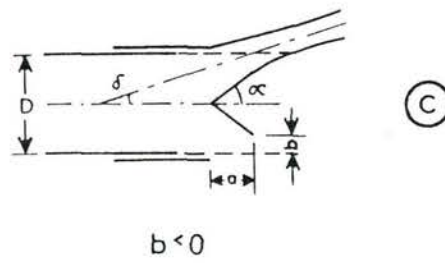
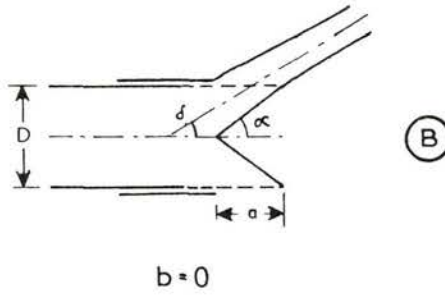
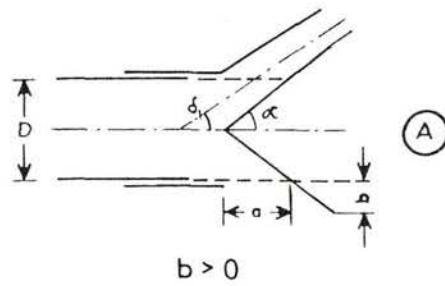
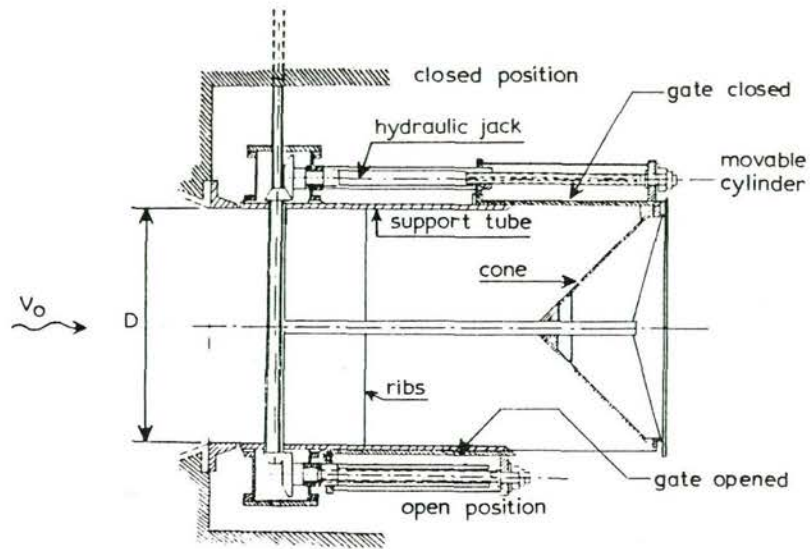


Figure 56 The Howell Bungler valve and the schematisations investigated by Gieseke [14]

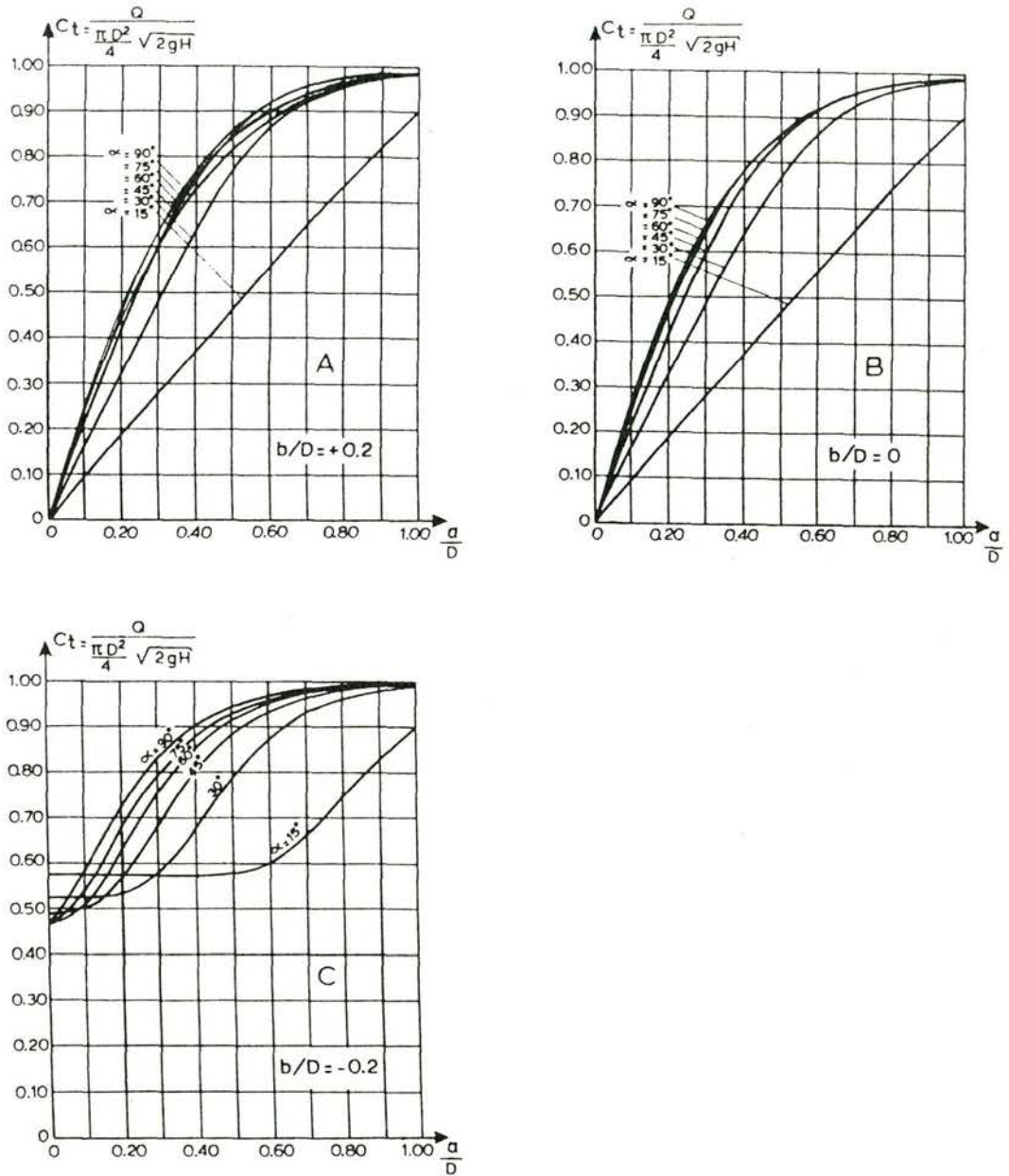


Figure 57 Discharge relations of the Howell Bunger valve for $b/D=0$, for $b/D = -0.2$ and for $b/D = +0.2$, from Gieseke [14].

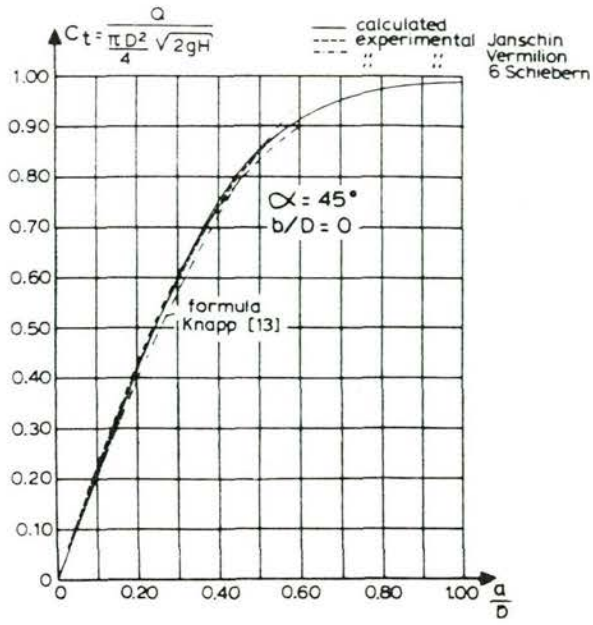


Figure 58 Comparison of calculated values with experiments, from Gieseke [14]

3.12 Conduit outlet

The free flow loss of the conduit outlet depends on the Froude number similarly to a gate with underflow at free flow conditions (section 3.8). If the water in the fully filled conduit flows into the air, the discharge capacity of the whole tube depends on the level at which the atmospheric pressure can be assumed to act. At high discharge (great Froude number) the influence of the gravity tends to disappear and the centre of gravity of the pipe section should be taken as pressure head. Figure 59 shows results for a circular conduit, published by the US army Waterways Experiment Station [43].

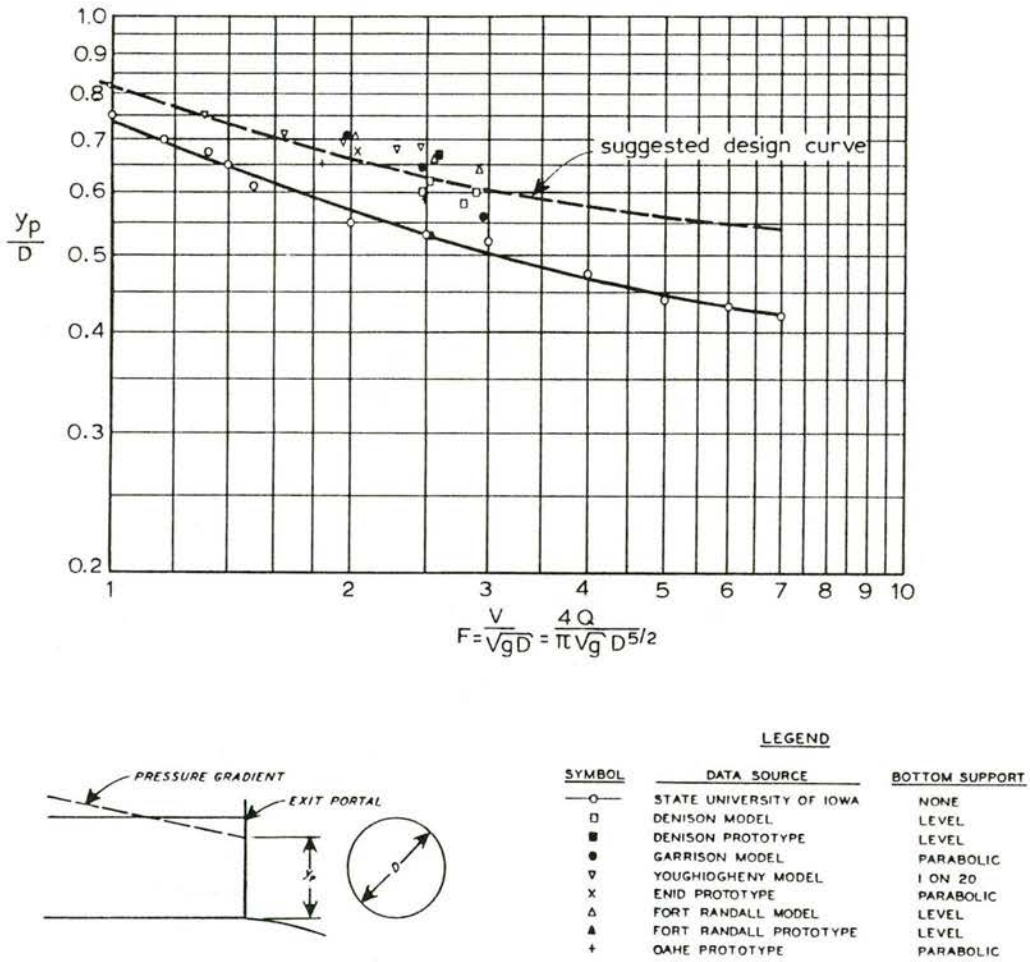


Figure 59 Level at which the pressure head is zero, at a circular conduit exit, from WES [43].

4. LOSSES OF COMPONENTS UP- AND DOWNSTREAM OF THE CONTROL SECTION

4.1 Orifice and intake losses

When the flow contraction is known, both orifice and intake (or entrance) losses can be calculated with the momentum equation in the region downstream of the section with maximum flow contraction (assuming hydrostatic pressure at this section). Or, at submerged flow, the Carnot equation can be applied. The flow-contraction coefficient in the orifice or in the entrance is C_c with an average velocity in the contraction V_m and a culvert velocity V_c downstream (Figure 60). Now introducing for the average flow velocity in the orifice V_o the Carnot equation is:

$$\Delta H = (V_m - V_c)^2 / 2g = (V_o / C_c - V_c)^2 / 2g \tag{67}$$

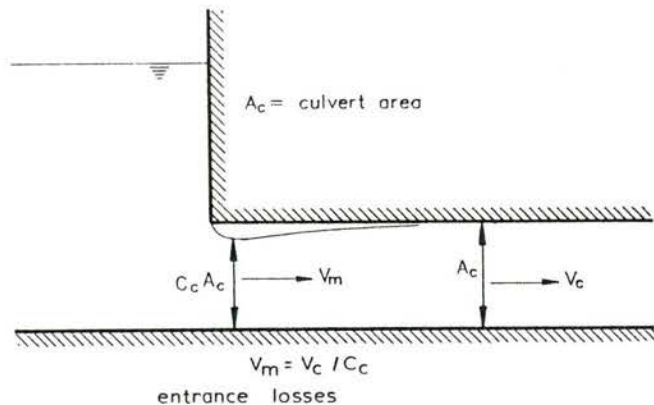
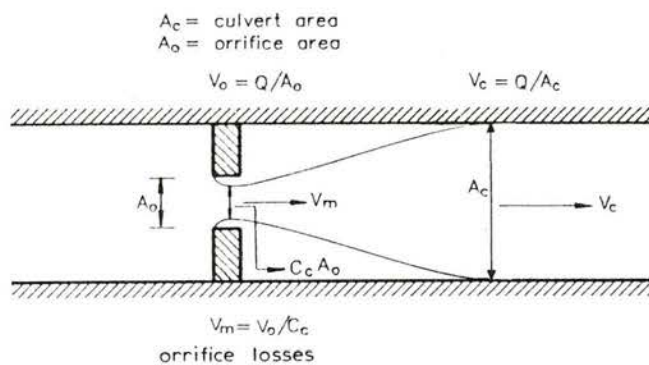


Figure 60 Orifice and entrance losses

When the culvert is wide, compared to the orifice, the influence of V_c can be neglected. When the culvert section is not widening (intake condition) then $V_c = V_o$ and the entrance loss becomes:

$$\Delta H_e = K_e V_c^2/2g = (C_c^{-1} - 1)^2 V_c^2/2g \quad (68)$$

The flow contraction coefficient C_c is derived from the orifice tests presented in USBR [38] and shown in Figure 61, series 1. The conversion from the discharge coefficient C from Figure 61 to the contraction coefficient C_c is done as follows:

At low velocities (low Froude number) it can be derived that:

$$\Delta h \approx \Delta H$$

The discharge relation of Figure 61 can be read as:

$$\Delta H = Q^2/C^2 A^2 2g$$

From (67) it follows that:

$$\Delta H = (V_o^2/2g)(C_c^{-1} - A/S)^2 = (Q^2/A^2 2g)(C_c^{-1} - A/S)^2$$

Combining the two expressions for ΔH :

$$C_c = C S/(S + CA) \quad (69)$$

From the contraction coefficient the entrance-loss coefficient of a long culvert can be derived by using Eq. 68:

$$K_e = (C_c^{-1} - 1)^2 \quad (70)$$

From the C_c values presented in Figure 61, the K_e values of a culvert become:

$$C_c \quad 0.56 \quad 0.58 \quad 0.61 \quad 0.69 \quad 0.83$$

$$K_e \quad 0.62 \quad 0.52 \quad 0.41 \quad 0.20 \quad 0.04$$

The discharge coefficients of Figure 61 clearly show that the discharge coefficient C will increase when the culvert length increases. This is caused by the spreading of the jet into the culvert (two-step flow expansion) resulting in outlet loss reduction. The small value of C_c for a sharp-edged orifice is in agreement with other experiences.

Figure 62 is an example showing an inlet of a sloped culvert which can remain partially filled with air or become fully submerged, only depending on the shape of the entrance and H/D . In the case of the sharp-edged entrance there is a control section formed at the inlet and due to the sharp edge the flow section is largely reduced. These elements affect the discharge capacity much. The line for the full culvert is only an example, the real discharge curve depends on the culvert slope, the culvert length and maybe the presence of air caused by vortices.

Figure 63 shows the sharp-edged box culvert inlet with a discharge behaviour similar to the sharp-edged condition of the circular culvert of Figure 62.

The discharge formula which is used in Figure 63 is:

$$Q = C_d w D \sqrt{(2gh)} \quad (71)$$

where h is the height of the upstream water level above the bottom, D the culvert height and w the culvert width. The expression (71) is similar to the one that is often applied for gates (see Equation 64). The results are comparable as well. (Figure 39 and 46).

Figures 64 to 66 show intake losses of concrete culverts. The section where the gates are located is used as reference culvert section.

It can be seen that the nicely-shaped inlet of Figure 64, upper part without slots, piers etc. has the lowest intake-loss coefficient, namely 0.16. For other conditions the loss coefficients vary between 0.2 and 0.8. The losses in hydraulic models all seem to be lower than in prototype; an explanation was not found in the reference [43]. Piers, slots, support beams, etc. they all are elements that influence the hydraulic losses.

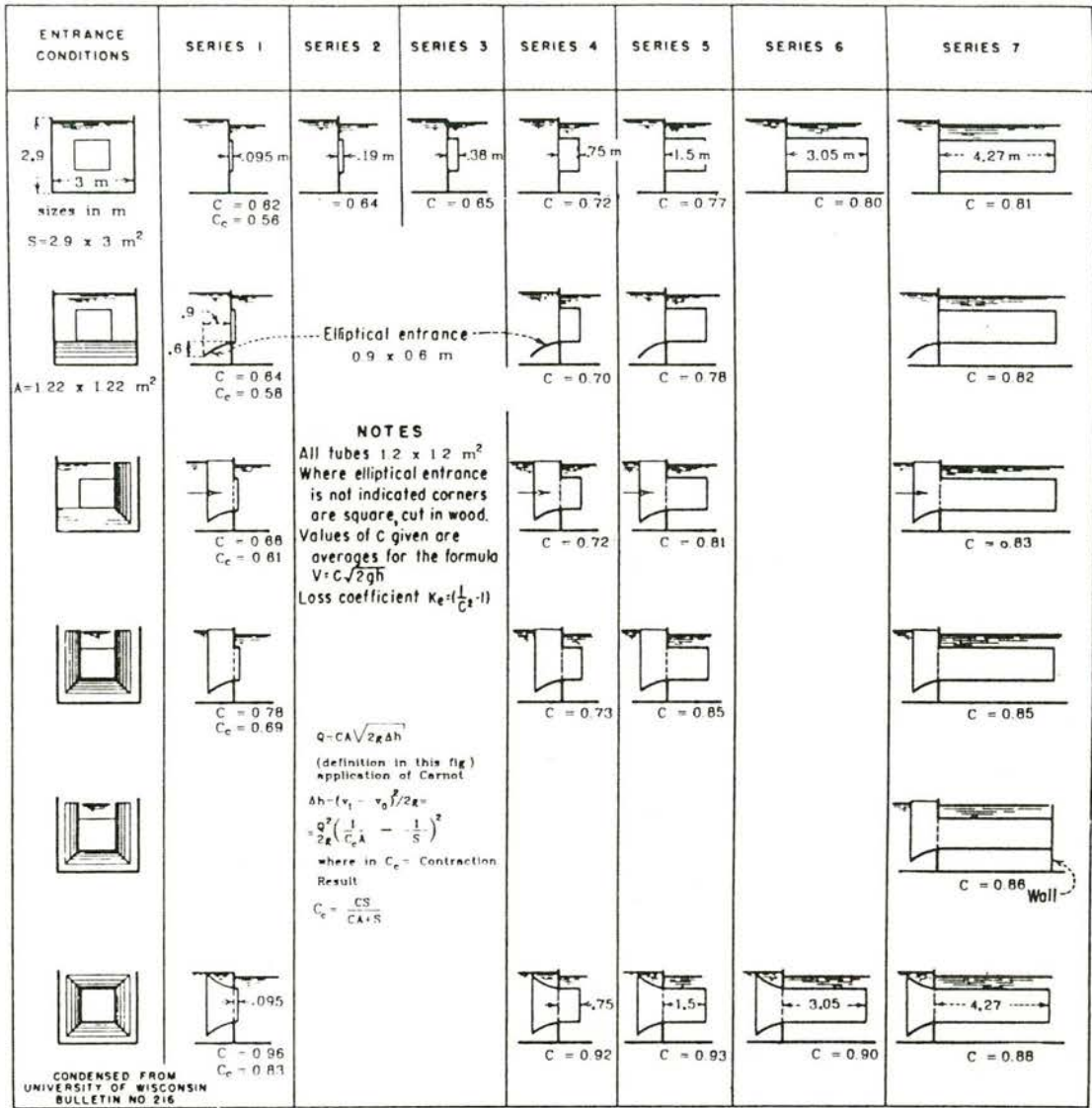


Figure 309. Flow through submerged tubes. 288-D-2531.

Figure 61 Discharge coefficients of submerged rectangular orifices without and with tubes, from USBR [38], and their derived contraction coefficients C_c .

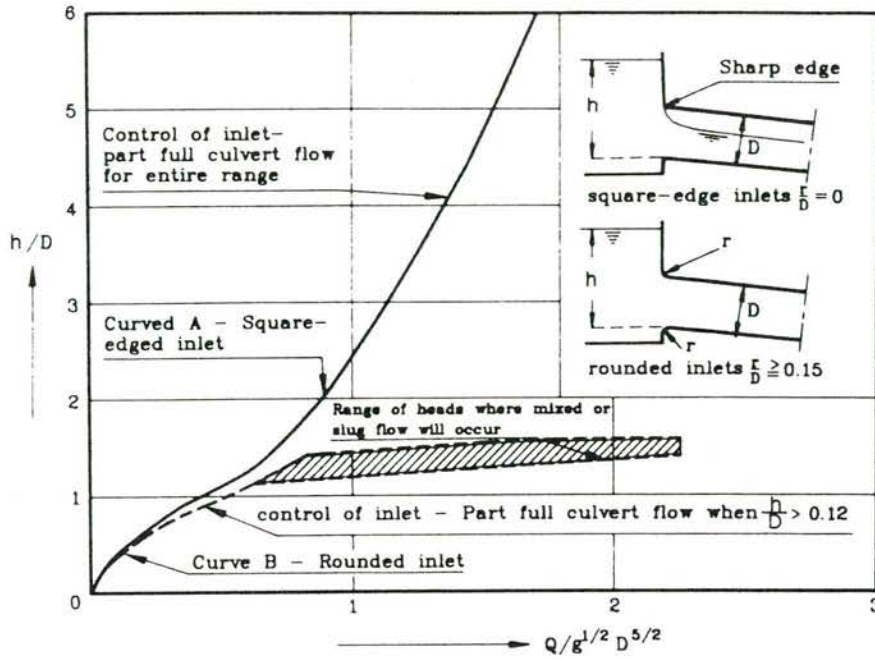


Figure 62 Head-discharge curves for square-edged and rounded inlets for circular culverts on steep slopes, form USBR [38]

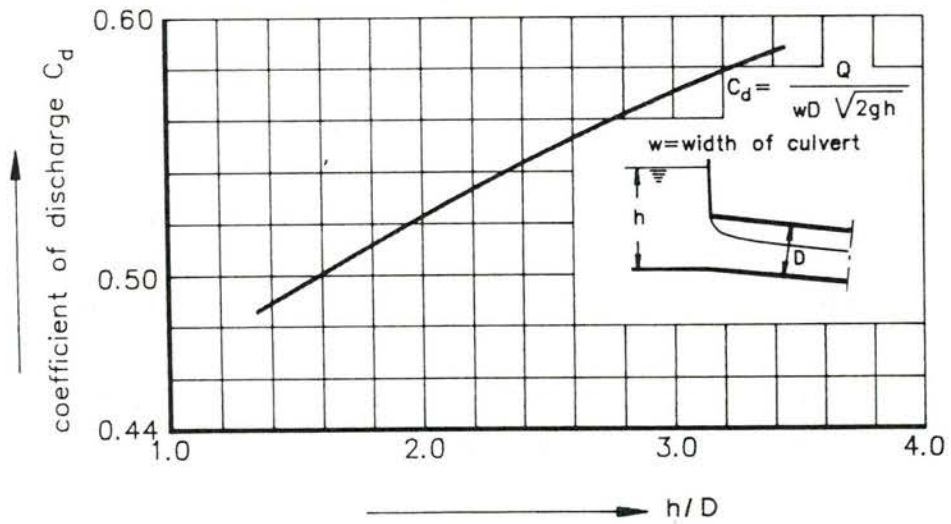
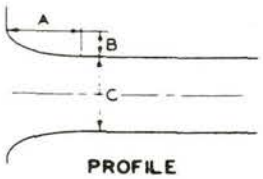
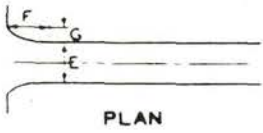
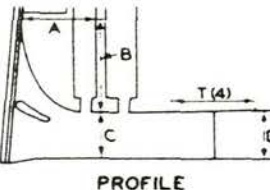
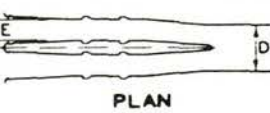
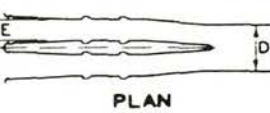
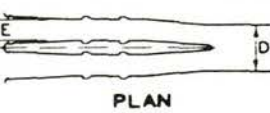
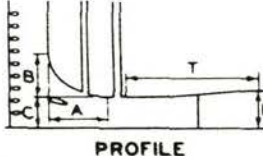
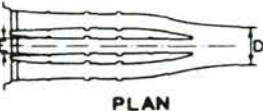


Figure 63 Discharge coefficient for submerged box culvert spillway with square-edged top opening, dimensionless redesign after USBR [38]

SHAPE	PROJECT (1)	CONDUIT PROPER			AVERAGE INTAKE COEFFICIENT K_e
		LENGTH DIAM (2)	REYNOLDS NUMBER (2)	VELOCITY HEAD (1)	
SINGLE INTAKE (CONCRETE DAM CONDUITS)					
 <p>PROFILE</p>	<u>PINE FLAT</u>	54	29-3.8 x 10 ⁷	65-81	0.16
	(PROTOTYPE) A=90, B=30 C=90, E=50 F=50, G=17		(PROTOTYPE)		
 <p>PLAN</p>	<u>ES 802</u>	83	6.7 x 10 ⁵	97	0.07 (3)
	(1/20 MODEL) A=7.5, B=2.5 C=10.0, E=5.7 F=4.3, G=1.4		(MODEL)		
DOUBLE INTAKE (EARTH DAM TUNNEL)					
 <p>PROFILE</p>	<u>DENISON</u>	40	1.2 x 10 ⁸	66	0.19
	(PROTOTYPE) A=250, B=390 C=190, D=200 E=90, T=530		(PROTOTYPE)		
 <p>PLAN</p>	<u>DENISON</u>	47	8.2-9.6 x 10 ⁵	61-62	0.12
	(1/25 MODEL) (SEE ABOVE)		(MODEL)		
 <p>PROFILE</p>	<u>FT RANDALL (5)</u>	39	0.7-1.5 x 10 ⁸	16-72	0.25
	(PROTOTYPE) A=240, B=160 C=230, D=220 E=110, T=490		(PROTOTYPE)		
 <p>PLAN</p>	<u>FT RANDALL</u>	39	0.9-1.0 x 10 ⁸	46-66	0.16
	(1/25 MODEL) (SEE ABOVE)		(MODEL)		
TRIPLE INTAKE (EARTH DAM TUNNEL)					
 <p>PROFILE</p>	<u>TIONESTA</u>	98	1.5-4.1 x 10 ⁵	7-50	0.33
	(1/36 MODEL) A=300, B=220 C=160, D=190 E=7.5, T=660		(MODEL)		
 <p>PLAN</p>					

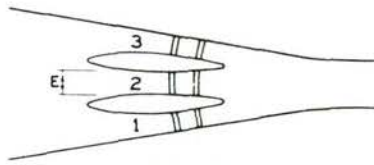
INTAKE HEAD LOSS

$$h_e = K_e \frac{V^2}{2g}$$

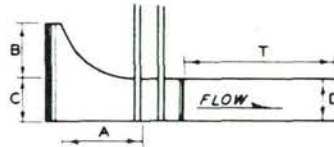
V = VELOCITY IN CONDUIT PROPER

- (1) DIMENSIONS IN PROTOTYPE FEET.
- (2) EQUIVALENT DIAMETER FOR NONCIRCULAR SECTIONS BASED ON HYDRAULIC RADIUS
- (3) DOES NOT INCLUDE GATE-SLOT LOSSES
- (4) LENGTH OF TRANSITION
- (5) ROOF CURVE MAJOR AXIS HORIZONTAL

Figure 64 Entrance losses of concrete conduits, form WES [43]



PLAN



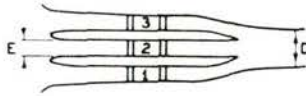
PROFILE

WAPPAPELLO*

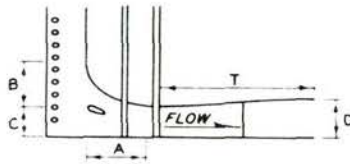
(1:25 MODEL)

A=31', B=25'
C=20', D=20'
E=10', T=50'

K_e (THREE GATES)=0.50
 K_e (GATES 1 & 3)=0.37



PLAN



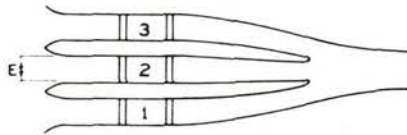
PROFILE

TIONESTA

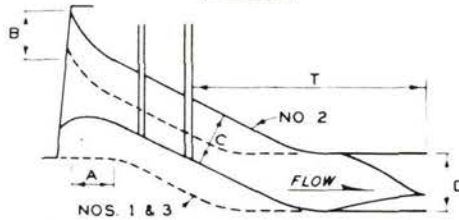
(1:36 MODEL)

A=30', B=22'
C=16', D=19'
E=7.5', T=66'

K_e (THREE GATES)=0.53
 K_e (GATES 1 & 3)=0.45



PLAN



PROFILE

ARKABUTLA*

(1:25 MODEL)

A=10.5', B=16'
C=17', D=18.25'
E=8.5', T=75'

K_e (THREE GATES)=0.79
 K_e (GATES 1 & 3)=0.68

* CONDUIT NOT CIRCULAR

INTAKE HEAD LOSS h_e

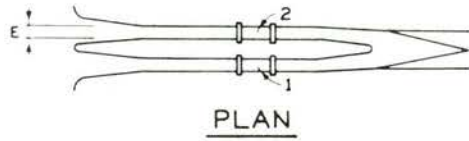
$$h_e = K_e \frac{v^2}{2g}$$

WHERE:

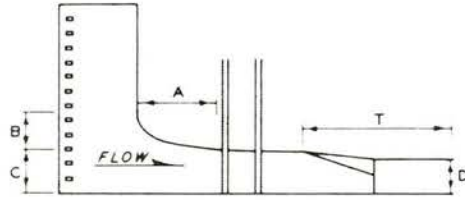
- K_e = LOSS COEFFICIENT
- v = GATE PASSAGE VELOCITY
- g = ACCELERATION, GRAVITATIONAL

NOTE: TO CONVERT LOSS COEFFICIENTS INTO TERMS OF CONDUIT VELOCITY HEAD, MULTIPLY K_e BY THE SQUARE OF THE RATIO OF THE CONDUIT AREA TO THE GATE PASSAGE FLOW AREA $\Sigma(C^2K_e)$ OF THE GATES CONCERNED.

Figure 65 Entrance losses of three gate conduits, from WES [43]



PLAN



PROFILE

EAST BRANCH

(1:25 MODEL)

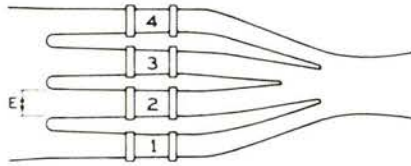
A= 23', B= 8'
 C= 12', D= 10'
 E= 3.33', T= 42.5'
 K_e (TWO GATES) = 0.23
 K_e (ONE GATE) = 0.45

SEE CHART 221-1 FOR
 DIMENSIONS OF FORT
 RANDALL INTAKE

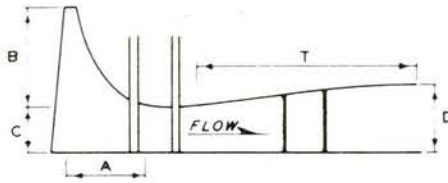
FORT RANDALL

(PROTOTYPE)

K_e (TWO GATES) = 0.44
 K_e (ONE GATE) = 0.78



PLAN



PROFILE

SARDIS

(1:25 MODEL)

A= 16', B= 23.5'
 C= 12', D= 17'
 E= 6', T= 62.5'
 K_e (FOUR GATES) = 0.32
 K_e (GATES 1, 2, & 3) = 0.33
 K_e (GATES 1, 3, & 4) = 0.37

INTAKE HEAD LOSS h_e

$$h_e = K_e \frac{v^2}{2g}$$

WHERE:

- K_e = LOSS COEFFICIENT
- v = GATE PASSAGE VELOCITY
- g = ACCELERATION, GRAVITATIONAL

NOTE: TO CONVERT LOSS COEFFICIENTS INTO TERMS OF CONDUIT VELOCITY HEAD, MULTIPLY K_e BY THE SQUARE OF THE RATIO OF THE CONDUIT AREA TO THE GATE PASSAGE FLOW AREA $\Sigma(C \times E)$ OF THE GATES CONCERNED.

Figure 66 Entrance losses of two and four gate passages, from WES [43]

4.2 Friction losses

In Figure 67 the Moody diagram is presented. This diagram shows the wall friction for pipe flow. The results can also be applied for free-surface flow if the pipe diameter D is replaced by the hydraulic diameter D_h or the hydraulic radius R_h .

$$D = D_h = 4R_h \quad (72)$$

R_h is the hydraulic radius which is defined as the ratio flow-section wetted-perimeter.

The Moody diagram presents the friction coefficient related to the fully developed boundary layer where the velocity profile harmonize with the pipe diameter and the wall roughness.

The C_f coefficient is related to the wall friction which equals the boundary shear stress τ in the flow:

$$\tau = C_f (0.5 \rho \bar{U}^2) \quad (73)$$

(\bar{U}^2 represents the averaged velocity in the pipe).

The Reynoldsnumber $\bar{U} D/\nu$ is related to the average pipe velocity and the pipe diameter (ν represents the kinematic viscosity, with a magnitude of about 10^{-6}). For prototype structures the Reynolds numbers are so large and the walls so rough that only the horizontal line parts of Figure 67 are relevant. The friction formula for large Reynolds numbers is approximately:

$$c_f = 0.0606 \{\log (3 D_h/k)\}^{-2} \quad (74)$$

For instance, in Thijsse [36] the following k values are found:

old concrete	$k = 10-20 \text{ mm}$	rusty steel	$k = 1-2 \text{ mm}$
plaster	$k = 0.5 \text{ mm}$	riveted steel	$k = 0.5-2 \text{ mm}$
smoothed concrete	$k = 0.2 \text{ mm}$	welded steel	$k = 0.1 \text{ mm}$
rock excavation	$k = 0.2-2 \text{ m}$		
sand in movement	$k = 10-100 \text{ mm}$	stone revetment	$k = 5-20 \text{ mm}$
slopes (+ vegetation)	$k = 0.1-0.2 \text{ m}$	riprap	$k = D_{90}$

Figure 68 illustrates how at the entrance of a rough pipe the local friction develops with respect to the distance. C_{fx} is the friction coefficient averaged from the mouth to the distance x . The higher C_f at the mouth, is due to the greater velocity gradients near the wall (at a contraction the velocity profile tends to be block-shaped, without a boundary layer).

More general information about how friction develops with respect to the distance can be found in Figure 69, from Harrison [15].

The friction coefficient has again been expressed in terms of a distance-averaged value. Such friction tests are performed with a plate in an unbounded flow. In practice, friction in a pipe or in a culvert will not fall below the friction belonging to the fully developed flow in the culvert section over long distances. The latter can be derived from the Moody diagram. Harrison [15] shows that in the transition region between laminar and turbulent flow there can exist lower C_f values than presented in Figure 69. This is similar to what is indicated in the Moody diagram of Figure 67 in the transition region. Related velocity profiles are, among others, found in Kolkman [20].

Pugh [26] presents measurements in a rectangular prototype conduit. The friction that was measured at the pipe inlet was greater than Tullis found [ref. 37]. Shear stress became constant at a distance $x/D = 20$ which is in the range of what Tullis found. The other test results of Pugh confirmed what is already known about velocity profiles and boundary layer development.

B. The developed flow

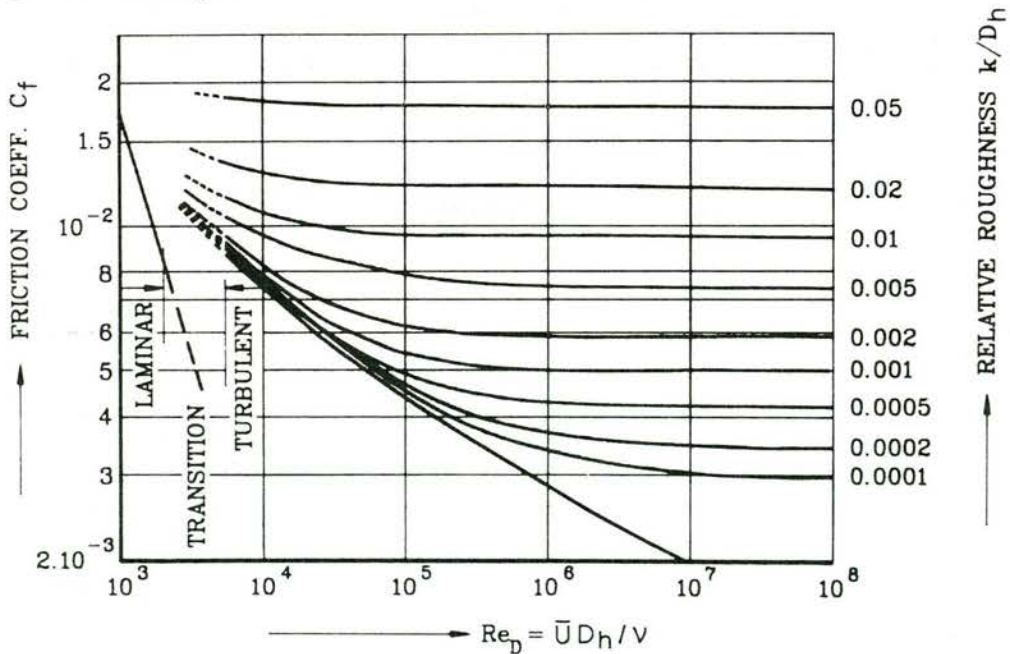


Figure 67 The Moody diagram

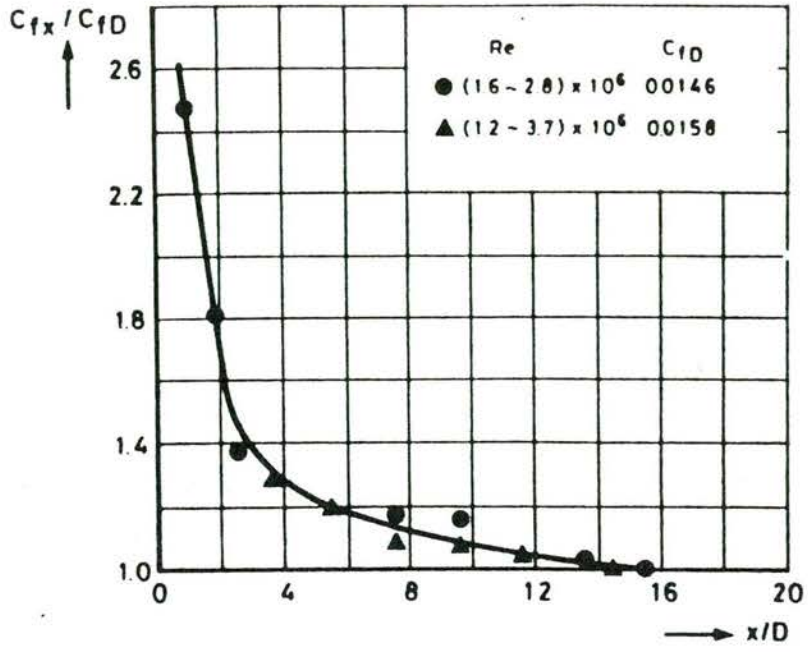


Fig. 68 Distance-averaged friction factor at a pipe entrance from Tullis/Wang [37]

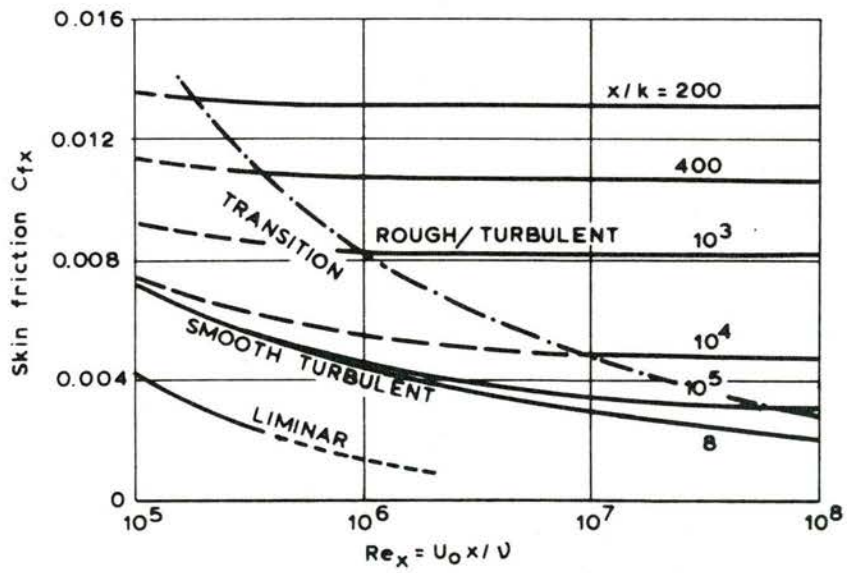


Figure 69 Distance-averaged friction factor at a plate (Harrison [15])

4.3 Slots

Loss coefficients of slots are presented as fractions of the velocity head of the average flow velocity in the culvert section where the slot is located.

$$\Delta H = K_s \bar{U}^2 / 2g \quad (75)$$

In general, the slot coefficients are small compared to other losses. A possible additional effect of a slot is, when located just upstream of a diverging section, that the flow spreads better over the divergence owing to the induced turbulence. Then there is a greater recovery of potential energy and reduction of energy loss.

Levin [22] tested a number of slot shapes located in a round tube (diameter 210 mm) along the whole circumference and in the walls of a squared section, having a height and width of 150 mm. Figure 70 shows the investigated slot sections.

The results of the test in the squared tunnel were not accurate because of the deformation of the test section caused by hydrodynamic pressures.

Conclusions were:

1. Between Reynolds numbers of $3.5 \cdot 10^5$ and $8 \cdot 10^5$ (related to the tunnel section) no effect of the Reynolds number was found
2. Low pressures locally appearing downstream of the slot faded out at a distance of 12 diameters behind the slot
3. Rounded corners gave a decrease in loss in the order of 7-15%

The tests in a circular tube with the slot all around (only the slots with sharp edges were tested again) show that the influence of the Reynolds number was still observed till $Re = 10^6$; this is amazingly high. The losses are shown in Figure 71.

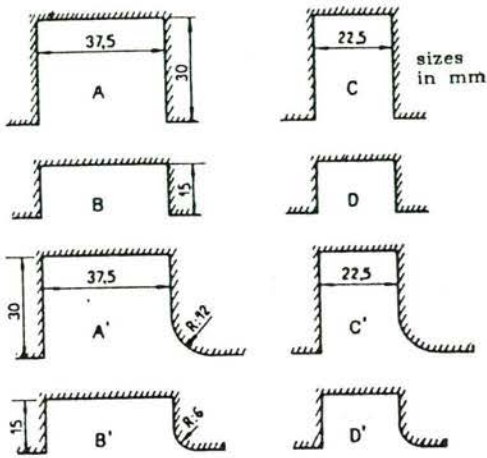


Figure 70 Slot sections of the tests by Levin [22]

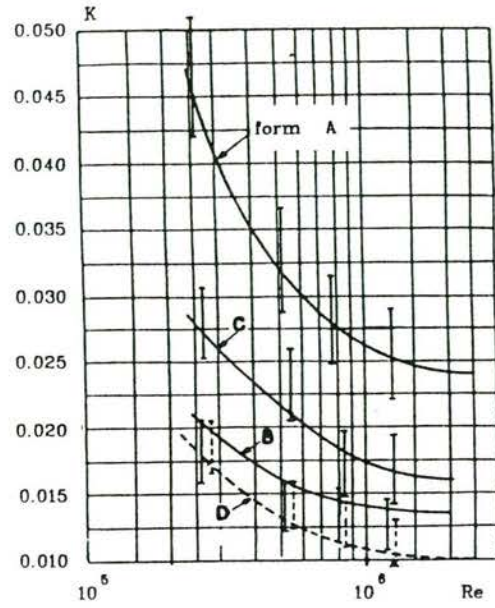


Figure 71 Test results with the circular tube section (D = 209.5 mm)

A theoretically plausible approximation is that losses are proportional to the length (along the perimeter of the culvert) and inversed proportional to the culvert section.

The further elaboration performed by Levin is not presented here; the empirical formula are complex and slot losses as he found them are low compared to other losses and their inaccuracies.

4.4 Exit losses and hydraulic jump relations

Exit losses are defined here as losses which occur at the transition of an outlet into a downstream canal or a larger basin like a lake or the sea. In certain cases the control section of the structure can also be at the exit. The exit can be an abrupt expansion or a gradual expansion with divergent walls and/or a sloping bottom.

A reduction in exit losses gives an increase in discharge in the case of submerged flow or intermediate flow (for definitions see Chapter 1). However it has no effect on the discharge if the downstream water level is so low that modular flow is involved. On the other hand, the modular (maximum) flow will still occur at a higher downstream water-level. So it is meaningful to calculate exit losses in case of a fully submerged flow (at low velocities), and of intermediate flow till the limit of modular flow.

The difference between submerged and intermediate flow causes that at intermediate flow the exit losses with abrupt expansions should always be calculated with the momentum equation whereas at fully submerged flow the Carnot equation can be applied as well.

When no special measures are taken, the exit loss coefficient at an (abrupt) large expansion is equal to 1, which means that all kinetic energy is lost.

If the outflow runs into a canal that having a limited section, it follows from the momentum equation that some of this energy is regained.

From the Carnot equation can be found for instance:

$$\Delta H = (V_1 - V_2)^2 / 2g$$

This shows that a greater V_2 yields smaller losses.

Expansions that diverge gradually also regain potential energy, leading to a further reduction of losses.

At modular flow conditions in the control section, super-critical flow will occur downstream of this section, where energy loss takes place by bottom friction and/or a hydraulic jump.

It has been decided to include in this section also the hydraulic jump relations. They are important when studying the limit-conditions downstream, where modular flow can still occur.

A. Abrupt expansions downstream of the control section

It has been discussed in Chapter 1, that at an abrupt (90°) expansion the momentum equation can be applied and losses can be calculated because then the hydrodynamic forces, exerted on the back face of a weir, a gate or an orifice are known to be hydrostatic. So the forces exerted on the downstream water by the rear side of the outlet are related to the local water level. At the inflow of the downstream water, the pressures and the advective momentum flux (fluid density \times discharge \times velocity ρQV) are often also known, being the pressure and momentum advection which belongs to the modular flow condition of the control section.

If there is a nappe over a sharp-crested weir, the highest downstream water level at which modular flow in the control section can exist, is the water level equal to the crest level. Together with the nappe momentum, the downstream water level h_3 at some distance further downstream can be determined. In Figure 72 this is illustrated for a nappe with width w , flowing into a downstream basin with width W . The coefficients m_1 and m_2 refer to discharge coefficients. The aim of Figure 72 is to calculate h_3 when a certain H_1 is introduced. Solving these equation is laborious but the procedure of Chapter 2 can be helpful.

A similar computation can be set up for a submerged hydraulic jump. The discharge relation of flow under a gate can be treated similarly to Q_1 in Figure 72.

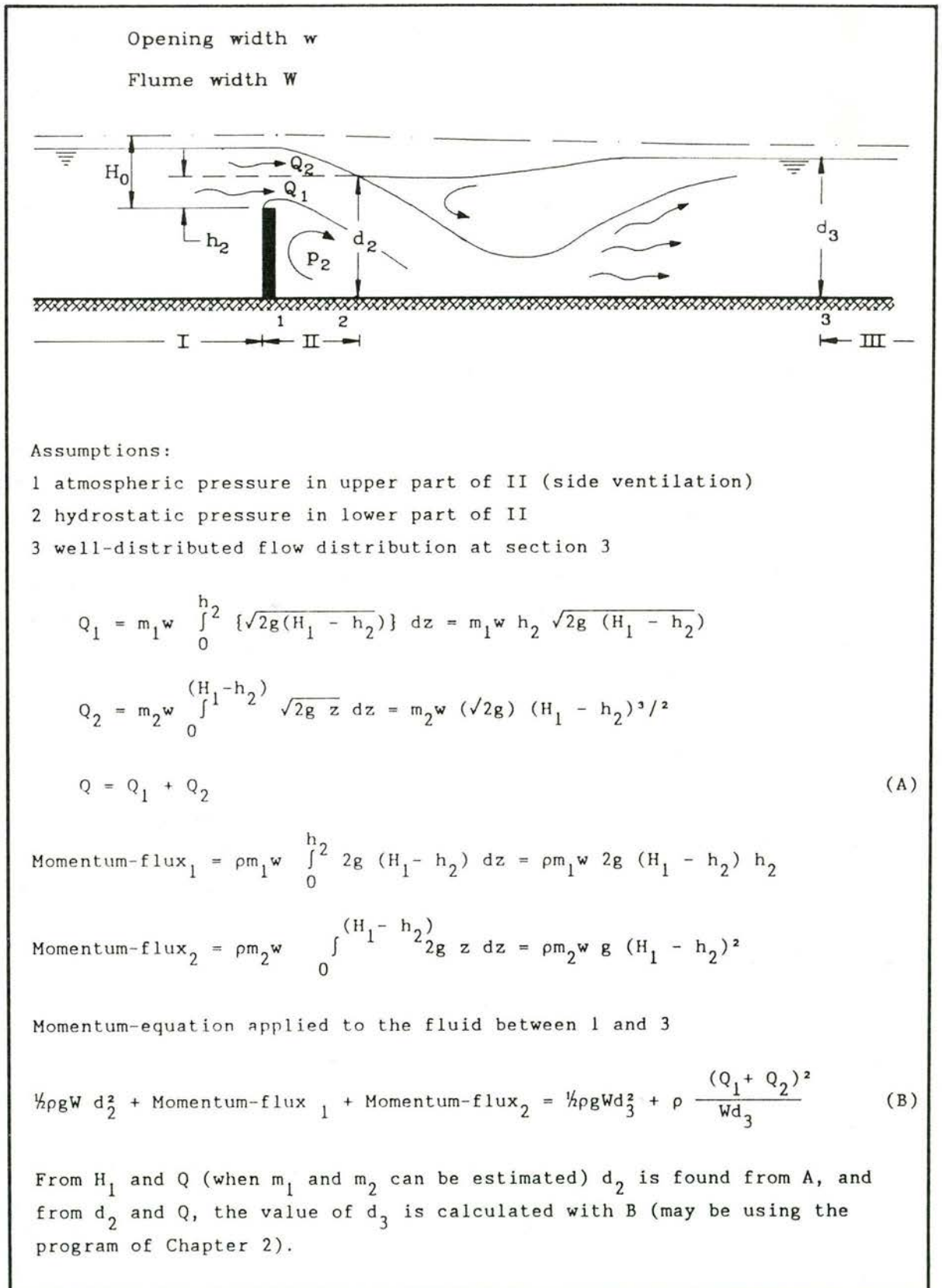


Figure 72 Exit conditions with a submerged hydraulic jump calculated with the momentum equation

B. Hydraulic jump relations (two-dimensional)

Only those hydraulic jump data which are related to the computation of hydraulic losses are presented here. Not included are considerations about the jump stability, the design of stilling basins etc.

The application of the momentum equation for the hydraulic jump is well-known, the results are presented in Figure 73.

Figure 73 is based on the momentum equation for a rectangular prismatic canal:

$$\frac{1}{2}\rho g d_1^2 + \rho q(q/d_1) = \frac{1}{2}\rho g d_2^2 + \rho q(q/d_2) \quad (76)$$

Division by ρg and introducing the Froude number F_1 for the upstream side ($F_1 = V_1/\sqrt{gd_1}$) gives

$$\frac{1}{2}d_1^2 + d_1^2 F_1^2 = \frac{1}{2}d_2^2 + (d_1^3/d_2) F_1^2 \quad (77)$$

or:

$$(1 - d_2/d_1)(1 + d_2/d_1) = 2 F_1^2(1 - d_2/d_1)/(d_2/d_1)$$

resulting in

$$d_2/d_1 = \frac{1}{2} (-1 + \sqrt{1 + 8F_1^2}) \quad (78)$$

This expression is found in many references. It is only valid at a well distributed flow, because the momentum-flux does not contain a correction factor.

In Figure 73 the following symbols are used. The index 1 refers to the oncoming supercritical flow with depth d_1 , velocity V_1 , and index 2 to the conditions behind the jump.

The term h_j refers to the difference in depth $h_j = (d_2 - d_1)$. The symbols H_1 and H_2 refer to the energy levels.

Figure 73 can be well applied for the hydraulic jump at a horizontal bottom when the starting conditions upstream of the jump are known. This is for instance the case at free flow models of a gate.

For the design of stilling basins the author has designed a chart variant from which directly the level of the bottom of the stilling basin can be derived, see Figure 75. This is done by introducing the critical depth d_c as the length by which all other length parameters are made dimensionless. d_1 and d_2 again refer to upstream and related conjugate waterdepth. H_1 and H_2 is respectively the upstream and downstream energy head.

The critical depth represents the discharge per unit of width:

$$d_c = (q^2/g)^{1/3} \quad (77)$$

The required energy loss ΔH of the hydraulic jump related to d_c determines the Froude number. The bottom level of the stilling basin also follows directly, because H_2/d_c can be read in Figure 75. A second curve with 10% extra reserve in conjugate depth (advised for the USBR stilling basins, see Ven Te Chow [40]) is also included.

The use of the graphs, Figures 73 and 75, can be replaced by the computation procedure of Chapter 2 (introducing directly the momentum equation). In that case the momentum-flux can contain correction coefficients for the uneven velocity distribution.

Particularly the momentum flux of the incoming flow will be sensitive to β values greater than 1. (see further Chapter 1, Figure 1.3).

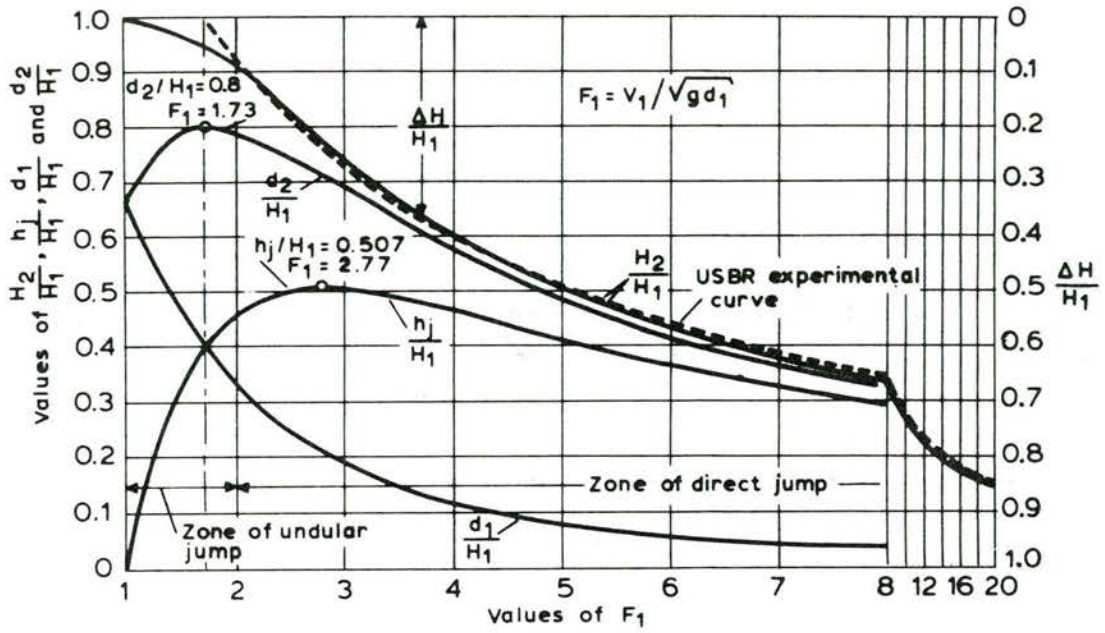


Figure 73 Relations for the hydraulic jump, from Ven Te Chow [40].

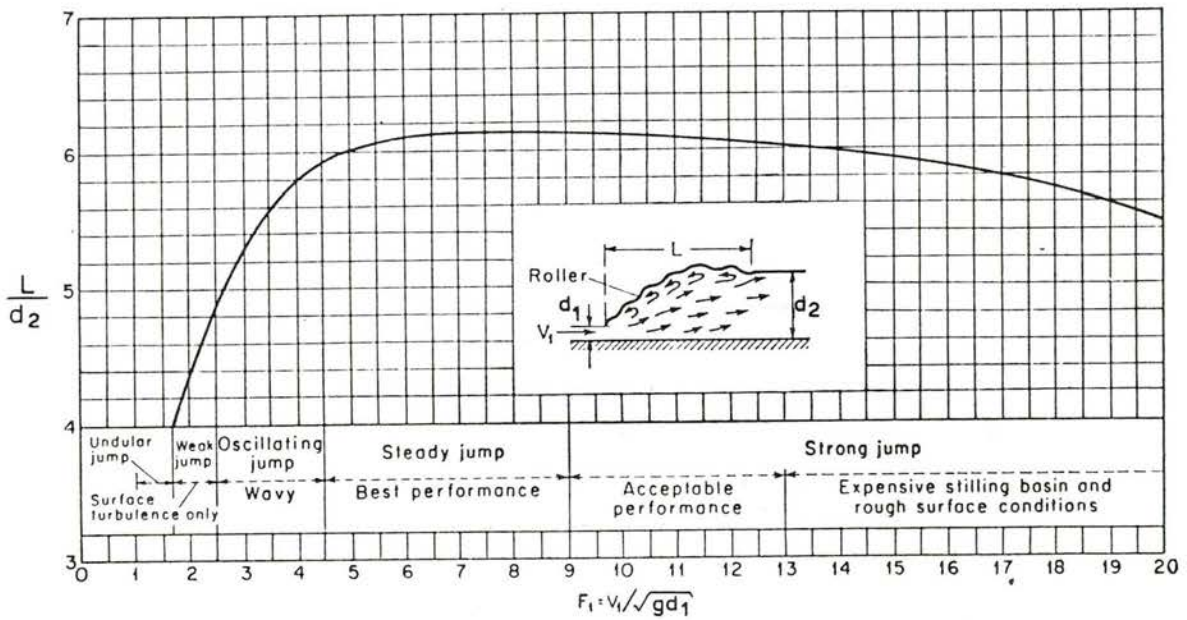
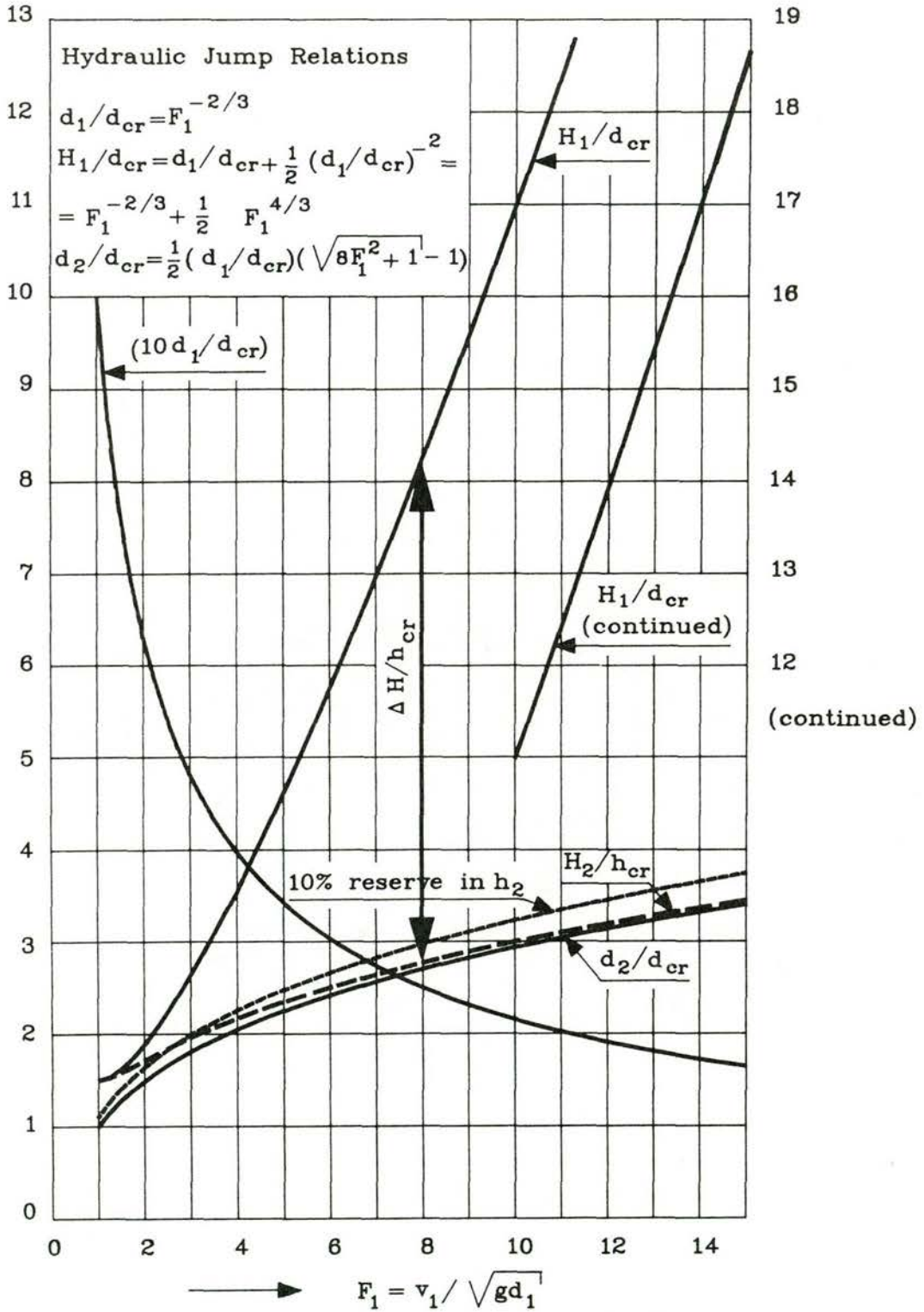


Figure 74 The length of a hydraulic jump, from [40].



Index 1 refers to inflowing (super-critical) flow
 Index 2 refers to outflowing (sub-critical) flow

Figure 75 Revised hydraulic jump relations for stilling basin design

C. Hydraulic jump on a slope

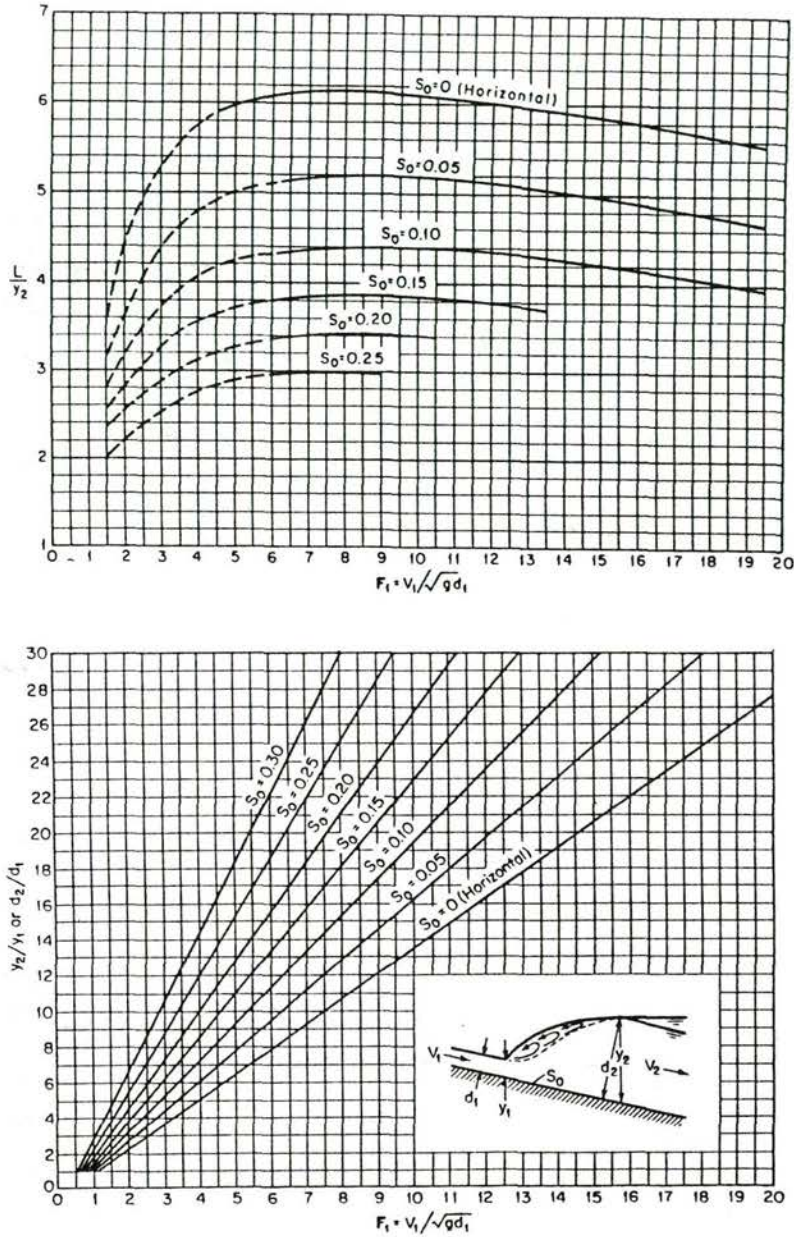
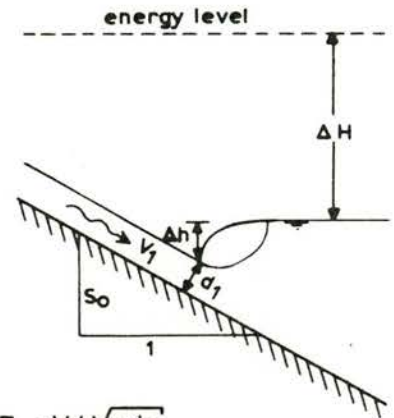
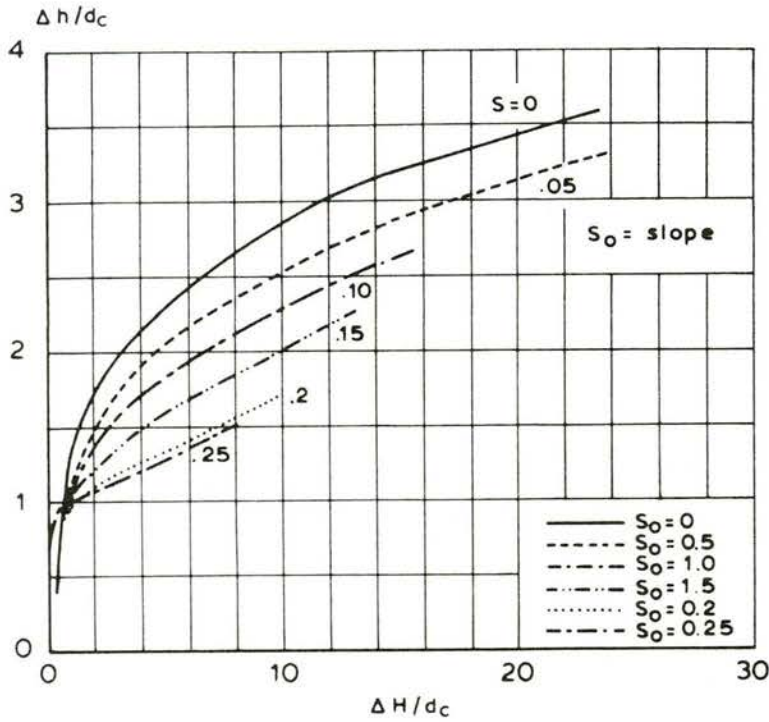


Figure 76 The hydraulic jump data sloping bottom (from Ven Te Chow [40])

For a sloping bottom the two-dimensional hydraulic jump relations are also known, see Figure 76. It is important to know at which downstream water level the modular flow gets (partially) submerged if the upstream jet is the outflow of a gate or a weir nappe . With Figure 76 this can only be found with an iterative search. Therefore another graph has been prepared in Figure 77, using the results of Figure 76. If ΔH , and d_{cr} are known, the dip in the water level can directly be read. ΔH the difference between the energy level of the incoming flow and the downstream water level, and the

dip is defined as Δh . If the dip is known the Froude number $V_1/\sqrt{g d_1}$ can be found, see the expression mentioned in Figure 77, and from that the length of the jump can be read in Figure 76.



$$F_1 = V_1 \sqrt{g d_1}$$

$$F_1 = \left[\frac{2(\Delta H + \Delta h)}{d_c} \right]^{3/4}$$

Figure 77 The dip in the water level at the hydraulic jump on a slope.

D. Gradual expansions

For submerged flow at very low Froude number, losses in gradual expansions are known from internal flow data.

The expression to define the losses is related to the Carnot equation at abrupt expansions:

$$\Delta H = \xi (V_1 - V_2)^2 / 2g \quad (78)$$

Free-surface flow tests were carried out by Formica [13]; Bos [7] compared these results with Idel'cik's results for internal flow with various top angles (see Figure 78). Other types of expansion investigated by Formica are shown in Figure 79.

The scale of the Formica tests was quite small and presumably the Reynolds number will still have had influence. This, however, cannot be the explanation of these losses which are twice as low as those of Idel'cik. Idel'cik suggested that the expansion ratio is of little relevance. This is not a priori evident. The curves of Idel'cik are for $\alpha = 90^\circ$ a little higher than the Carnot losses which were based on a hydrostatic pressure distribution just after the expansion. This agrees with other references. So for this moment it seems advisable to multiply all formica coefficients by 1.2. In Figure 80 Idel'cik data are presented for a gradual expansion with outflow in a large canal, using an optimal diffusor angle (low losses).

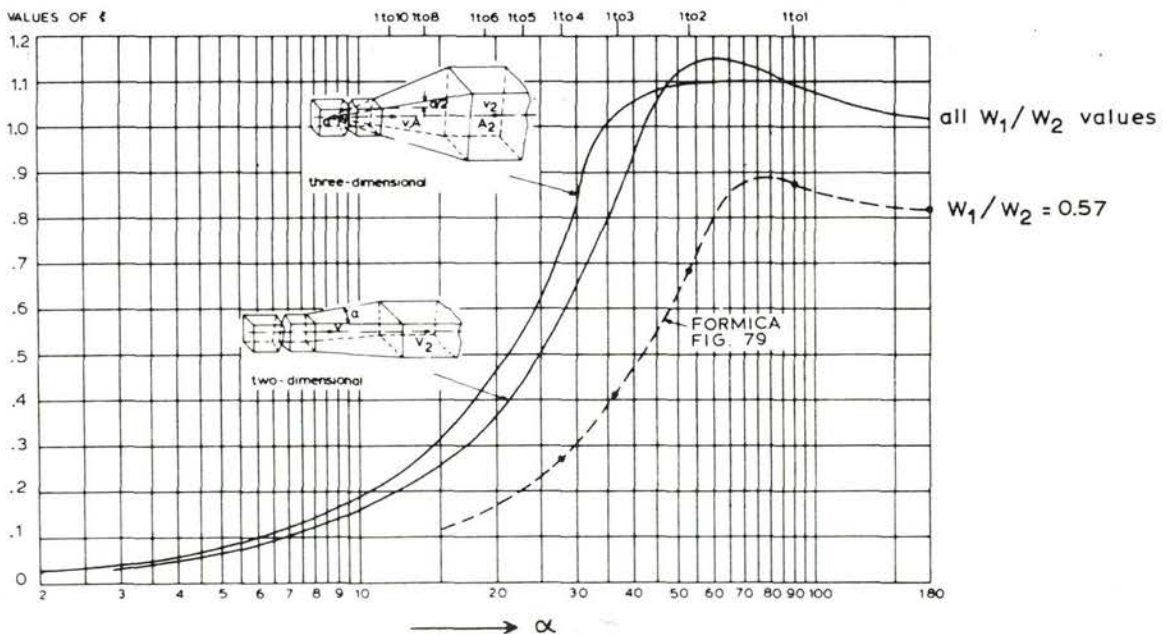


Figure 78 Expansion losses in closed and open conduit flow, from Bos [7] and after Formica [13] and Idel'cik [17]

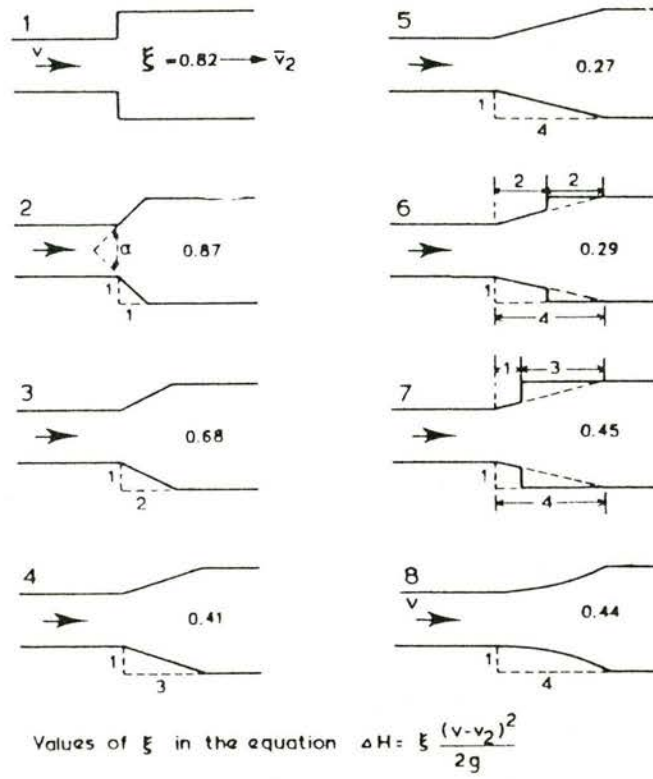
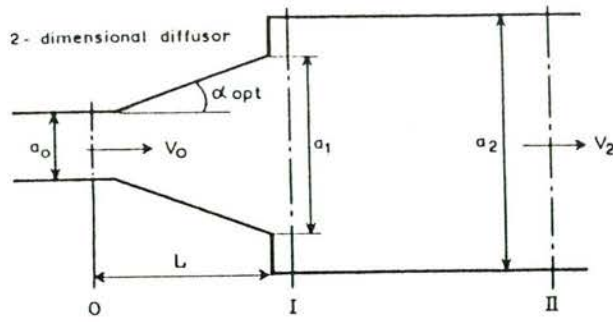


Figure 79 Losses at expansions of different shapes at free surface flow at an expansion rate of 335 mm/205 mm, (taken from Bos [7] after Formica [13])



Loss of energy head:

$$\Delta H_{0-II} = \xi_t (V_0^2 / 2g)$$

Constant depth:

$$n = a_2 / a_0 = A_2 / A_0$$

$$n_1 = a_1 / a_0 = A_1 / A_0$$

Optimal diffuser angle α_{opt} when L/a_0 is given:

n	L/a ₀										
	0,5	1,0	2,0	3,0	4,0	5,0	6,0	8,0	10	12	14
1.5	25	18	11	8,0	6,4	5,4	4,7	3,5	2,8	2,4	2,0
2.0	33	23	15	12	9,7	8,4	7,5	6,0	5,2	4,7	4,3
2.5	37	26	18	14	12	10	9,4	8,0	7,0	6,3	5,6
3.0	39	27	20	16	13	12	11	9,1	8,0	7,2	6,4
4.0	42	30	21	17	15	13	12	10	9,0	8,2	7,4
6.0	45	31	23	18	16	14	13	11	10	9,4	8,5
8.0	47	32	23	19	17	15	14	12	11	10	9,1
10	48	33	24	20	17	15	14	12	11	10	9,5
14	49	34	25	20	17	16	14	13	12	11	9,9
20	50	35	25	21	18	16	15	13	12	11	10

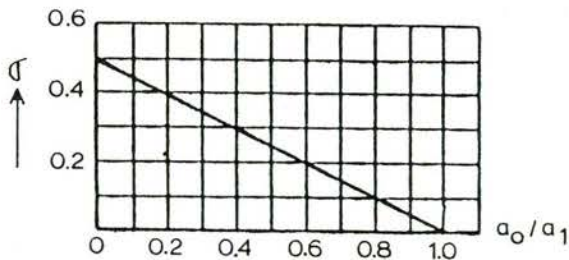
α_{opt} in degrees

$$n_1 = 1 + (2 L/a_0) \operatorname{tg} \alpha_{opt}$$

n	L/a ₀										
	0,5	1,0	2,0	3,0	4,0	5,0	6,0	8,0	10	12	14
1.5	0,04	0,04	0,04	0,04	0,05	0,06	0,06	0,08	0,10	0,11	0,13
2.0	0,12	0,09	0,07	0,07	0,06	0,07	0,07	0,07	0,08	0,10	0,12
2.5	0,18	0,14	0,11	0,10	0,09	0,09	0,09	0,09	0,09	0,10	0,10
3.0	0,23	0,18	0,14	0,12	0,11	0,11	0,10	0,10	0,10	0,10	0,11
4.0	0,30	0,24	0,19	0,16	0,15	0,14	0,13	0,12	0,12	0,12	0,12
6.0	0,38	0,31	0,25	0,21	0,19	0,18	0,17	0,16	0,15	0,14	0,14
8.0	0,43	0,36	0,28	0,25	0,22	0,20	0,19	0,17	0,16	0,16	0,15
10	0,46	0,38	0,30	0,26	0,24	0,22	0,21	0,19	0,18	0,17	0,16
14	0,50	0,41	0,33	0,29	0,26	0,24	0,22	0,20	0,19	0,18	0,18
20	0,53	0,44	0,35	0,31	0,28	0,25	0,24	0,22	0,20	0,19	0,19

Basic loss coefficient

ξ_0



$$\xi_t = \xi_0 (1 + \sigma)$$

Figure 80 Determination of optimal diffuser outlet shape at constant depth condition, from Idel'cik [17]

E. Hydraulic jump in a gradual expansion

Downstream of a control section often divergent sections are applied. These have two advantages:

- lower losses, particularly at the submerged flow conditions
- spreading of discharge over a larger width

Systematic test results are only available about conditions with a horizontal bottom.

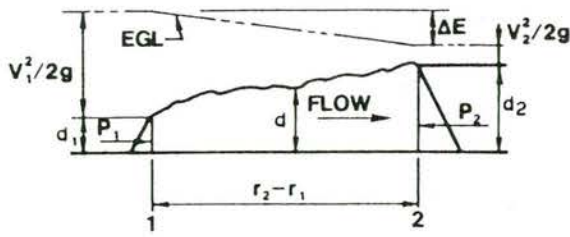
Two conditions can be considered:

- Free hydraulic jump, systematically investigated by Woodbury and Padmanabhan, ref. [44]
- Submerged hydraulic jump (behind a gate with non-modular flow), investigated by Abdel-Gawad and Carquodale, ref. [1].

The hydraulic jump in a divergent section is called "radial hydraulic jump". The width at the throat w and the divergence angle 2θ determine the radius r_1 before the jump (being $\frac{1}{2} w/\sin(\theta/2)$) and the phenomena in the divergent part are supposed to be a part of a circular hydraulic jump condition.

For the free radial hydraulic jump the sequent depth can be derived from Figure 81. There is still a slight dependence on the ratio of the radius r_2 and r_1 , so only a first estimate is obtained.

For the submerged hydraulic jump (definition sketch is Figure 84) the relations found by Abdel-Gawad and Corquodal [1] are presented in Figure 85 and 86.

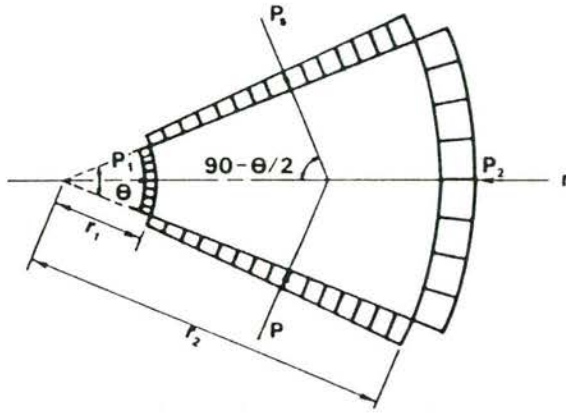


Notation

$$Y_0 = d_2 / d_1$$

$$F_1 = V_1 \sqrt{g d_1}$$

$$r_0 = r_2 / r_1$$



P = pressure
 P_s = side pressure etc.

Figure 81 Definition sketch free radial jump

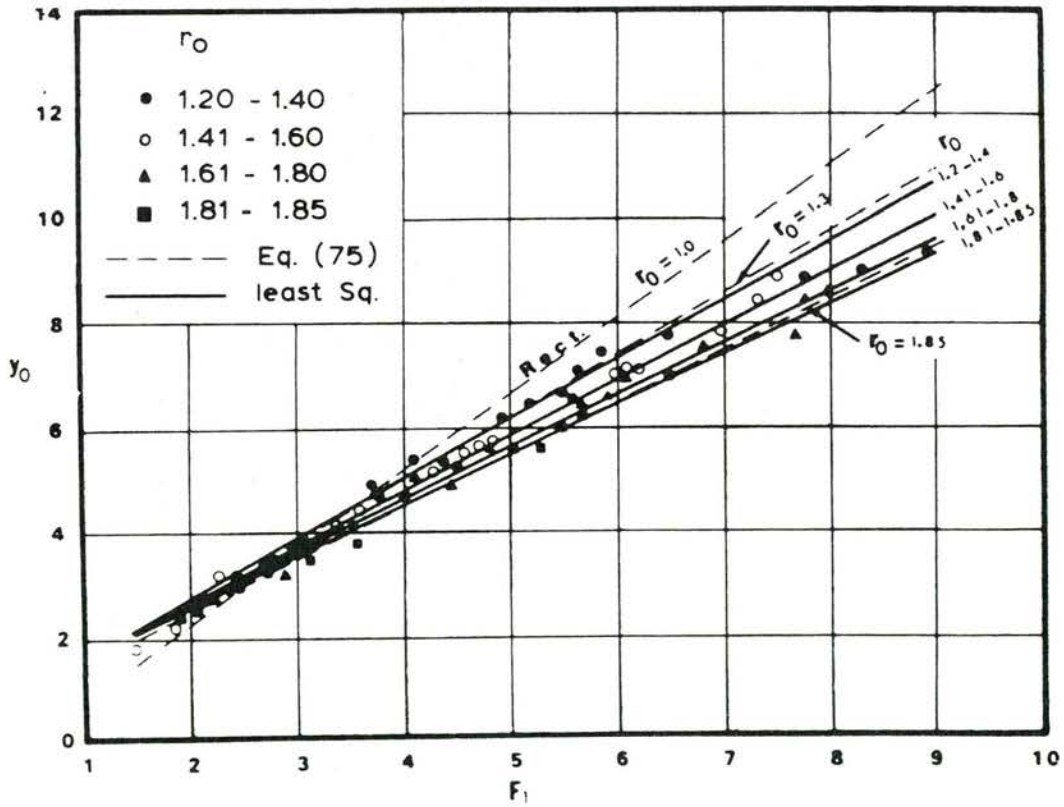


Figure 82 Radial jump sequent depth ratio as function of approaching Froude number and radius ratio, from Woodbury and Padnahabnan [44]

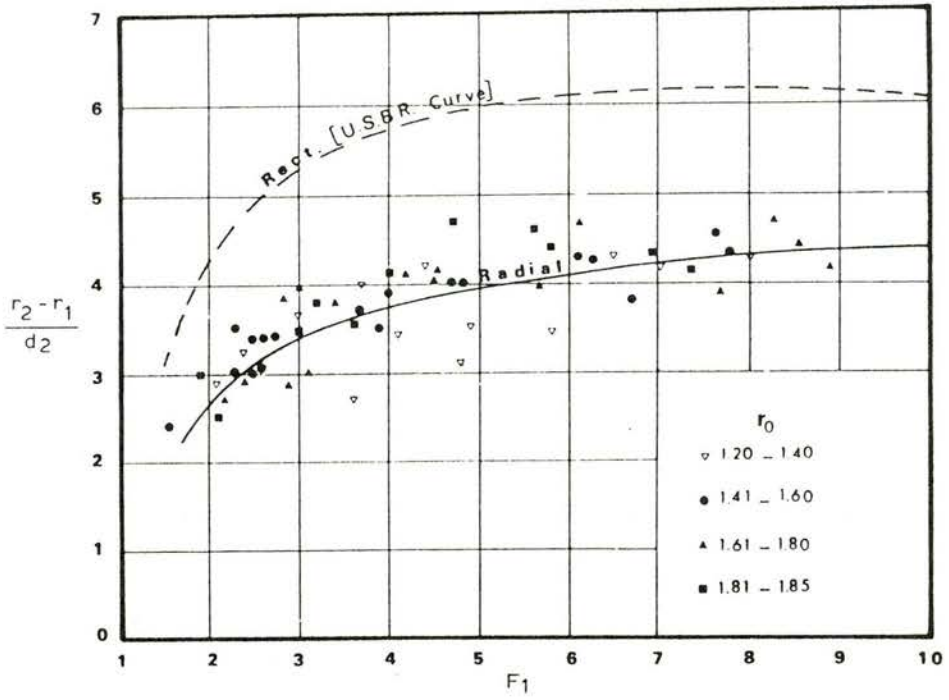


Figure 83 Free radial jump length [44]

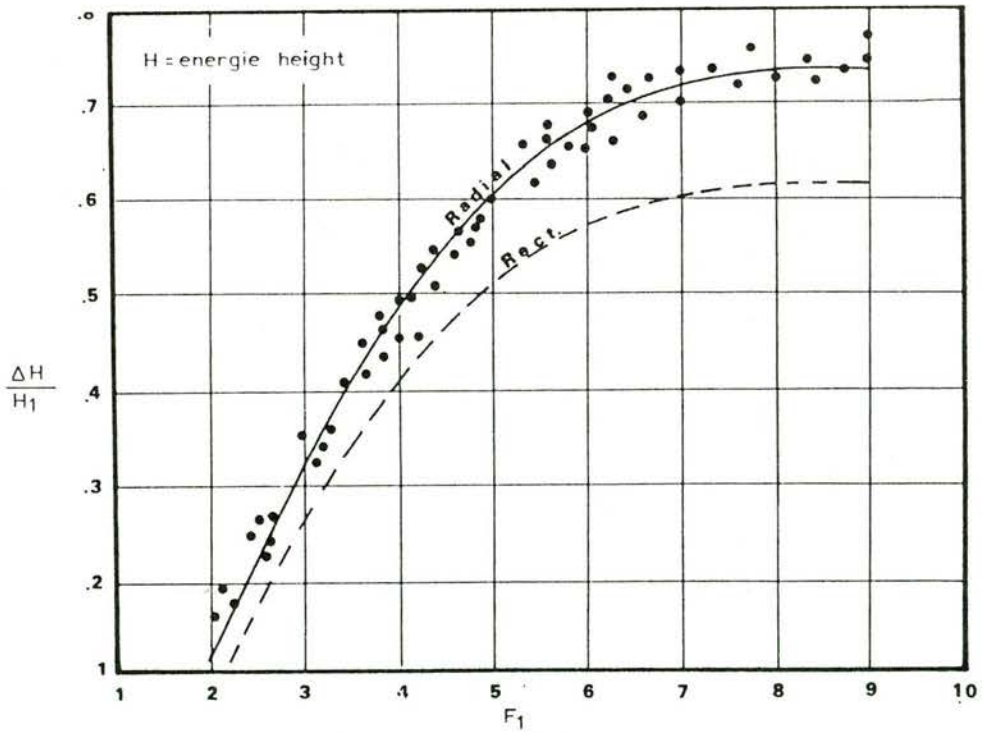
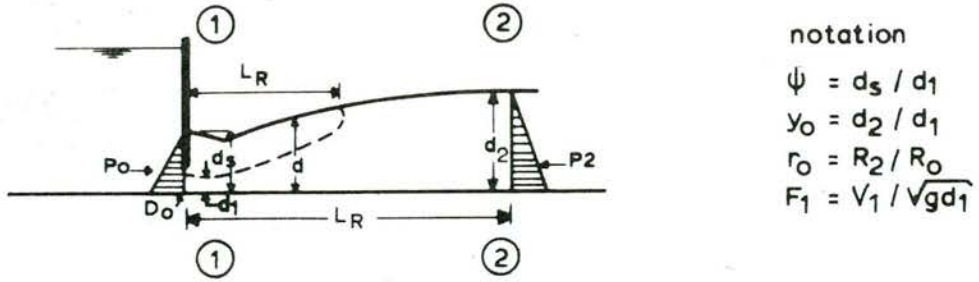


Figure 84 Free radial jump relative energy loss, also [44]



notation
 $\psi = d_s / d_1$
 $y_0 = d_2 / d_1$
 $r_0 = R_2 / R_0$
 $F_1 = V_1 / \sqrt{gd_1}$

Figure 85 Definition sketch submerged radial jump

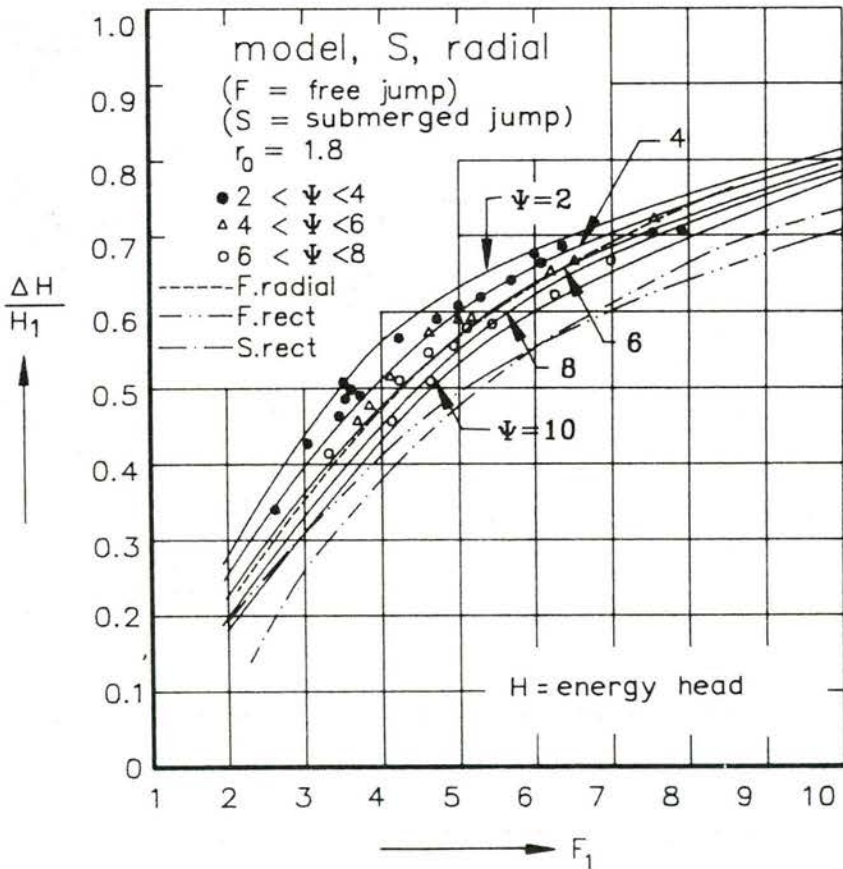


Figure 86 Relative energy loss of the submerged radial jump, after Abdel-Gawad and Corquodale [1]

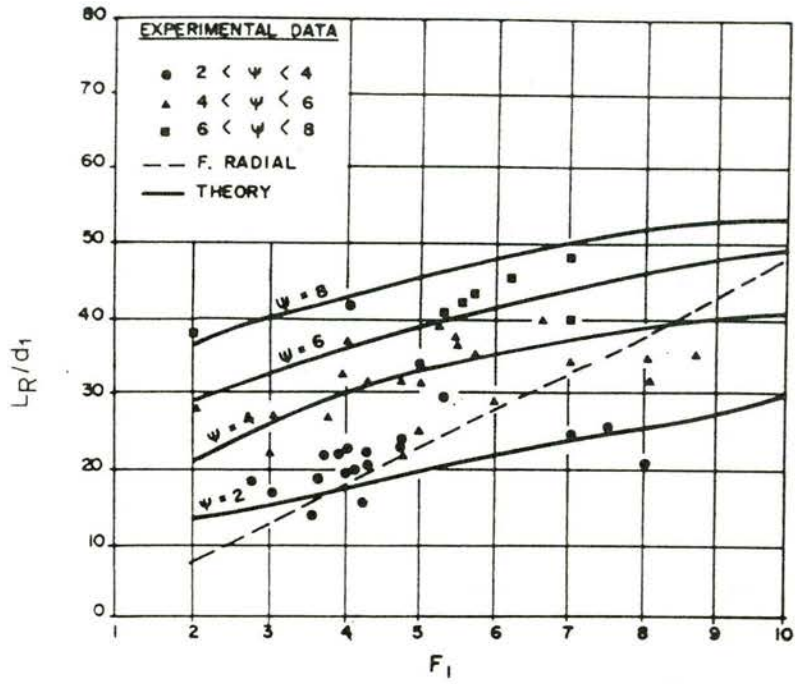


Figure 87 Jump length of the submerged radial jump [1]

4.5 Trash racks

The losses at trash racks depend on:

- A. shape of the bar section,
- B. blockage factor or solidity (S) which can also be written as $\Sigma w/W$ (w = width of one single bar, W = width of the whole flow section if bars are absent),
- C. the angle of approach of the flow. If there is horizontal flow and the bars stand inclined, the $\sin(\theta)$ is introduced, with $\theta = 90^\circ$ when the bars are vertical.
- D. when the bars stand vertical and the flow is horizontal but not perpendicular to the plane of the rack, the skewness angle α is introduced with $\alpha = 0^\circ$ if the flow is perpendicular,
- E. the other structure elements such as trusses, sills, slots which are related to the rack.

Losses can be largely influenced by a skew approach angle, irregular flow distribution, trash and ice.

If V_a is the approach velocity (or, when there are no bars, V_a is the average flow velocity in the trash rack section) the losses are expressed in terms of:

$$\Delta H = C_{tr} (V_a^2/2g) \quad (79)$$

(this is method C of section 1.9 and Figure 8)

When the trash rack is inclined, the loss reduces to:

$$\Delta H = C_{tr} (V_a^2/2g) \sin \theta \quad (80)$$

Short bars (seen in flow direction) have higher losses than longer bars. This is caused by the tendency of reattachment of the flow at the longer bars.

If the length is introduced as t , the increase in t is effective until $t/w > 5$, see Figure 90. The effect of streamlining is important, see Figure 88, but the effect reduces when there is a skew approach flow. For further data of flow resistance of different shape see also next section on bridge piers.

Figure 89 shows C_{tr} values for different sections of bars and various values of the solidity S .

Figure 90 contains information for greater blockage of flow. This information is important because if the other trash-rack elements (mentioned under point E) are taken into account the blockage of the flow is much greater than from the bars only.







Trusses are sometimes badly shaped so that loss coefficients correspond to bars with a small t value.

In section 1.9 the use of the Carnot formula for the computation of trash rack losses has been discussed. Orsborn [26] also discusses this point, referring to earlier work of Escande. For the contracted flow, a contraction coefficient of .9 should be applied if S is in the order of 8% and this coefficient is 0.65 if S is in the order of 50% (the contraction coefficient is related to the net area between the bars). The contraction coefficient is rather low and the important flow-area reduction can cause that at an increased discharge (at free surface flow), modular flow conditions occur causing a further decrease of discharge capacity.

In Figure 91 the losses are presented at skew approach velocities. Although an empirical formula, constituted by multiplication of two independent factors has its inherent inaccuracies, the losses correspond within 20% with the other presented data. But in view of other inaccuracies in the estimation of trashrack losses this is still acceptable.

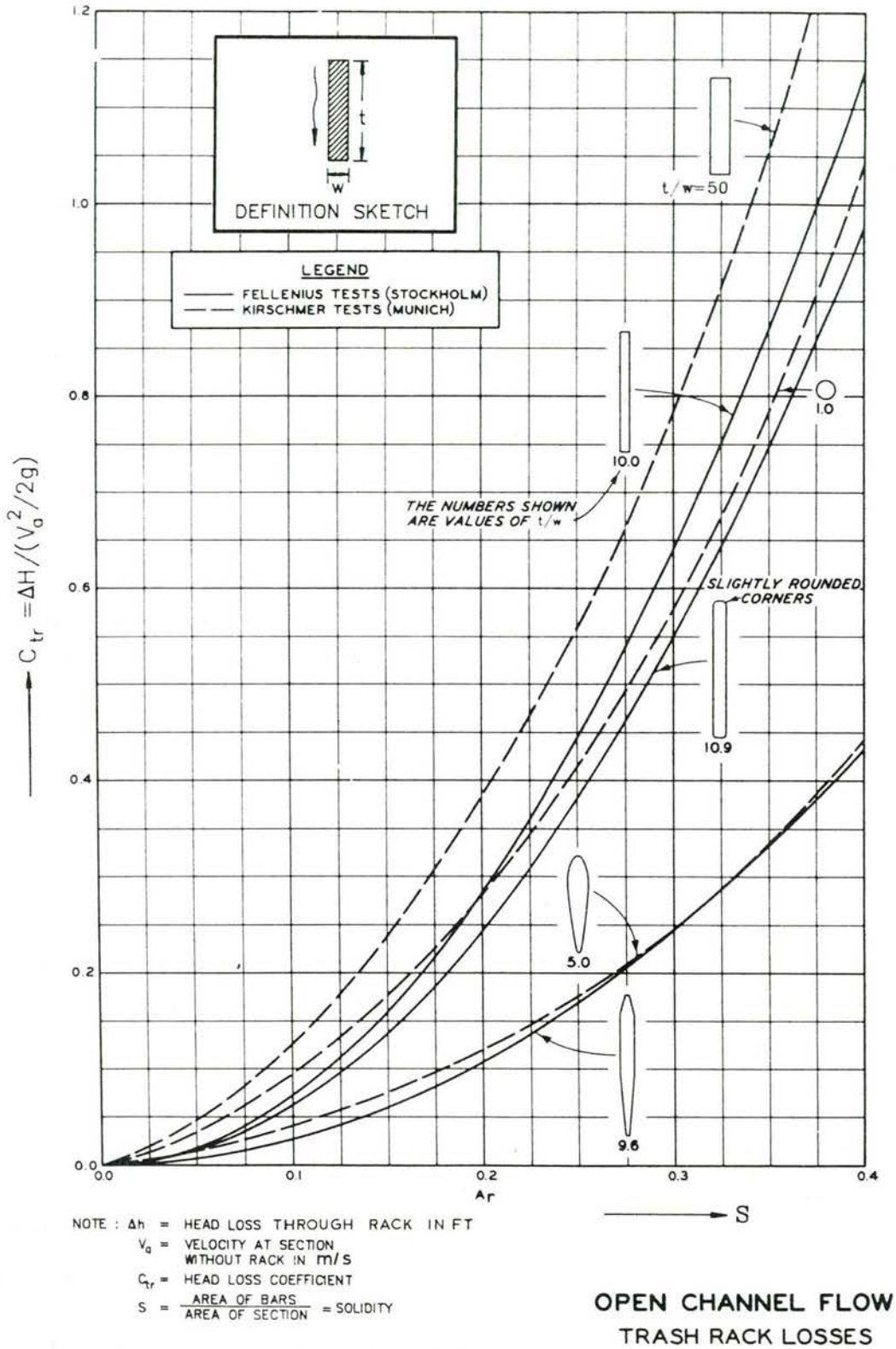
INFLUENCE OF APPROACH-FLOW ANGLE ON BAR-LOSS COEFFICIENT

Conditions: Solidity = 0.37; Vertical angle $\theta=90^\circ$

Bar Shape						
Flow Angles	Bar Loss Coefficient*, C_{tr}					
$\alpha=0^\circ$	1.13	0.86	0.78	0.48	0.42	0.35
$\alpha=30^\circ$	1.46	0.76	0.71	0.43	0.68	0.22
$\alpha=45^\circ$	2.05	1.29	1.29	0.94	1.29	0.67
$\alpha=60^\circ$	4.26	2.45	2.81	2.19	3.05	1.84

* C_{tr} is loss coefficient $\Delta H=C_{tr} V_a^2/2g$

Figure 88 Trash-rack losses at skew approach flow, from Orsborn [26].



**OPEN CHANNEL FLOW
TRASH RACK LOSSES**

Figure 89 Losses of different types of bars, after WES [43]

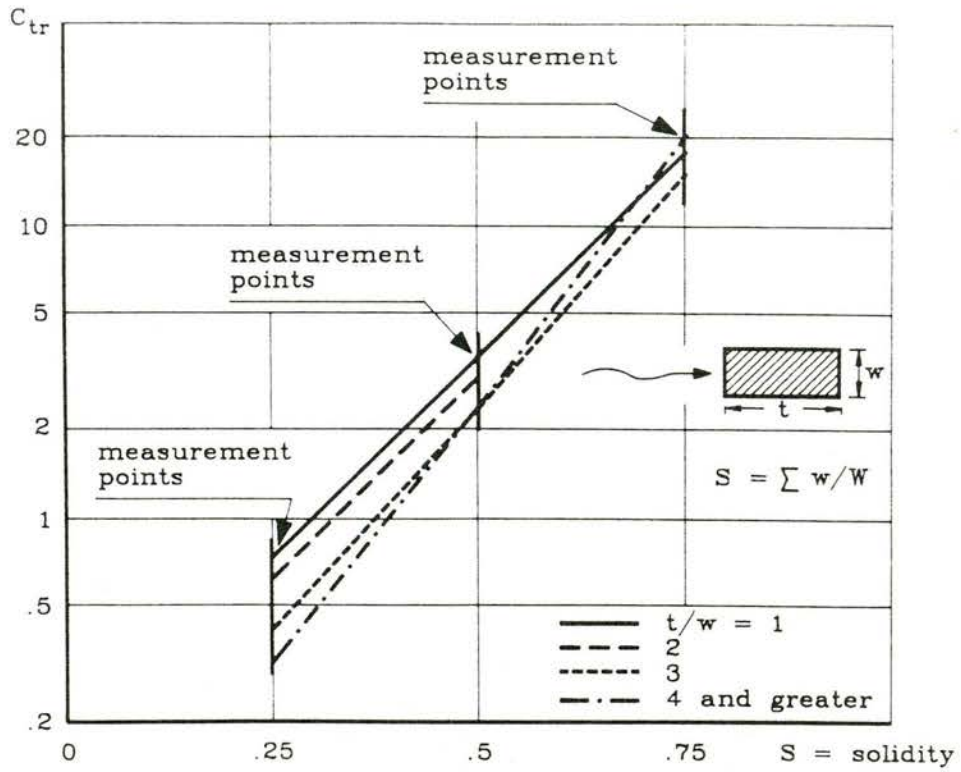


Figure 90 Loss coefficients for rectangular bars at greater solidity after Orsborn [26]

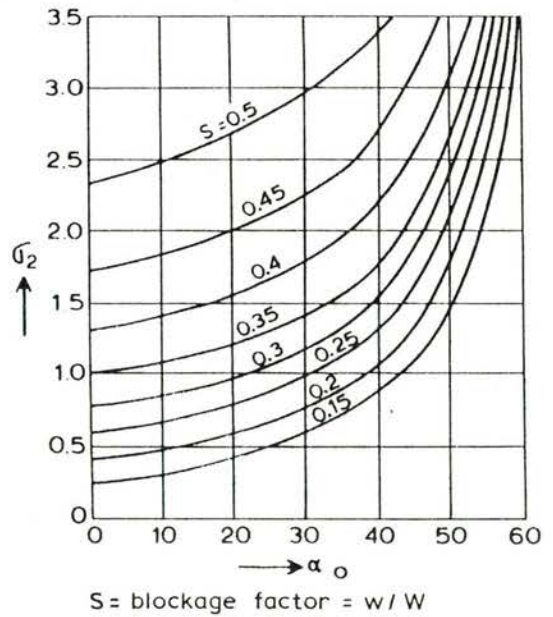
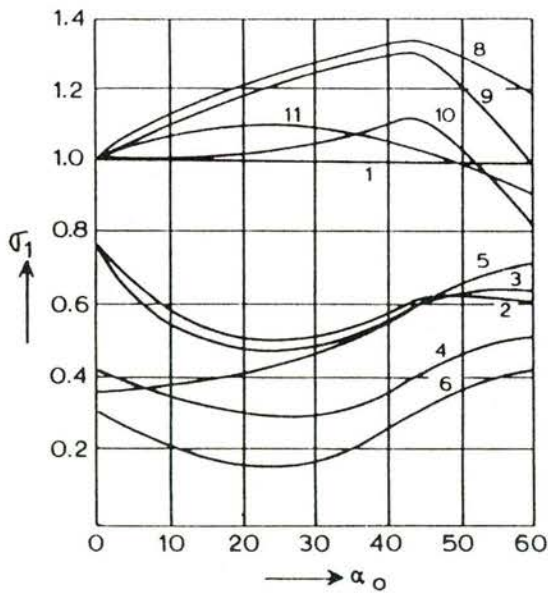
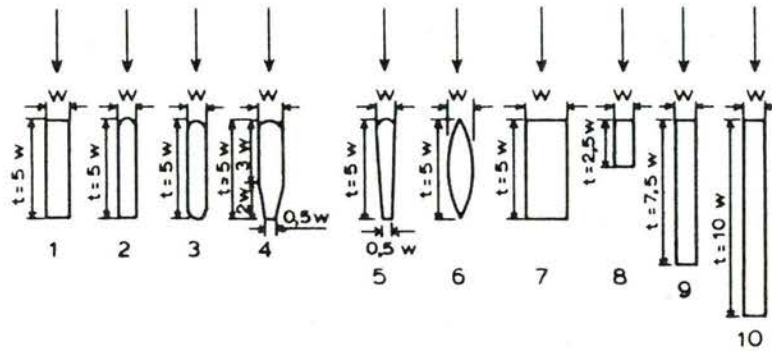
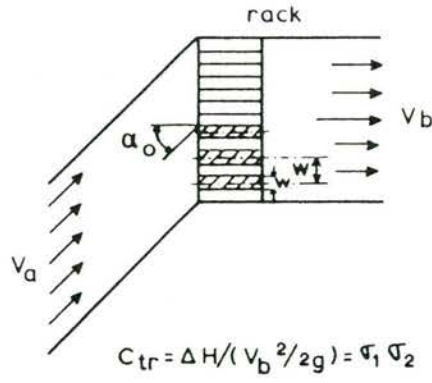


Figure 91 Trashrack-bar losses at skew approach velocities, after Idel'cik [17]

4.6 Resistance of bridge piers

In the following, only very schematised cases are considered. For example, no deepening between the piers by the locally enlarged bedload capacity or by scour and no rough bottom protection around the piers are taken into account. The flow is assumed to be parallel to the canal or river axis. Moreover, all experimental data were obtained by tests performed in rectangular flumes and all data presented here relate to rectangular flow sections. The ratio of water-depth over pier-width is not considered, although there are indications that this parameter might have some influence (Naudascher [25]).

The above simplifications permit the application of one-dimensional hydraulics, in the same way as discussed for other hydraulic structures in section 1.4.

Three regimes of flow are distinguished (Figure 92); types A, B and C refer to the WES classification [43].

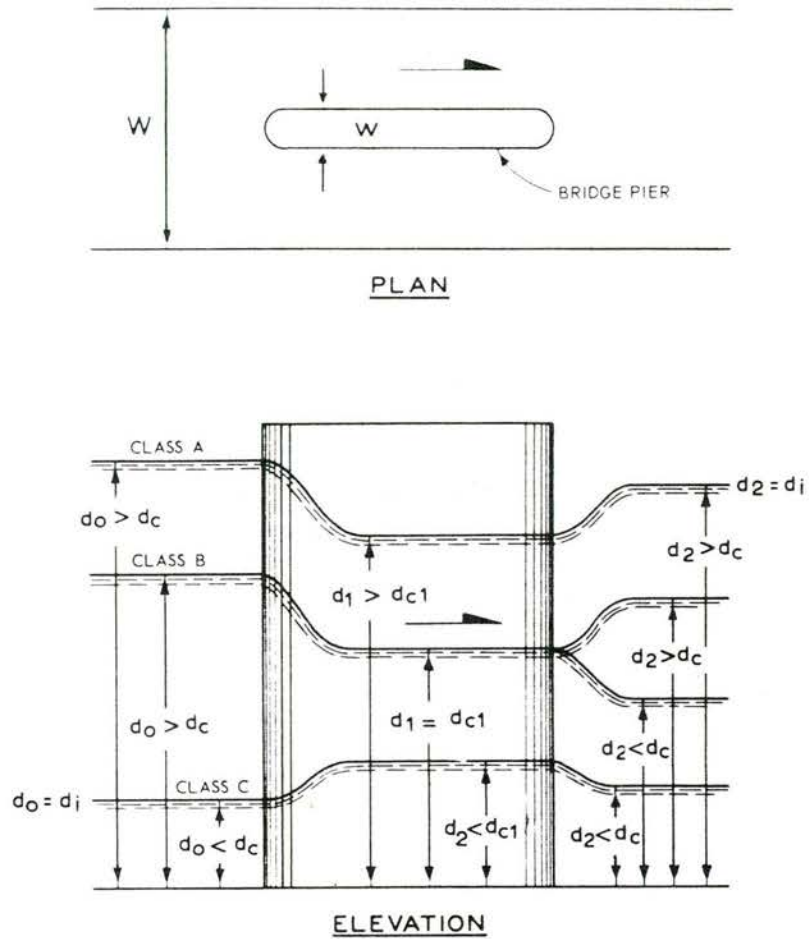
A Subcritical flow condition (fully submerged and intermediate flow).

In this situation the water level upstream of the bridge depends on the initial water depth (d_i) and the discharge of the undisturbed river. The initial water depth also corresponds to the depth downstream of the bridge (d_2 in Figure 92) apart from a slight modification by friction and head loss due to deceleration.

B Modular flow condition (critical flow).

A unique relation between the water level upstream of the bridge and the discharge will occur here. It is usual to define the critical depth in the control-section by using the full width of the flow section between the bridge piers, neglecting the effect of side contraction of the flow. The necessary correction coefficients are found from empirical data. The energy level which belongs to the critical depth between the piers determines the energy level upstream of the bridge and the corresponding upstream water level can also be calculated. The water level downstream of the bridge can be either supercritical or subcritical (see Figure 92). If the initial water level is in between these levels, the supercritical water-level will occur in combination with a hydraulic jump further downstream. If a downstream loss coefficient is estimated the local downstream water-level can be derived, but this has no practical importance.

Which condition - the supercritical or the subcritical one - will exist is found from a further analysis of the flow downstream of the bridge.



Note: $S = w/W =$ blockage ratio
 $w =$ total pier width
 $W =$ gross channel width
 $d_o =$ upstream depth
 $d_1 =$ depth within pier section
 $d_2 =$ downstream depth
 $d_c =$ critical depth within the unobstructed channel section
 $d_{c1} =$ critical depth within the pier section
 $d_i =$ initial depth

Figure 92 Water levels for the three flow regimes, A, B and C

C Super-critical flow condition.

At high river velocities the water level just upstream of the bridge as it is found for type B flow is not sufficient to evoke a hydraulic jump (upstream of the bridge) and the flow under the bridge remains thus also supercritical. All water levels are now fully determined by the upstream conditions and the upstream water level d_0 equals now the initial water level d_i . Regime C, which occurs at mountain rivers, is not of interest for backwater effects; its interest is mainly in forces exerted by the flow on the piers and the maximum water level under the bridge.

In table 4.6.1 the properties and needed calculations for each of the flow regimes are summarized.

name	per definition	influence initial depth	needed calculations
A Subcritical	$d_1 > d_{c1}$	$d_2 = d_i$	$d_o = f(q, S, d_2)$
B Modular (critical)	$d_1 = d_{c1}$	no influence	$d_o = f(q, S)$
C Supercritical	$d_1 < d_{c1}$	$d_0 = d_i$	$d_2 = f(q, S, d_0)$

Table 4.6.1: Properties of flow regimes A, B and C

Figure 93, from WES [43], shows the limits of type A, B and C flow regimes as function of the initial conditions and the blockage ratio.

Curve 1 is obtained by taking the critical depth in the section between the piers and its corresponding energy head, from which the (equal) water levels up- and downstream at the wider sections are derived (subcritical condition without additional losses). The calculated water level applies to the downstream limiting condition between modular flow and submerged flow. Curve 2, now including hydraulic losses, follows from interpretation of experiments; at the same critical flow condition between the piers the downstream energy head and corresponding water level (which equals at the limiting condition also the initial water level) is lower when losses are involved. Curve 1 represents the subcritical depth upstream of the bridge at modular flow. This depth is also the available sequent depth of a hydraulic jump which can occur for supercritical flow in the upstream region. From this depth the sequent supercritical flow conditions can be derived, which results in curve 3.

In the following the three flow regimes will be considered in more detail in the sequence C, B and A. For definitions see Figure 92. The discharge per unit width, q , is defined in the initial situation without bridge piers.

Flow type C (supercritical flow): No further experimental data are available; WES advises to get insight in the flow behaviour by application of the momentum equation. In Figure 94 a computation result for the water level under the bridge is presented. The assumption was a constant energy level without additional losses. However, this computation is on the unsafe side so a factor α for flow contraction must be applied. It shows clearly that an important set-up of the water level can be expected. The graph has been obtained by application of the Bernoulli equation:

$$d_0 + q^2/2g d_0^2 = d_1 + \{q/(1-\alpha S)\}^2/2g d_1^2 \quad (81)$$

(d_0 and d_1 refer to the water depth upstream and between the piers)

In the figure d_c applies to critical depth at the section without the bridge piers. Between the piers the discharge per unit width is higher than upstream of the bridge

$$q_1 = q/(1-\alpha S) \quad (82)$$

Type B (modular flow): Figure 95 presents the upstream water level for two nose shapes of a bridge pier. Contrary to subcritical flow where pier losses are determined by the nose and the afterbody shape, only the contraction induced by the nose shape will determine the flow section at modular flow.

Type A flow (fully-submerged and intermediate flow): the bridge pier losses for low flow-velocities (due to the near-horizontal water level) are fully comparable with the bar-losses at trashracks presented in the former section. But at higher velocities a dip in the water level occurs, giving an increase of losses. The higher velocity is expressed in terms of an increased Froude number, a decreased relative water depth d/d_c or an increased relative velocity head $V^2/2gd$. (These numbers have in fact all three the same significance, for instance $F^{-2} = (d/d_c)^3$.)

For increasing velocity, the dip in the water level initially increases in proportion to the velocity squared, but when the dip increases the velocity

in the contraction increases more rapidly due to the additional effect of a decrease in water depth.

Two formula for bridge pier resistance are discussed below, the Rehbock formula and the Yarnell formula (applied in the WES charts [43]). To have a basis for comparison some uniform parameters are introduced in both formula.

Rehbock (taken from Reh [29]) developed the following formula:

$$\Delta H = C_{br} V_2^2 / 2g \quad (83)$$

$$C_{br} = \{\delta_0 - S(\delta_0 - 1)\} (0.4 S + S^2 + 9 S^4)(1 + F_2^2) \quad (84)$$

(δ_0 = factor depending on the shape of the pier, S = blockage ratio = w/W , F_2 = Froude number downstream = $V_2 / \sqrt{gd_2}$). The downstream Froude number is also the Froude number for the initial condition. It is seen that Rehbock took into account interaction between blockage and pier shape (the product terms with δ_0 and S) but in his expression the amplification due to the Froude numbers is the same for all bridge pier types. This indicates that he tested the piers at relatively low velocities (near the modular flow conditions it is mainly the flow contraction at the pier nose which is important and not the total pier shape).

To enable comparison with other formulae for bridge pier losses Eqs. 83 and 84 are transformed.

Making use of the fact that the drag coefficient of one single bridge pier equals (this will be discussed hereunder)

$$C_d = C_{br} / S \quad (85)$$

the drag coefficient (derived from Equation 84) at low flow velocity $F_2^2 \ll 1$ and zero blockage ($S = 0$) becomes:

$$C_{do} = 0.4 \delta_0 \quad (86)$$

and Equation 84 transforms into

$$C_{br} = (C_{do} - C_{do} S + 0.4 S)(S + 2.5 S^2 + 22.5 S^4)(1 + F_2^2) \quad (87)$$

Remark:

Equation 85 is not formally derived here but when the drag of a pier is defined as

$$D = C_d \frac{1}{2} \rho V_0^2 w d_0 \quad (a)$$

and when the momentum equation is applied at a condition where there are small velocities and a small head differences it can be found that the pier drag is just compensated by the force induced by the difference in water level

$$D = \Delta h (\rho g w d_0) \quad (b)$$

And also can be found

$$\Delta h \approx \Delta H \quad (c)$$

Now equation (b) in combination with (c) and (83) results, taking into account that $V_2 \approx V_0$, in:

$$D = C_{br} (V_0^2/2g) (\rho g w d_0) = C_{br} \frac{1}{2} \rho V_0^2 w d_0 \quad (d)$$

Equation a and d combined result in eq. 85.

In Figure 96 the C_{do} of a number of piers as investigated by Rehbock is presented. Although not all sizes are explicitly mentioned the drawing is undistorted and all piers unless indicated otherwise, have a length of 6 to 6.7 times w (probably 6.66).

WES [43] proposes for C_{br} in eq. 83 the use of the Yarnell formula:

$$C_{br} = (d_0 - d_2)/(V_2^2/2g) = 2K\{K + 10(V_2^2/2g d_2) - 0.6\}(S + 15 S^4) \quad (88)$$

The factor K can be transformed, using Eq. 85, into C_{do} ($V = 0$ and $S = 0$)

$$C_{do} = 2 K^2 - 1.2 K \quad (89)$$

from which:

$$K = 0.3 + (0.09 + 0.5 C_{do})^{0.5} \quad (90)$$

The proposed Yarnell K factors are transformed in the next table into C_{do} and compared with the Rehbock values of corresponding shapes. Especially for case a (the semicircular nose and tail), a great difference is seen.

Pier shape	K	derived C_{do}	from Fig. 96
a. Semicircular nose and tail	0.90	0.54	0.84
b. Twin-cylinder piers with connecting diaphragm	0.95	0.67	
c. Twin-cylinder piers without diaphragm	1.05	0.95	
d. 90 deg. triangular nose and tail	1.05	0.95	1.15
e. Square nose and tail	1.25	1.63	1.56

Table 4.6.2: The Yarnell K factors, the derived C_{do} factors therefrom and corresponding values from Rehbock

The Yarnell formula is presented graphically in Figure 97. Figure 98 gives a comparison with Rehbock results for shapes a, d and e (as indicated in Table 4.6.1) for varying d_2/d_c values.

The differences are probably due to the fact that the Rehbock formula is here applied in the range beyond the experimental range from which it was derived. Very small S values were probably not tested either, nor were the very large d_2/d_c values (to prevent too low values of the Reynolds number). It is interesting that the best agreement is found for d_2/d_c in the range of 3 and for the square-nosed and -tailed piers.

In recent years an investigation of Al-Nassri and McBean [3] has been published which covers a variety of shorter pier shapes. The range of F_2 was between 0.25 and 0.6 the blockage varied between 12 and 35%. Figure 99 shows the test results. Instead of water depths the energy levels H with respect to the bottom level were used.

A direct comparison with the Yarnell formula is difficult because the two presentations are quite different; therefore only a comparison with the Rehbock formula is presented. Shape 1 and 5 of Figure 96 was compared with b and a of Figure 99; the comparison is presented in Figure 100. In general the Rehbock formula gives higher water level differences (where the Al-Nassri resistance is higher the diamond pier was also shorter and hence less streamlined).

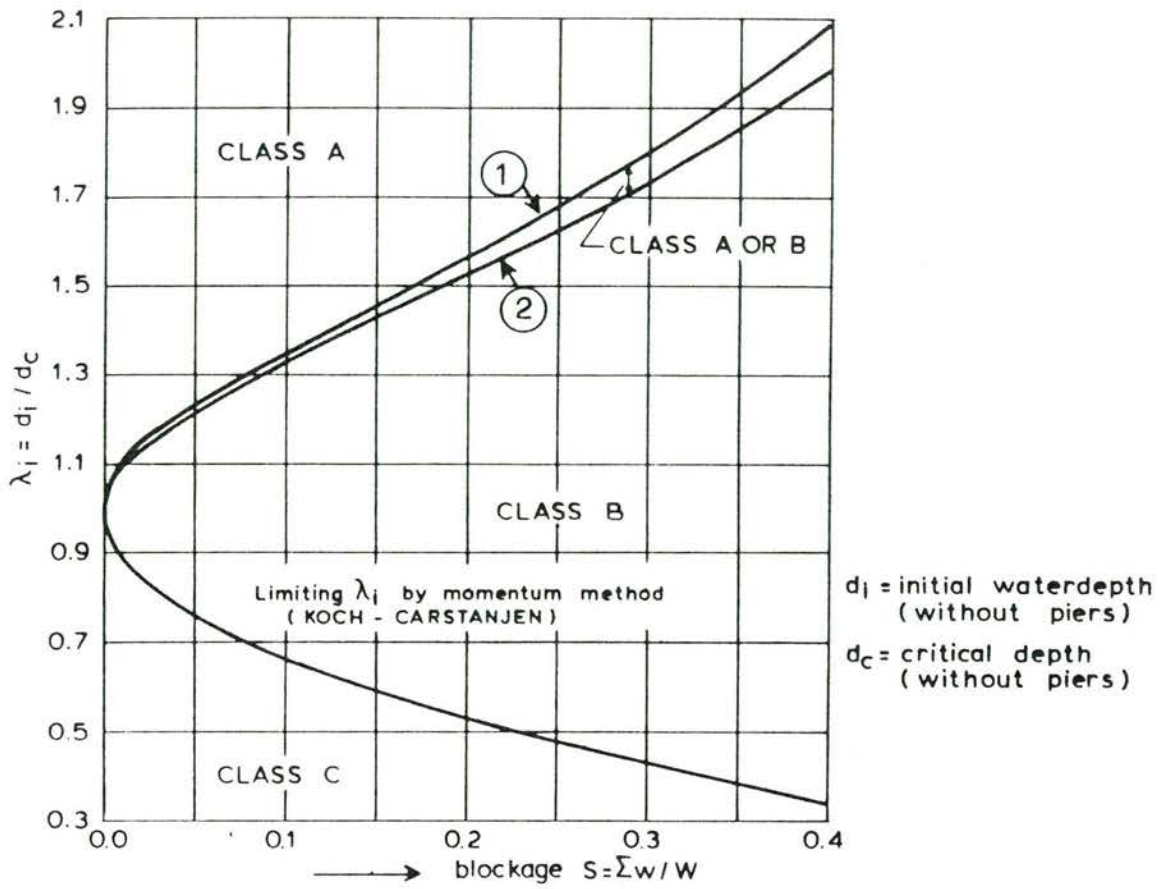


Figure 93 Flow regime as function of the initial flow conditions in a rectangular canal, from WES [43]

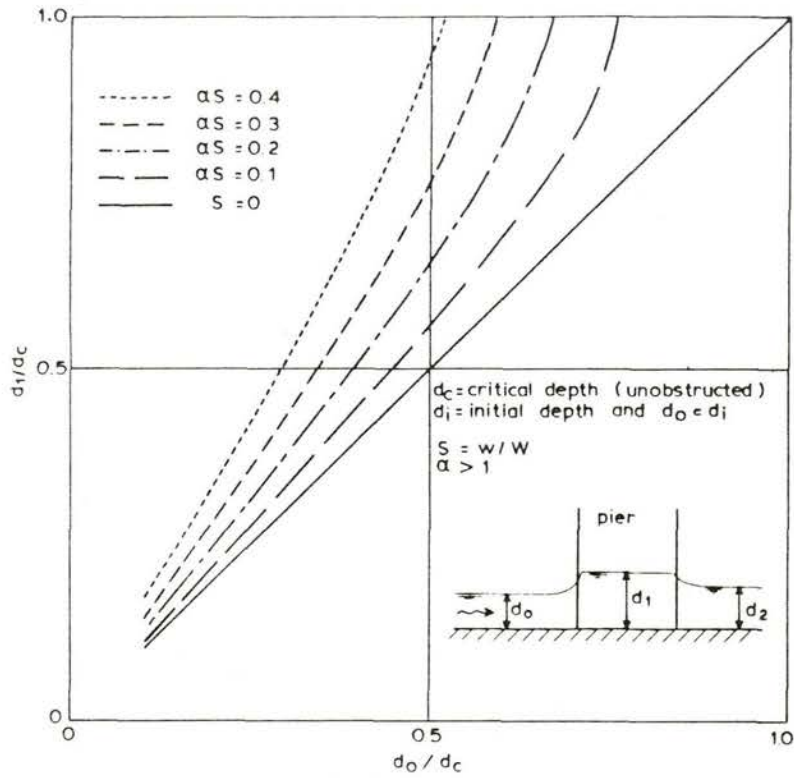


Figure 94 Theoretical minimum change of the water level under the bridge for flow type C (supercritical).

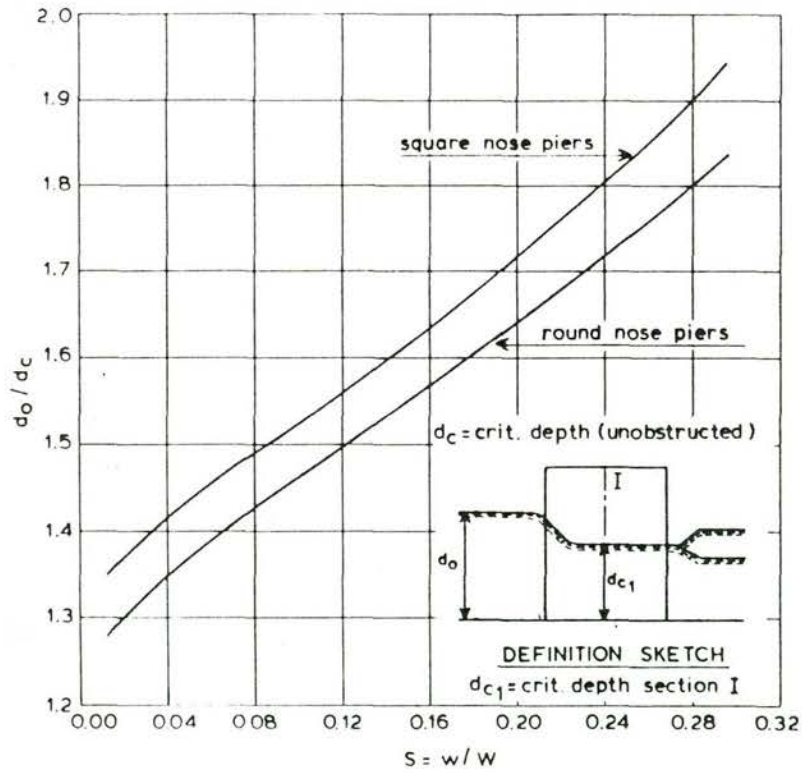


Figure 95 Upstream water depth for type B (modular) flow, from WES [43]

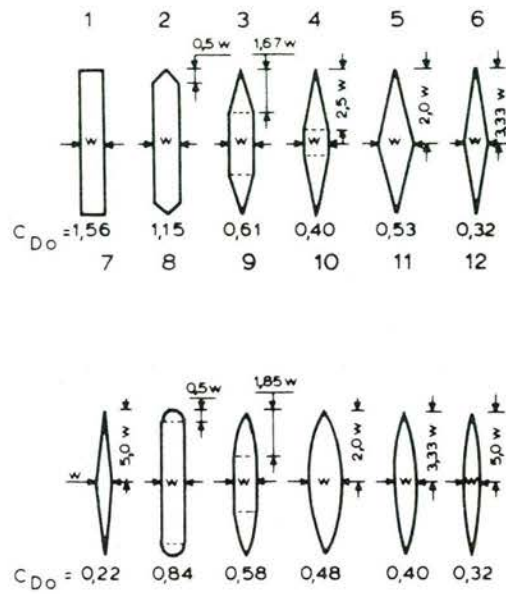


Figure 96 Drag coefficients of piers investigated by Rehbock after Reh [29]

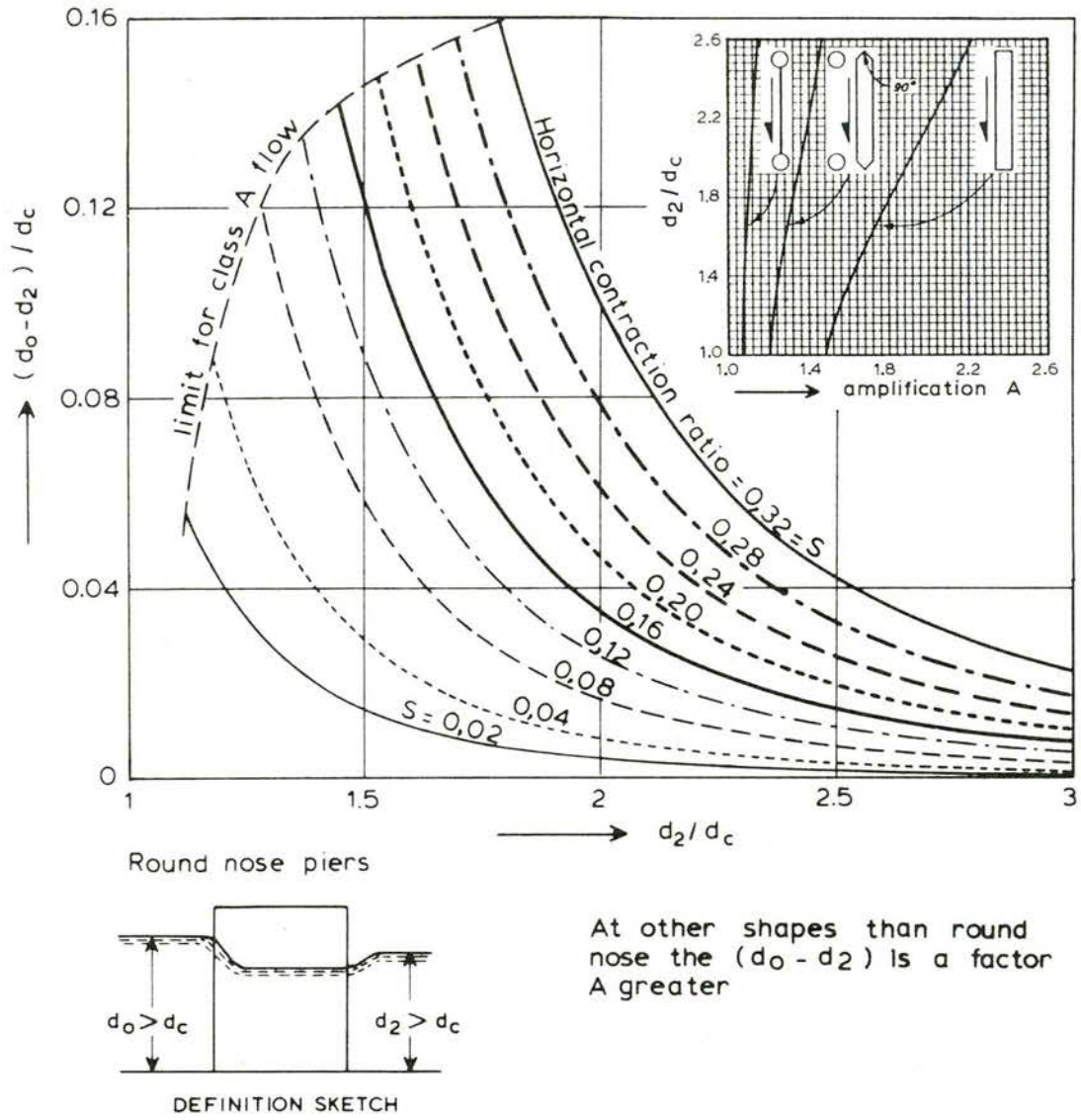
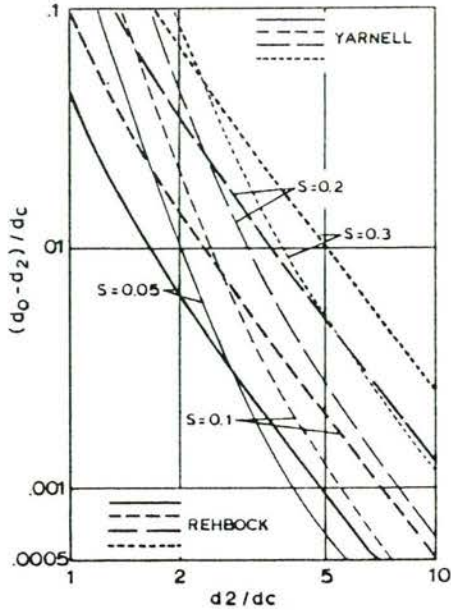
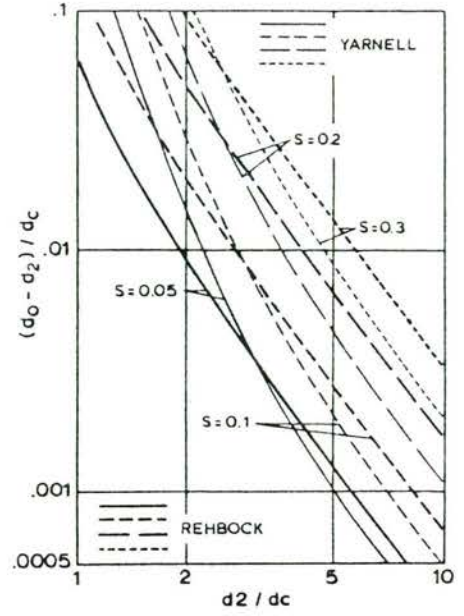


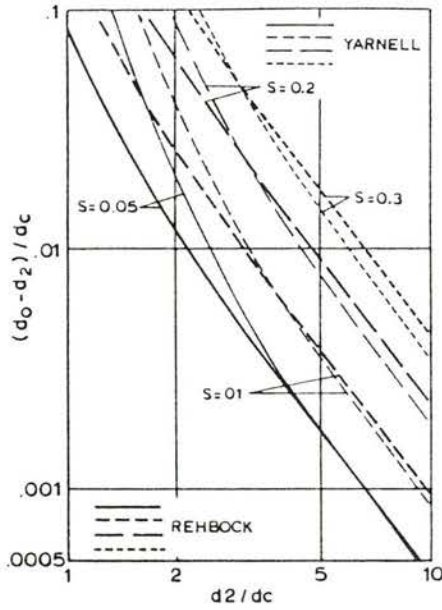
Figure 97 Bridge pier losses for regime A (fully submerged and intermediate flow) based on the Yarnell equation, after WES [43]



case a (table 4,6,2):
 semicirc nose / tail
 Rehbock $C_{Do} = 0.84$
 Yarnell $K = 0.90$

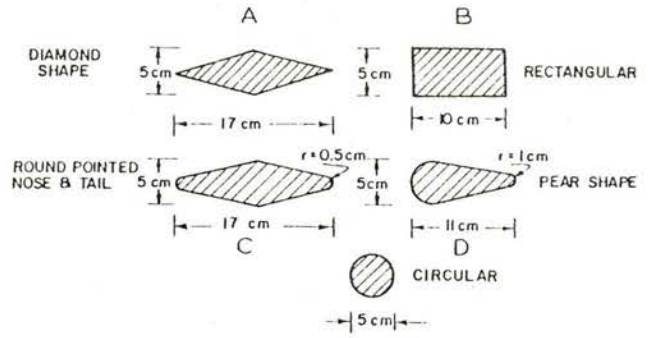
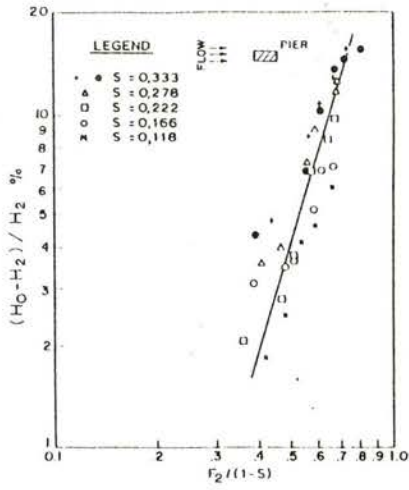


case d:
 90° angle nose / tail
 Rehbock $C_{Do} = 1.15$
 Yarnell $K = 1.05$



case e:
 square nose / tail
 Rehbock $C_{Do} = 1.56$
 Yarnell $K = 1.25$

Figure 98 Comparison between bridge pier losses computed from the Yarnell and Rehbock equations



$F_2 = V_2 / \sqrt{g d_2}$
 (equals F_1 (unobstructed condition))

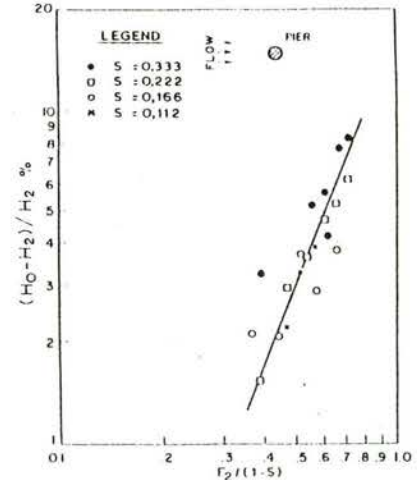
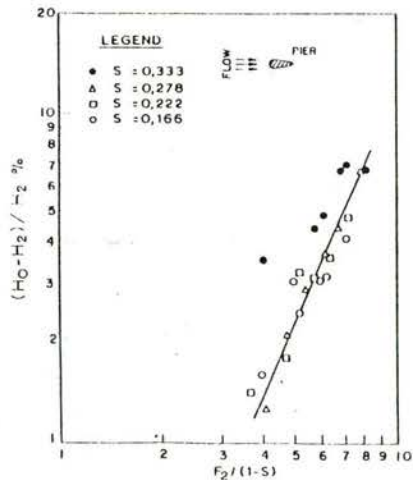
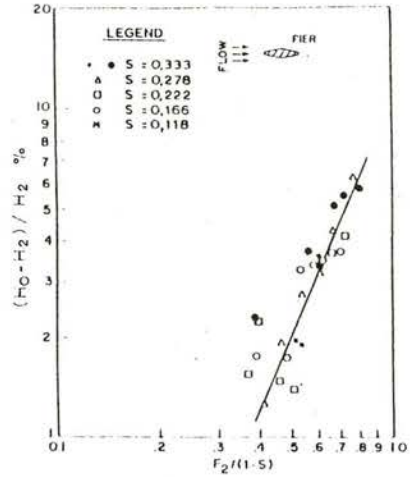
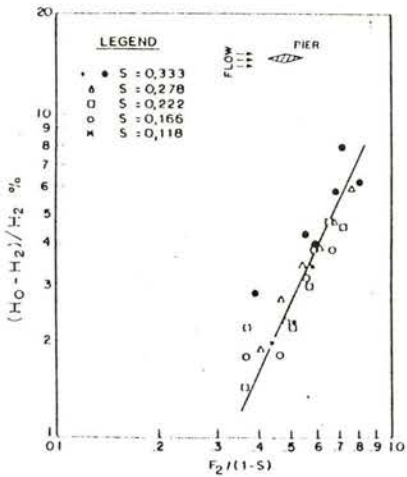


Figure 99 Test results at regime A according to Al-Nassri and McBean [3]

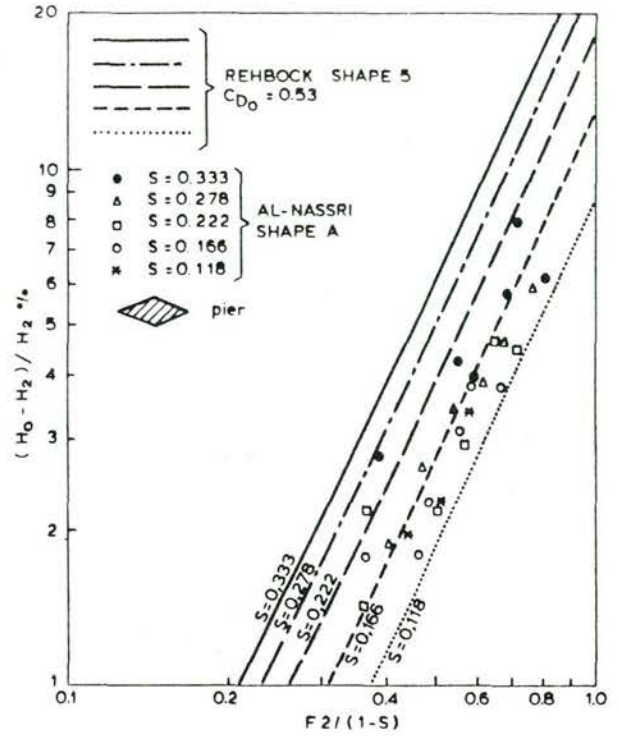
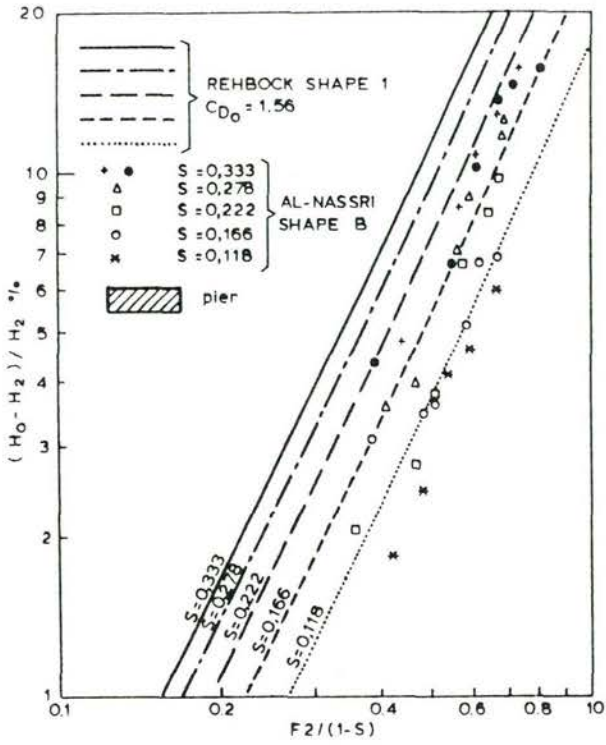


Figure 100 Comparison of pier resistance of the Rehbock formula and the tests of Al-Nassri and McBean

REFERENCES

1. Abdel-Gawad, S.M. and Corquodale, J.A.Mc.,
"Analysis of the submerged radial hydraulic jump" in *Canad. Journ. of Civ. Eng.* Vol 12, 1985 pp. 593-602
2. Abou-Seida, M.M., Quraishi, A.A.; "A flow equation for submerged rectangular weirs", *Proc. Inst. Civil Engineers*, Vol. 61, 1976.
3. Al-Nassri, S.A. and McBean, E.A.: "Bridge pier shape and contraction ratios". *Journal of Engineering and Applied Sciences*, Vol. 2, pp. 115-129, 1983
4. Billoré, J., Jaoui, A., Kolkman, P.A., Radu, M.T., de Vries, A.H.:
"Hydraulic investigation for the diversion, the morning glory spillway and the bottom outlet of the M' Dez dam in Marocco" (in French language). 13th Congress on large Dams, Q50, A62 ICOLD, 1979.
5. Boiten, W.; "Ice flap of the Borgharen barrage. Determination of discharge coefficients." (original in Dutch), DELFT HYDRAULICS Rep. M1318, 1980.
6. Boiten, W.; "Vertical underflow gates discharge characteristics", Research Report No 93. Agricultural University of Wageningen, dept, of Hydraulics and Catchment Hydrology, November 1989.
7. Bos, M.G. (ed); "Discharge measurement structures" publ. DELFT HYDRAULICS nr. 161 and Int. Inst. for Land Reclamation (ILRI), Wageningen 1976.
8. Bready, J.N.; "Rating curves for flow over Drum Gates", *Transactions ASCE* Vol. 119, pp. 403-420, 1954.
9. Cozzo, G.; "A formula to calculate the discharge coefficient of gates" (original in Italian); *l'Energia Elettrica* nr 11-12, pp. 504-513, 1978.
10. DELFT HYDRAULICS " Discharge coefficients at overflow" (original in Dutch), report M647, 1959.

REFERENCES (continued)

11. DELFT HYDRAULICS: "The rectangular broad-crested weir", report S170-VIII, 1981.
12. DELFT HYDRAULICS: "The trapezoidal profile broad-crested weir", report S170-XI, 1983.
13. Formica, G.,
"Preliminary experiments of head losses in canals with divergent or convergent section" (in Italian).
L'energia elettrica, Milano, Vol. 32 No 7, pp. 554-568, July 1955.
14. Gieseke, J.; "Computation of discharge coefficient for Hower Bunger valve" (original in German); "Die Wasserwirtschaft", 56, no. 10, pp. 315-323, 1966.
15. Harrison, A.J.M., "Boundary layer displacement thickness on flat plates", Proc. ASCE, Journal Hydraulic div. HY4, July 1967 paper 5339 pp. 79-91
16. Hay, N and Taylor, G.; "Performance and design of labyrinth weirs", ASCE, Journ of Hydr. Div HY11, pp. 2337-2357, Nov. 1970.
17. Idel'cik, I.E.; "Momento des pertes de charge" Publ. Eyrolles, France 1969 (translated from Russian)
18. ISO, International Organization for Standardization: "Measurement of liquid flow in open channels"; ISO Standards Handbook 16, Geneva 1983.
19. Kinsvater, C.E. and Carter, R.W.C.; "Discharge characteristics of rectangular thin-plate weirs" Journ. Hydr.Div ASCE vol 83, HY6, paper 1453, Dec.1957.
20. Kolkman P.A.; "Considerations about the accuracy of discharge relations of hydraulic structures and the use of scale models for their calibration" IAHR symp. on "Modelling hydraulic structures" Esslingen, Sept 1984.

REFERENCES (continued)

21. Kooman, D. and Korthof, R.M.; "Sill beam loads due to flow and waves"; In "Hydraulic Aspects of Coastal Structures; Developments in Hydraulic Engineering related to the design of the Oosterschelde Storm Surge Barrier in the Netherlands", part 2, pp 47-66, Delft University Press, 1980.
22. Levin, L.; "Theoretical and experimental study of flow in slots" (original in French); in "Le genie civil" No. 5, pp. 1-12, May 1971.
23. Nago, H.; "Influence of Gate-Shapes on Discharge Coefficients"; Transactions Jap. Soc. of Civ. Engrs, Vol. 10, pp 116-119, Nov 1978.
24. Naudascher, E.; "Hydraulics in open channels and hydraulic structures" (original in German); Publ. Springer, Vienna 1987.
25. Naudascher, E.; "Forces on hydraulic structures, Manual about hydraulic structures design information"; Int. Ass. for Hydraulic Research IAHR, publ. Balkema 1989 (in preparation).
26. Orsborn, J.F.,
"Rectangular-bar trashrack and baffle head losses", Proc. ASCE, Journ. Power Div., paper 6223, pp. 111-123, Nov. 1968.
27. Pickering, G.A.; "Lock culvert valve loss coefficients" Hydr. Lab US Army Engin. Waterways Experiment Station WES. Sept 1981.
28. Pugh, C.A.,
"Turbulent flow in rectangular outlet conduit, Rend Lake dam, Big Muddy river, Illinois"; Rep. H75-2, Hydr. Lab. of US Army Waterw. Exp. Station WES, Jan. 1975.
29. Reh, U; "Simplified application of the Rehbock backwater formula for bridges" (original in German). "Die Wasserwirtschaft", 1957 - 1958 pp. 240-242.
30. Rehbock, TH; "The constantness of the discharge relation at sharp edged weirs" (original in German), in "Der Bau-ingenieur" Vol.11, No.48 pp. 821-826, 1930.

REFERENCES (continued)

31. Rouse, H.; "Engineering Hydraulics", publ. John Wiley 1950.
32. Rouvé, G. and Inlekofer, H.; "Discharge over straight weirs with semi-cylindrical crest" (original in German); "der Bauingenieur 49, pp. 250-256, publ. Springer, 1974.
33. Rouvé, G. and Khader, M.H.A.; "Transition from a conduit to free surface flow" IAHR Journal of Hydraulic Research, Vol. 7 No.3, 1969.
34. Sarginson, E.J.; "The influence of surface tension on weir flow"; IAHR Journal of Hydraulic Research, Vol. 10, no.4, pp. 431-446, 1972.
35. Schönfeld, J.C.; "Tidal computations by integration along characteristics" (original in Dutch language); Note 55-14 of Central Study Office, Rijkswaterstaat, 1935.
36. Thijsse, J.Th.; "Hydraulica, in The Technical Vademecum" (originally in Dutch the "technische vraagbaak") part W, publ. Kluwer, the Netherlands, 1951.
37. Tullis, J.P. and Wang, J.S.; "Turbulent flow in the entry region of a rough pipe", Transactions ASME, pp. 62-68, March 1974.
38. USBR; "Design of small dams", US dept. of Interior, Bureau of Reclamation USBR, revised edition 1977.
39. Varshney, R.S. and Mohanty, S.K.; "Discharge relations for submerged weirs" Indian journ. of Power & River valley development, pp. 225-228, July 1973.
40. Ven Te Chow; "Open Channel hydraulics", Publ. Mc Graw-Hill 1959.
41. Villemonte, J.R.; "Submerged weir discharge studies", Engin.News Record, pp. 866-869, Dec. 25, 1947.
42. Wagner, W.E.; "Determination of pressure-controlled profiles of Morning-Glory shaft spillways, "Symposium ASCE, transactions 1956.

REFERENCES (continued)

43. WES; "Hydraulic Design Criteria", US Army Waterways Experiment Station, Corps of Engineers, 17th issue 1977.
44. Woodbury, L.H. and Padmanabhan, G.; "Design implications of radial hydraulic jumps" in "Civil Engineering for Practicing and Design Engineers" Vol. 4, pp. 965-984, Publ. Pergamon USA, 1983.





main office
Rotterdamseweg 185
p.o. box 177
2600 MH Delft
The Netherlands
telephone (31) 15 - 56 93 53
telefax (31) 15 - 61 96 74
telex 38176 hydel-nl

location ' De Voorst '
Voorsterweg 28, Marknesse
p.o. box 152
8300 AD Emmeloord
The Netherlands
telephone (31) 5274 - 29 22
telefax (31) 5274 - 35 73
telex 42290 hylvo-nl

